Chem Soc Rev

REVIEW ARTICLE

View Article Online
View Journal | View Issue

Open Access Article. Published on 24 January 2025. Downloaded on 11/7/2025 6:47:57 AM.
This article is licensed under a Creative Commons Attribution 3.0 Unported Licence.

Check for updates

Cite this: *Chem. Soc. Rev.*, 2025, **54**, 2054

Influence of π–π interactions on organic photocatalytic materials and their performance†

Liquan Jing,‡[a] Pandeng Li,‡[a] Zheng Li,[a] Dongling Ma*[b] and Jinguang Hu*[a]

Received 31st August 2024

DOI: 10.1039/d4cs00029c

rsc.li/chem-soc-rev

Currently, organic photocatalyst-based photocatalysis has garnered significant attention as an environmentally friendly and sustainable reaction system due to the preferable structural flexibility and adjustable optoelectronic features of organic photocatalysts. In addition, π–π interactions, as one of the common non-bonded interactions, play an important role in the structure and property adjustments of organic photocatalysts due to their unique advantages in modulating the electronic structure, facilitating charge migration, and influencing interfacial reactions. However, studies summarizing the relationship between the π–π interactions of organic photocatalysts and their photocatalytic performance are still rare. Therefore, in this review, we introduced the types of π–π interactions, characterization techniques, and different types of organic photocatalytic materials. Then, the influence of π–π interactions on photocatalysis and the modification strategies of π–π interactions were summarized. Finally, we discussed their influence on photocatalytic performance in different photocatalytic systems and analyzed the challenges and prospects associated with harnessing π–π interactions in photocatalysis. The review provides a clear map for understanding π–π interaction formation mechanism and its application in organic photocatalysts, offering useful guidance for researchers in this field.

1. Introduction

Photocatalysis driven by solar energy is a promising future technology for energy transformation, storage and environmental restoration, including H_2 generation, CO_2 reduction, organic pollutant degradation, and N_2 fixation.[1–4] The key to the development and eventual practical implementation of photocatalysis technology is the design of novel, high-performance photocatalysts, which should possess strong photo-redox

[a] Department of Chemical and Petroleum Engineering, University of Calgary, 2500 University Drive, NW, Calgary, Alberta T2N1N4, Canada. E-mail: jinguang.hu@ucalgary.ca

[b] Institut National de la Recherche Scientifique (INRS), Centre Énergie Materiaux et Télécommunications, 1650 Boulevard Lionel-Boulet, Varennes, Québec J3X1S2, Canada. E-mail: Dongling.Ma@inrs.ca

† Electronic supplementary information (ESI) available. See DOI: https://doi.org/10.1039/d4cs00029c

‡ These authors contributed equally to this work.

Liquan Jing

Liquan Jing earned his PhD in Environmental Science and Engineering from Jiangsu University in 2021. He is now a postdoctoral researcher in the Department of Chemical and Petroleum Engineering at the University of Calgary, working under the guidance of Prof. Jinguang Hu and Prof. Ian D. Gates. His research primarily focuses on designing and synthesizing functional photocatalysts for sustainable hydrogen production, converting biomass into high-value-added bioproducts, and methane conversion.

Pandeng Li

Pandeng Li earned his PhD from the Institut national de la recherche scientifique (INRS) in Canada in 2021. He is currently a postdoctoral researcher in Prof. Jinguang Hu's research group in the Department of Chemical and Petroleum Engineering at the University of Calgary. His research primarily focuses on developing large-scale reactors for biomass photoreforming, aiming to concurrently produce valuable chemicals and sustainable hydrogen.

 This journal is © The Royal Society of Chemistry 2025

Open Access Article. Published on 24 January 2025. Downloaded on 11/7/2025 6:47:57 AM.
This article is licensed under a Creative Commons Attribution 3.0 Unported Licence.

ability, efficient charge migration, rapid surface reactions, high selectivity and durability.[5–10] Over the last two decades, different types of photocatalytic materials have been developed. Inorganic semiconductor nanomaterials are promising photocatalysts, including oxide-based photocatalysts (TiO_2, ZnO, $SrTiO_3$, $BiVO_4$, *etc.*), chalcogenide-based photocatalysts (ZnS, CdS, CdSe, MoS_2, $Zn_{1-x}Cd_xS$ ($0.2 \leq x \leq 1$), $ZnIn_2S_4$, $AgInS_2$, *etc.*), and nitride-based photocatalysts (GaN and Ta_3N_5).[11–14] To further improve photocatalytic performance, the size, shape, and doping of inorganic photocatalysts are optimized, and a co-catalyst strategy is also applied.[13,15–21] Additionally, another type of photocatalyst is based on organic materials with a delocalized π-electron system, such as covalent organic frameworks (COFs), metal–organic frameworks (MOFs), organic small-molecule compounds, conjugated polymers, carbon-based materials, and other aromatic compounds (Fig. 1a).[22–38] The conjugated (or aromatic) photocatalytic materials exhibit structural flexibility and precise tuning of optoelectronic features. Fig. 1b shows that the number of publications related to π–π interactions in photocatalysis (mainly photocatalysts) has increased exponentially since 2002, reflecting the increasing importance of applying π–π interactions in photocatalysis.

In addition, another important feature of the π–π interactions arises from the strong dispersion and dipole–dipole interactions when the planes of aromatic rings are stacked on one another.[39–41] These interactions can be classified into different groups based on the geometric arrangement of stacked aromatic rings, and typically exist in conjugated intermolecular interactions or between conjugated molecules and reactant organic molecules. The former can influence the crystallization properties, optical properties, electronic properties, and stability of organic conjugated photocatalytic materials. In contrast, the latter can alter charge transfer between conjugated photocatalytic molecules and reactant organic molecules, ultimately influencing the corresponding photocatalytic reaction.[42–44] Hence, π–π interaction as an important factor must be carefully considered when designing novel conjugated photocatalysts and optimizing the related photocatalytic performance. To date, the related reviews about the influence of π–π interactions on conjugated photocatalysts and photocatalytic performance are still rare. Therefore, it is of great significance to summarize the influences of π–π interactions in different conjugated (or aromatic) photocatalysts on photocatalytic performance in particular, which can provide a direction for researchers in this aspect.

In order to understand the π–π interactions of conjugated (or aromatic) photocatalysts in depth, this article first provides an introduction to the types of π–π interactions and the characterization methods, and then summarizes, in turn,

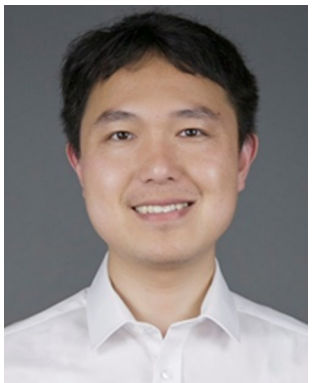

Zheng Li

Zheng Li earned his PhD from the Dalian Institute of Chemical Physics and is currently an Eyes High Postdoctoral Research Fellow in the Department of Chemical and Petroleum Engineering at the University of Calgary, under the guidance of Dr Jinguang Hu and Dr Zhangxin (John) Chen. His research primarily focuses on the photo(electro/piezo/bio)-catalytic conversion of biomass-derived and energy-related molecules for the production of sustainable hydrogen and value-added chemicals.

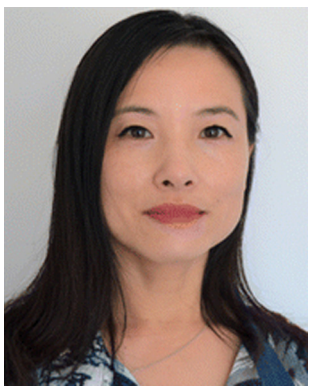

Dongling Ma

Prof. Dongling Ma holds the Canada Research Chair in Advanced Functional Nanocomposites and serves as a full professor at the Center of Energy, Materials and Telecommunications, INRS. She earned her PhD in materials science and engineering from Rensselaer Polytechnic Institute (USA) in 2004. From 2004 to 2006, she was awarded Natural Sciences and Engineering Research Council Visiting Fellowships and worked at the National Research Council of Canada. Her primary research focus is on developing various nanomaterials including semiconductor quantum dots, transition metal catalytic nanoparticles, and plasmonic nanostructures, as well as different types of nanohybrids for applications in the energy, catalysis, and biomedical sectors.

Jinguang Hu

Prof. Jinguang Hu is an Associate Professor and Schulich Research Chair at the University of Calgary. His current research focuses on biomass valorization, sustainable energy and bioinspired materials/systems for Energy, Environmental and Biomedical application. He has received the Chemical Institute of Canada's Bao and Zhu Innovation Award, presented annually to a single early-career researcher across Canada for distinguished contributions to chemical engineering; the Schulich Early Research Excellence Award; and the S.C. Trindade Award. He is an External Advisory Board member of the Canada Biomass Energy Network, a member of the "China-Canada Joint Centre for BioEnergy", a Research Fellow of Grizzly Bear Institute of Canada (GBIC), and serves on the editorial boards of several journals.

Open Access Article. Published on 24 January 2025. Downloaded on 11/7/2025 6:47:57 AM.
This article is licensed under a Creative Commons Attribution 3.0 Unported Licence.

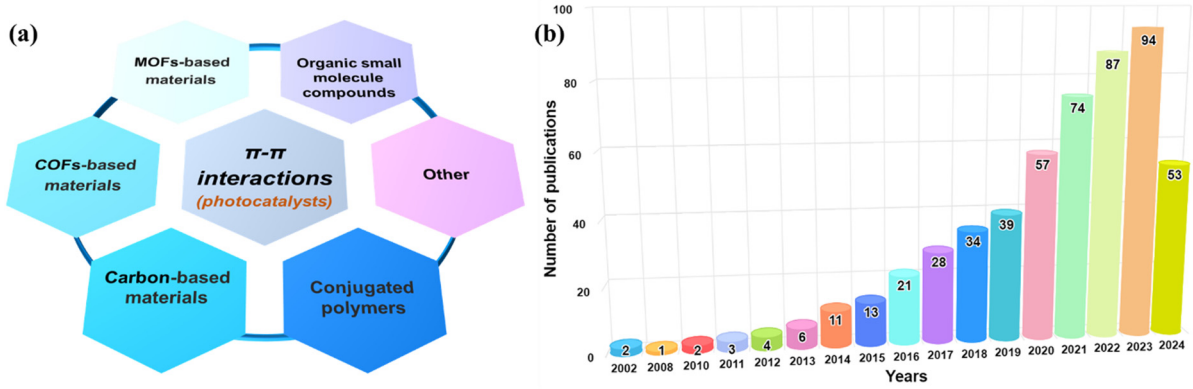

Fig. 1 (a) Photocatalysts involving π–π interactions. (b) Yearly publications on π–π interactions (including the catalyst itself, between different catalysts, and between the catalyst and the substrate) for photocatalytic applications based on keyword search of "π–π" and "photocata*" in the Web of Science (as of September 1, 2024).

different types of photocatalytic materials with π–π interactions and the influences of π–π interactions on their photocatalytic performance. Further, we discuss the modification strategies of π–π interactions to improve the photocatalytic performance and their applications and advantages in various photocatalytic reactions. Lastly, the challenges of π–π interactions in photocatalytic systems and the potential for subsequent development are discussed.

2. Characteristics of π–π interactions

2.1. Definition and geometric configurations of π–π interactions

In recent years, noncovalent interactions (π–π interactions, hydrogen bonds, van der Waals forces, ionic interactions, *etc.*) have attracted widespread attention, particularly in chemistry, biology, and materials sciences.[45] Specifically, the noncovalent interactions enhance the adsorption capacity, durability and activity of the catalyst by enhancing the interaction between the reactant and the catalyst, while affecting the adsorption configuration of the reactant, optimizing the stability of the catalyst, and enhancing the catalytic efficiency and selectivity.[46] Among them, π–π interactions mainly caused by intermolecular orbital overlap are most prominent in aromatic systems. They exist mainly between benzene rings, and their energy magnitudes range from about 1 to 50 kJ mol^{-1}, with the majority around and below 10 kJ mol^{-1}.[39] Their magnitude and direction depend on the intermolecular distances and their dihedral angles. Based on the electrostatic interaction of σ backbone and π electrons, Christoph Janiak's research proposed that the two aromatic ring planar spacings around 3.3 Å constitute a strong π–π interaction, while 3.6–3.8 Å is a weak interaction.[47] In addition, the common π–π interactions are divided into four types, as shown in Fig. 2:[39,48,49] (a) T-shaped stacking (two

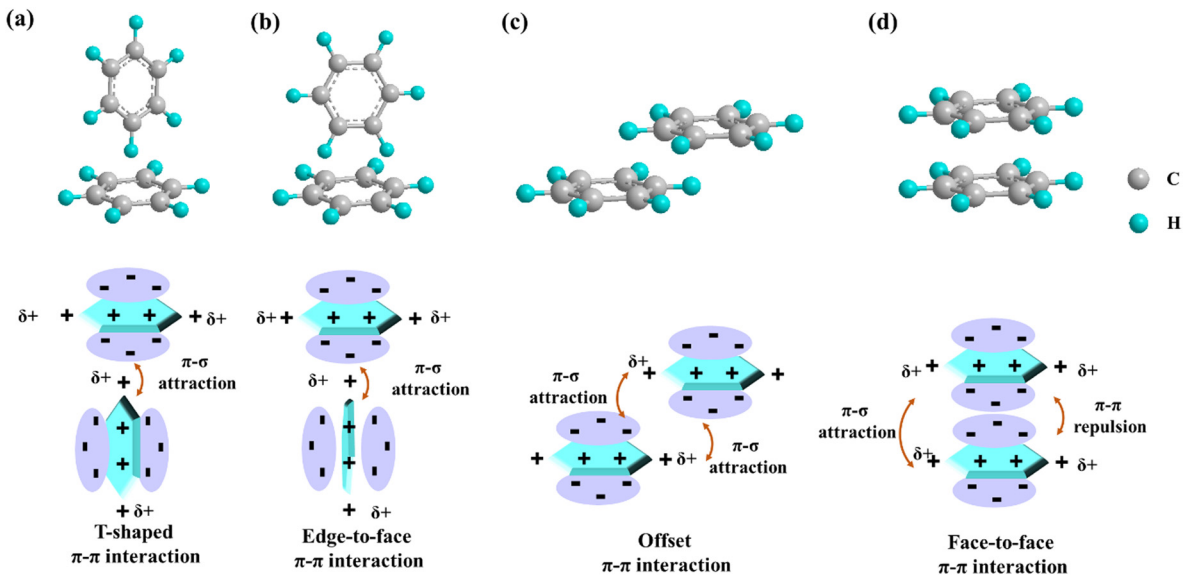

Fig. 2 Schematic of different geometries of interactions between aromatic rings and their corresponding electrostatic interaction diagrams (taking benzene rings as an example): (a) T-shaped, (b) edge-to-face, (c) offset and (d) face-to-face.

Open Access Article. Published on 24 January 2025. Downloaded on 11/7/2025 6:47:57 AM.
This article is licensed under a Creative Commons Attribution 3.0 Unported Licence.

aromatic systems are perpendicular to each other, with the point of the aromatic ring opposite to the face of the other aromatic ring); (b) edge-to-face stacking (the two aromatic systems are perpendicular to each other, with the side of the aromatic ring facing the face of the other aromatic ring); (c) offset face-to-face stacking (the two aromatic structures are essentially parallel, but there is a mismatch); and (d) face-to-face stacking (the two aromatic structures are basically parallel, with no dislocation and perpendicular to each other).

Furthermore, the strength and physicochemical characteristics of π–π interactions are influenced by the molecular structure and geometric arrangement, size and shape of π-electron clouds, molecular spacing, environmental conditions, molecular aromaticity, and multifarious substituents.[39,41,48,50] For effective π–π interactions, the spatial arrangement and geometry of molecules must allow for optimal overlap of π-electron clouds, forming stable interactions. Generally, larger π-electron clouds result in stronger interactions due to their increased overlap and attraction capabilities. In addition, the

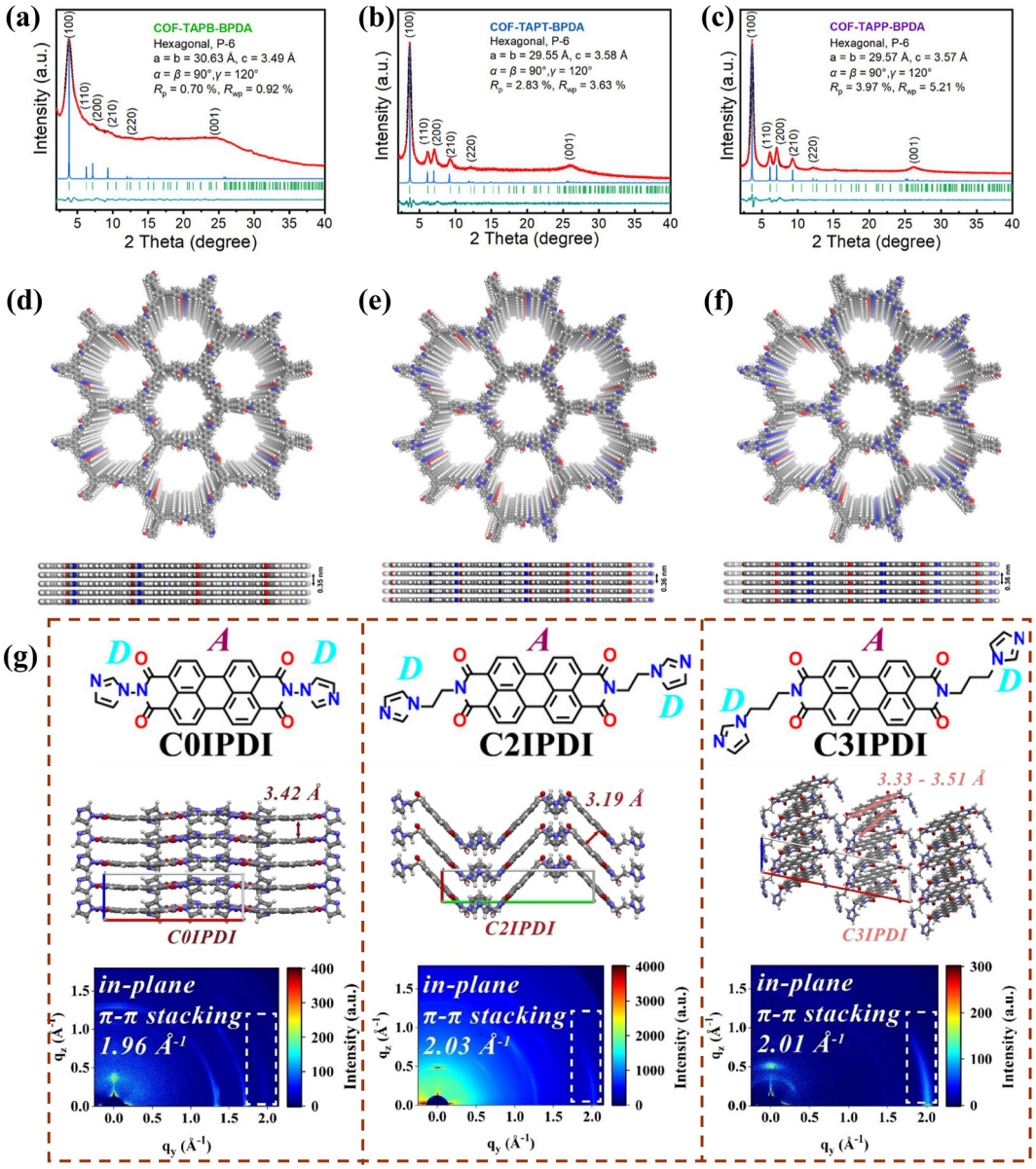

Fig. 3 (a)–(c) PXRD patterns of several different COF materials, where the experimental results are indicated in red lines, the refined profiles are in black, the computationally simulated patterns are in blue (indicating the overlap (AA) stacking mode), the Bragg position in green color, and the difference between the experimental and refined PXRD patterns in dark cyan color. ((d)–(f) Top and side views corresponding to the above three structures showing perfect overlapping (AA) structures (red, gray, white, and blue spheres) representing O, C, H, and N atoms, respectively). ((a)–(f) Reproduced from ref. 54 with permission from the American Chemistry Society, Copyright 2023). (g) Molecular structural formulae of the three modified PDI materials and their corresponding grazing-incidence wide-angle X-ray scattering (GIWAXS) 2D images of spin-coated protonated films. ((g) Reproduced from ref. 22 with permission from Wiley-VCH, Copyright 2023).

Open Access Article. Published on 24 January 2025. Downloaded on 11/7/2025 6:47:57 AM.
This article is licensed under a Creative Commons Attribution 3.0 Unported Licence.

interaction is more robust when the molecular spacing is approximately 3–4 Å, which facilitates optimal π-electron cloud overlap. Moreover, environmental conditions such as solvent polarity, solubility, temperature, and pressure can significantly affect the formation and stability of π–π interactions. Non-polar solvents and lower temperatures are typically favorable for forming π–π interactions.[51–53] Additionally, both the molecule aromaticity and the electronic and steric effects of substituents play crucial roles in determining the strength of π–π interactions. These factors collectively determine the characteristics and potential applications of π–π interactions in the photocatalysis field.

2.2. Analytical methods for π–π interactions

The verification of π–π interactions can be accomplished through both theoretical calculations and experimental methods, with single-crystal X-ray diffraction standing out as an effective technique due to its direct and straightforward approach.[40] This method, when coupled with theoretical analysis, allows for the precise measurement of dihedral angles and intermolecular distances, which are critical for identifying the stacking modes of molecules within crystals. Through detailed examination of the diffraction data, not only can the strength of π–π interactions be assessed, but also different stacking arrangements, such as face-to-face or face-to-edge, can be distinguished.[39] Overall, single-crystal X-ray diffraction serves as a valuable tool in gaining a comprehensive understanding of π–π stacking interactions and their characteristics. For example, Yang *et al.* synthesized three COFs with varying structures (COF-TAPB-BPDA, TAPB: 1,3,5-tris(4-aminophenyl)benzene; BPDA: 4,4′,4″-(benzene-1,3,5-triyltris-(ethyne-2,1-diyl))tris(2-hydroxybenzaldehyde); COF-TAPT-BPDA, TAPT: 1,3,5-tris(4-aminophenyl)triazine; COF-TAPP-BPDA, TAPP: 5,5′,5″-(1,3,5-triazine-2,4,6-triyl) tris(pyridin-2-amine)) and characterized their crystal structures through powder X-ray diffraction (PXRD) analysis and theoretical simulations.[54] The broad (001) diffraction peak of COF-TAPB-BPDA at 24.78° suggests a typical interlayer π–π stacking distance of less than 3.5 Å, indicative of strong π–π interactions. In contrast, the sharper (001) diffraction peaks of COF-TAPT-BPDA and COF-TAPP-BPDA at 25.96° reflect their higher crystallinity and relatively weak π–π interactions (Fig. 3a–c). Additionally, using the Forcite module of Materials Studio software, they simulated and optimized the stacking modes of these COFs. The experimental PXRD patterns closely matched the simulated ones, confirming that the stacking distance in COF-TAPB-BPDA is smaller than that in the other two COFs (Fig. 3d–f). In addition, the π–π interaction stacking pattern can likewise be determined by a grazing-incidence wide-angle X-ray scattering (GIWAXS) characterization method. Liu *et al.* explored three molecular structures (C0IPDI, C2IPDI, and C3IPDI) using perylene diimide (PDI) as the building unit, focusing on the effects of varying alkyl chain lengths between imidazole (IMZ) and PDI on molecular and π–π stacking (Fig. 3g).[22] GIWAXS images revealed clear π–π stacking in the protonated thin films. The study concentrated on the structure–activity relationship concerning π–π stacking interactions. Directly connected IMZ and PDI resulted in a π–π stacking distance of 3.42 Å; introducing an ethyl group reduced this distance to 3.19 Å, leading to herringbone stacking in C2IPDI, which enhances charge transport. The insertion of an *n*-propyl group in C3IPDI led to non-parallel molecular alignment, with π–π stacking distances ranging from 3.33 to 3.51 Å, and a zigzag stacking pattern where the IMZ and PDI are further apart. The study concluded that variations in the σ-bond length effectively regulate the molecular stacking patterns and π–π stacking distances in CnIPDI molecules. Furthermore, ultraviolet photoelectron spectroscopy (UV) and fluorescence spectrophotometry are two methods for detecting molecular π–π interactions.[39,55,56] The conjugation effect causes a red shift in the UV spectrum because the conjugated system has a lower transition energy, which shifts the absorption peak to a longer wavelength.[57,58] The positive ion stacking of planar molecules promotes molecular aggregation. In fluorescence spectrophotometry, the energy transfer caused by molecular stacking leads to fluorescence quenching, reducing the fluorescence intensity.[59–61] Overall, with the eventual development of more advanced spectroscopy, it is expected that more characterization methods will emerge that can clearly reveal π–π interactions in materials.

3. Conjugated (or aromatic) photocatalytic materials with π–π interactions

To date, various organic photocatalytic materials with π–π interactions have been developed (Fig. 4), such as organic framework materials (COFs and MOFs), π-conjugated organic small molecules (PDI, phthalocyanines, porphyrins, and complexes), polymers (carbon nitride and others) and carbon-based materials (graphenes, graphene oxides, carbon nanotubes, graphite, graphdiyne, biochar, *etc.*). As mentioned above, ideal photocatalysts need to have strong visible light absorption, high carrier separation efficiency, high stability, large specific surface area, and tunable structure. First, dye molecules (phthalocyanines, porphyrins, *etc.*) appeared in the spotlight because of their good absorption and π-structures. Traditional polymeric materials with π-structures (polyaniline, polypyrrole, *etc.*) were also used in photocatalysis because of their good conductivity and light absorption. Afterwards, carbon materials are widely utilized in photocatalytic systems due to their robust sp^2 lattice structure, extensive conjugated systems, excellent physicochemical stability, and strong adsorption capacity. Since 2012, traditional MOF-based framework materials have also been utilized, primarily owing to their intricate pore structures and the high capacity for ligand modulation. Following this, g-C_3N_4 and PDI, because of their unique structures, have attracted attention; their ability to readily create an internal electric field and excellent visible-light responsiveness has gained growing interest. In recent years, the ongoing achievements in computational chemistry, spectroscopic methods, and synthetic techniques have steered researchers' interest towards organic frameworks, including new π-conjugated

Open Access Article. Published on 24 January 2025. Downloaded on 11/7/2025 6:47:57 AM.
This article is licensed under a Creative Commons Attribution 3.0 Unported Licence.

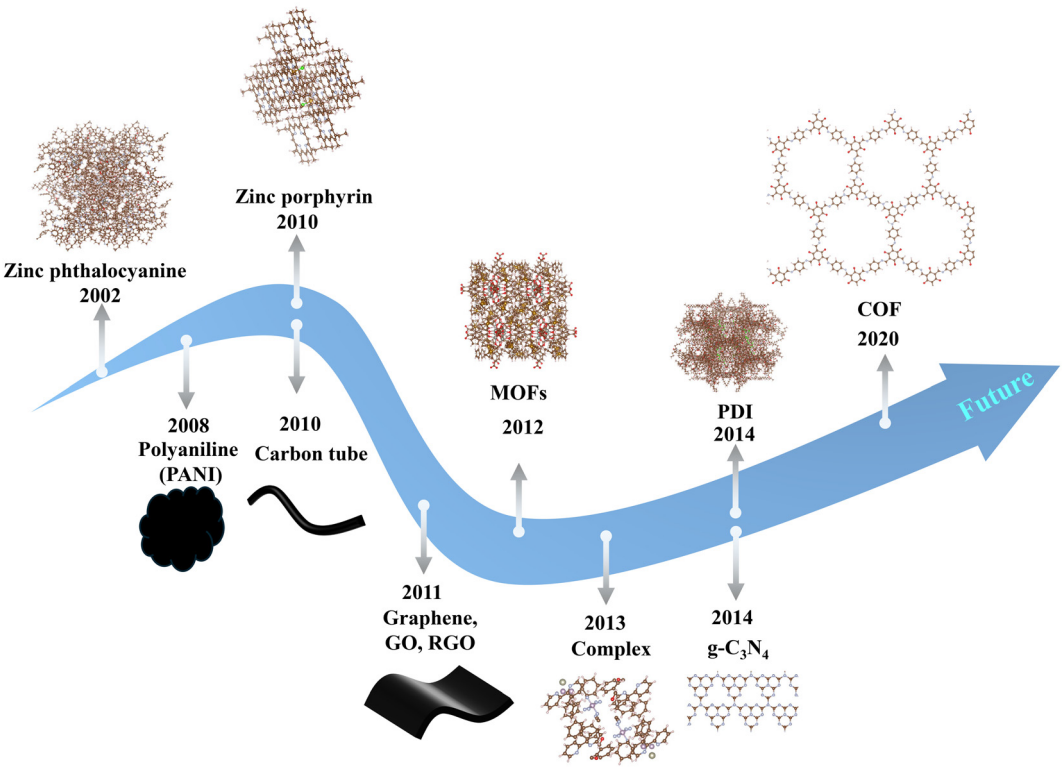

Fig. 4 Development history of materials with π–π interactions used in photocatalysis.

polymer materials, COFs, and innovative MOFs. This interest stems from their abundant, regularly arranged pores and easily modified structures. Throughout the evolutionary journey of photocatalysts that leverage π–π interactions, there has been a transition from simpler to more complex structures. This progression has been accompanied by increased structural tunability and designability, which facilitates the construction of active sites and charge separation, the fine-tuning of microenvironments, and the optimization of catalysts. Here, we focus on four widely used classes of materials: organic framework materials, organic conjugated small molecules, conjugated polymers, and carbon materials. Leveraging their distinct structural attributes, our ultimate goal is to provide a guideline for designing and fabricating high-performance, ideal photocatalysts that capitalize on π–π interactions. These photocatalysts will be characterized by their tunable absorption and emission spectra, elevated extinction coefficients, superior charge-transport capabilities, facile modifiability, and durability. Such features render them compelling and cutting-edge materials for a broad spectrum of photocatalytic applications. Additionally, Fig. 5 illustrates the distribution of materials featuring π–π interactions within the field of photocatalysis.

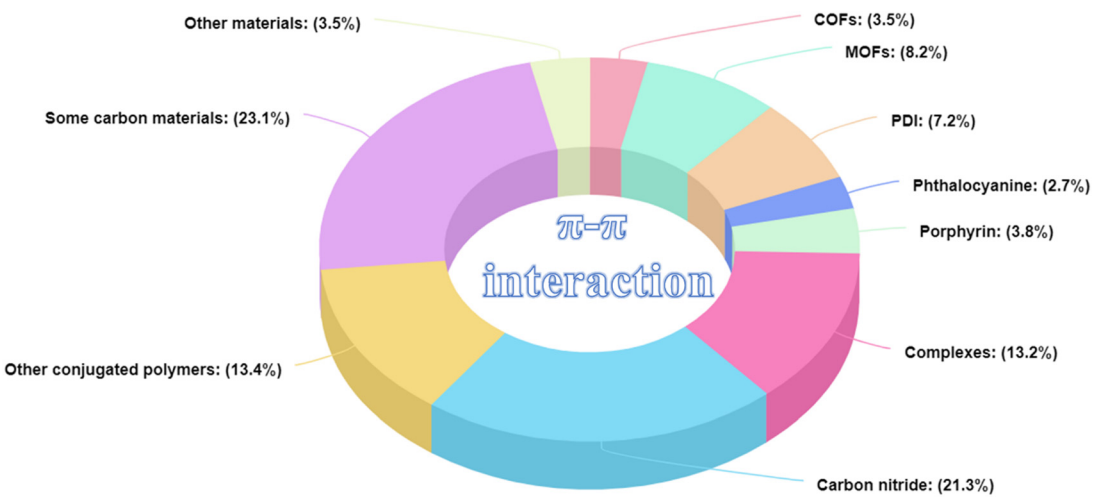

Fig. 5 Proportional distribution of various photocatalytic materials capable of forming π–π interactions.

Open Access Article. Published on 24 January 2025. Downloaded on 11/7/2025 6:47:57 AM.
This article is licensed under a Creative Commons Attribution 3.0 Unported Licence.

Conjugated polymers, carbon materials, organic framework materials, and small organic conjugated molecules represent the principal materials utilized in photocatalytic applications. Other materials featuring π–π interactions require further exploration and development to enhance their potential in photocatalysis.

3.1. Organic framework materials

3.1.1 Covalent organic frameworks (COFs). COFs are highly crystalline organic polymers formed by specific organic units linked by covalent bonds (*e.g.*, cyclic boroxanes, imines, hydrazines, boronic esters, acridines, or ketene amines), which can be constructed as two- or three-dimensional structures.[62] COFs exhibit high thermal and chemical stability, extensive porosity, and large surface areas.[62,63] Additionally, their π-conjugated structures and π–π stacked layers enhance their ability to absorb a broad range of visible light and facilitate efficient charge separation.[62,64,65] At present, the research on COF materials is primarily focused on two-dimensional structures. These two-dimensional COFs are structured and crystallized *via* interlayer π–π stacking interactions within a planar network created by rigid building units.[66,67] The synthesis of these two-dimensional COFs involves using building blocks with varying symmetries and molecular sizes to create monolayers of diverse macrocyclic shapes and sizes.[68,69] These molecular layers stack parallel to each other, guided by the principle of maximum π orbital overlap.[66] This involves the overlap of interlayer π–π electron clouds and conjugated connections within each layer, which facilitates a periodic distribution of pores and supports rapid carrier migration within the framework.[66] Additionally, the stability of two-dimensional COFs is enhanced by a combination of intralayer covalent bonds and interlayer non-covalent forces such as π–π interactions, hydrogen bonds, and van der Waals forces.[70] By adjusting the molecular structure and optoelectronic properties of two-dimensional COFs, the π–π interactions are enhanced, and structurally functionalized photocatalysts with customized properties can be developed.[71,72] This is primarily because π–π interactions influence several properties of COFs, such as charge transport properties, structural stability, crystallinity, morphology, adsorption capacity, and reaction selectivity.[73–76] These effects can enhance the performance of COF-based photocatalysts. Consequently, researchers can effectively design and fine-tune the π–π interactions within COFs to optimize their specific photocatalytic performance by selecting appropriate building blocks, functional groups, and synthetic conditions. Among the many above-mentioned COF structures, imine COFs have become the most widely used COF materials due to their ultra-high specific surface area, nano-sized pores, high porosity and excellent physical and chemical stability.[77] For example, Li *et al.* created a novel imine COF material through a solvothermal method and combined it with membrane PVDF for photocatalytic organic synthesis reactions.[78] Fig. 6a demonstrates the combination of a charge acceptor (naphthalene diimide (NDI)) and a charge donor (tetrakis(4-formylphenyl)pyrene (TFPPy)) constructed as DTF-ANDI-COF by Schiff base condensation. It is also demonstrated that DTF-ANDI-COF is a typical D–A-COF structure, which is a molecular structure with obvious H-kin and strong π–π interactions. Subsequently, they designed membrane-modulated catalysis to extend the existing catalytic advantages of stabilized DTF-ANDI-COF. The reaction performance of DTF-ANDI-COF/PVDF membranes selectively promoting amine-coupled catalysis, and from the results, the yields of the products of amine-coupled DTF-ANDI-COF/PVDF were all above 90%, which was mainly owing to the substantial π–π interactions formed within the structure of DTF-ANDI-COF constructing the charge transfer dynamics and the reactive oxygen radical's generation.

3.1.2. Metal–organic frameworks (MOFs). Unlike COF-based photocatalysts, MOFs represent a distinct class of nanoporous inorganic–organic hybrid materials.[80] These are formed from inorganic metal ions or clusters interconnected by organic ligands, available in one-dimensional, two-dimensional, or three-dimensional topological structures.[80–82] Among these, three-dimensional MOF materials are particularly valued in practical applications due to their versatile and porous nature.[83] This is mainly because the spatial 3D network formed by this type of material has the characteristics of high specific surface area, various structures, tunable pore shape and size, and modifiable pore surface.[83–85] By varying the structural units and synthesis methods, it is possible to tailor the functional groups, pore dimensions, and overall size of the MOFs to specific needs.[83] Furthermore, MOFs enhance the flexibility and practicality through assorted weak interactions (π–π stacking, electrostatics, hydrogen bonding, *etc.*) and coordination bonds.[86] Among them, the interaction formed by π–π stacking has received extensive attention. The conductivity and charge transfer efficiency of MOFs are enhanced by regulating the π–π stacking distance between electron-rich organic linkers (commonly using various planar aromatic cores such as naphthalene, pyrazine, naphthalene diimide, triphenylene, anthracene, and tetrathiafulvalene).[86] Moreover, π–π stacking not only alters MOFs' structural features such as porosity and packing density but also creates a continuous pathway for efficient charge transfer.[86] By selecting ligands with specific aromatic or conjugated structures and optimizing synthesis conditions, researchers can effectively control and design π–π interactions in MOFs, paving the way for substantial enhancements in photocatalytic performance. Zeolitic imidazolate framework-8 (ZIF-8) is a widely reported MOF composed of 2-methylimidazole and Zn, showcasing the inherent structural benefits of MOFs along with enhanced thermochemical stability.[87] Unlike many other MOFs, ZIF-8 is not only straightforward to synthesize but also retains its crystallinity and porosity after exposure to various solutions and remains stable up to 500 °C. Its surface active sites and effective charge separation attributes confer outstanding adsorption capacities and significant photocatalytic potential.[87] Furthermore, the π–π stacking interactions between the imidazole rings in ZIF-8 and aromatic ring-containing substances serve to further augment its photocatalytic capabilities.[88–90] Shi *et al.* constructed a complex

Open Access Article. Published on 24 January 2025. Downloaded on 11/7/2025 6:47:57 AM.
This article is licensed under a Creative Commons Attribution 3.0 Unported Licence.

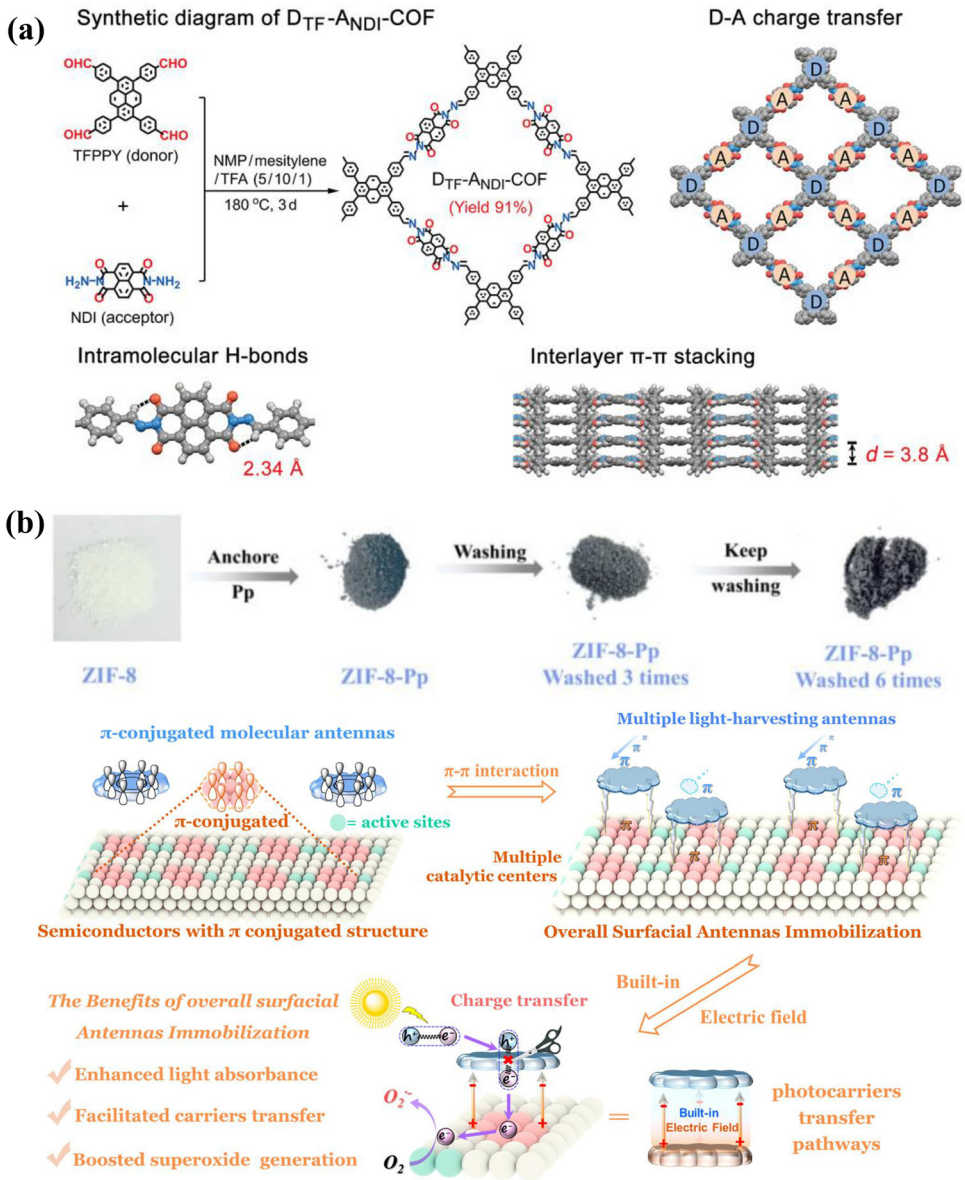

Fig. 6 (a) Preparation route of the novel COF and its structural features. ((a) Reproduced from ref. 78 with permission from Wiley-VCH, Copyright 2023). (b) Physical roadmap for the preparation of ZIF-8-Pp and the schematic of the large-scale and extensive built-in electric field that will be formed between the two through π–π interaction and the corresponding effect manifestation. ((b) Reproduced from ref. 79 with permission from the American Chemistry Society, Copyright 2022).

of porphyrin and ZIF-8 (ZIF-8-Pp) for the photolysis of organic pollutants and transformation of organic molecules by self-assembly.[79] Fig. 6b demonstrates the assembly process of ZIF-8 and 5,10,15,20-tetrakis(4-pyridyl)porphyrin (Pp), which is mainly owing to the substantial π–π interactions between Pp and ZIF-8, which results in a substantial built-in electric field's constitution, and ultimately, enhanced light absorption (antennae effect of porphyrin), efficient charge migration and high concentration of reactive oxygen radicals. As a result, the ZIF-8-Pp can efficiently convert phenylboronic acid and its congeners to the corresponding phenolics with yields of around 70%, and the study of the reaction process reveals that the photocarriers in Pp are excited under visible light, and then migrate to multiple metal nodes in ZIF-8 to form superoxide radicals, and the photogenerated holes resting on the Pp molecule oxidize the triethylamine molecule (TEA) on the Pp molecule to form TEA^+, which subsequently generates intermediates that are hydrolyzed to give the final phenol product. The above-mentioned results show that the substantial π–π interaction between Pp and ZIF-8 creates a built-in electric field that strongly pushes photocarrier migration, ultimately promoting the efficient utilization of solar energy.

3.1.3. Hydrogen-bonded organic frameworks (HOFs). Hydrogen-bonded organic frames (HOFs), a new type of porous material, are assembled by the non-covalent interaction of

Open Access Article. Published on 24 January 2025. Downloaded on 11/7/2025 6:47:57 AM.
This article is licensed under a Creative Commons Attribution 3.0 Unported Licence.

organic and organometallic components, and have the characteristics of easy synthesis, high crystallinity, low density, good biocompatibility and high flexibility.[91–95] The self-healing properties of HOFs help reduce damage, extend service life, and enhance stability through hydrogen bonding and π–π interactions.[94] Their metal-free composition, renewability and recyclability make them environmentally friendly and economic.[93] The versatility and designability of HOFs make them excellent candidates in photoelectric applications, and their hydrogen bonding properties make them superior to COFs and MOFs in solution processability and crystallinity.[94] Similar to COFs and MOFs, the high crystallinity network of HOFs facilitates electron transport and light utilization efficiency, and its conjugated structure and π–π packing interaction promote charge transfer, regulating energy levels to achieve efficient light absorption and utilization.[94] The sp^2-π conjugated connection of HOFs enhances π electron delocalization, promotes photoexcited carrier transfer, and expands the range of light absorption.[94,96] Currently, HOF-based photocatalysts have attracted increasingly more attention due to their excellent catalytic performance. One interesting HOF example is biohydrogen bond organic framework (HOF-25), which is derived from 2,2′-bipyridine (bpy) and uses a G-quadruplex as a rigid hydrogen bond backbone to further consolidate the hydrogen bond assembly by π–π stacking, and exhibits permanent porosity by co-stabilizing the G-quadruplex and the π–π interaction between layers. After post-modifying it with rhenium (Re) sites, which serve as the active center of photocatalysis, Yu *et al.* achieved a high visible light-driven carbon dioxide (CO_2) reduction efficiency of 1448 mmol g^{-1} h^{-1} with a CO selectivity of 93%.[97] The photocatalytic mechanism involves the transfer of electrons of the excited $[Ru(bpy)_3]Cl_2 \cdot 6H_2O$ photosensitizer to HOF-25-Re, triggering the photocatalytic reaction. This study not only provides a new strategy for constructing stable HOFs, but also offers new insights for heterogenizing molecular catalysts to achieve CO_2 photoreduction, opening up a new way to engineer functional HOFs.

3.2. Organic small-molecule compounds

3.2.1. Perylene imides (PDIs). The PDI molecules are the best-known n-type organic semiconductors composed of a planar perylene ring and the lactam units at two ends, and it has two main modification sites, including both end units called "imide positions" and "bay positions" at the middle of the perylene ring, which boosts diversity of PDI derivatives.[98] Excitingly, the conjugated π-electron system in the PDI molecule based on the formation between its planar (planar bicyclic structure with alternating single and double bonds) and aromatic structures (stilbene nuclei) allows for π–π stacking interactions between PDI units.[99–107] Because of excellent fluorescence quantum yields, excellent photochemical stability, and enhanced donor–acceptor property, the PDI-based materials in organic photocatalytic field have shown great progress through functionalizing a PDI molecular structure, functionalizing the PDI surface with anchoring groups that can bind with semiconductor metal oxides or $-NH_2$ terminal groups of graphitic carbon nitride (g-C_3N_4), and constructing self-assembled supramolecular architectures.[108–114] Among these strategies, π–π interactions play an important role in forming a supramolecular structure with a π–π stacking spacing of 3.4–3.5 Å.[115] In addition, the π–π stacking patterns in single PDI supramolecules can be mainly divided into H-aggregate (face-to-face arrangement) and J-aggregate (head-to-tail stacking).[116] The former exhibits the compact co-facial stacking structure and strong π–π stacking degree, and these features not only result in blue-shifted absorption and obvious photofluorescence quenching, but also promote rapid electron transfer to form superoxide radicals ($^{\bullet}O_2^-$) and holes. Differently, the J-aggregate of the perylene core structure with partial dislocation shows a lower π–π stacking degree, retaining the photoelectric property similar to that of a single PDI molecule. It not only causes red-shifted absorption and no distinct fluorescence quenching, but also facilitates energy transfer from the excited singlet state to the excited triplet state *via* intersystem crossing, ultimately generating singlet oxygen species ($^1O_2$). Clearly, the H-aggregate PDI supermolecules display more potential in the photocatalysis field because of more excellent mobility and separation capacity of photogenerated carriers, and deeper valence bands.[117,118]

In the self-assembling process of pure PDI supermolecules, the π–π stacking interactions are affected by side chains or substituents of monomer PDI. For instance, Li *et al.* found that the amide-modified PDI molecules formed self-assembled supramolecular (sAmi-PDI-HCl) nanofibers with high H-mode π–π interactions and hydrogen-bond networks that are beneficial for photogenerated charge carrier transport, finally enhancing organic pollutants' photodegradation.[119] Kong *et al.* further introduced a strong electron-withdrawing phosphate unit into two terminal positions of PDI, obtaining a multilayer P-PMPDI supramolecular nanobelt with the improved regularity of coplanar π–π interaction and strong dipole moment. Therefore, the resulting P-PMPDI provided a fast channel for the charge carrier separation and migration, resulting in high photocatalytic hydrogen evolution.[120] Additionally, the PDI supramolecules' π–π interactions further promoted their combination with other π-conjugated organic materials to build up extended π–π composites. For example, because of the π-conjugated structure in PTCDI and 7,7,8,8-tetracyanoquinodimethane (TCNQ), their self-assembling *via* π–π stacking successfully led to the formation of TCNQ-PTCDI co-catalysts under acid-based conditions. The formed strong electronic coupling and larger π-electron delocalization caused through the extended π–π stacking facilitate carrier transport and decrease carrier recombination, obviously promoting the photodegradation activity of phenol compared with the pure PTCDI.[121] Sun *et al.* synthesized various supramolecular structures by substituting the terminal groups of PDI with different organic acids (6-aminonicotinic acid (NA), benzoic acid (BA), and propionic acid (PA)).[122] Among these, the PDI conjugated with NA formed a biplanar π–π conjugated porous supramolecular photocatalyst (hp-PDI-NA). As depicted in the π–π stacking schematic of Fig. 7a, hp-PDI-PA did not form a biplane

Open Access Article. Published on 24 January 2025. Downloaded on 11/7/2025 6:47:57 AM.
This article is licensed under a Creative Commons Attribution 3.0 Unported Licence.

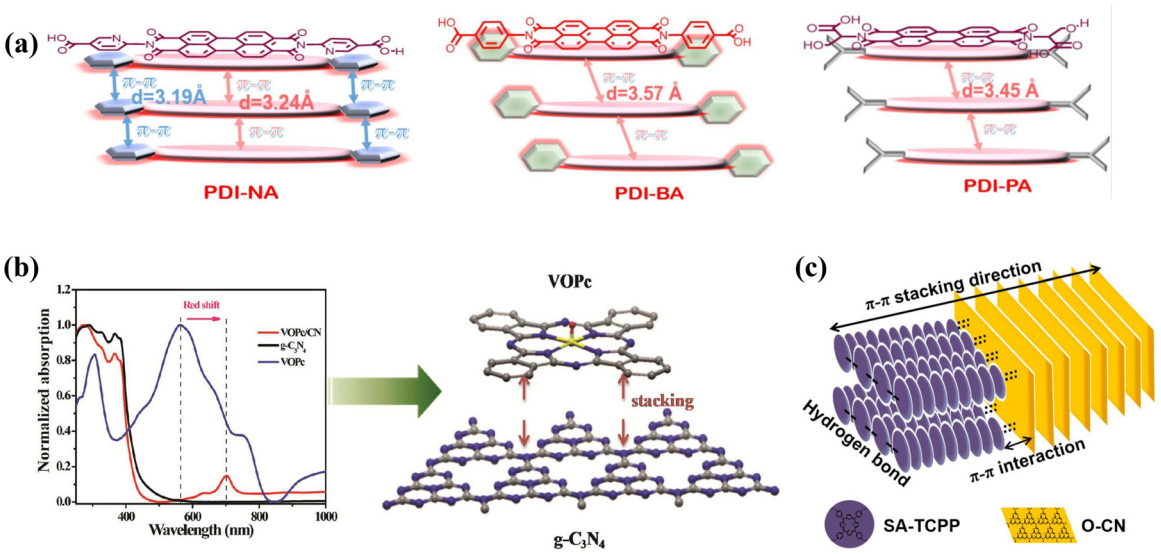

Fig. 7 (a) Schematic of PDI-BA, PDI-PA and PDI-NA. ((a) Reproduced from ref. 122 with permission from Elsevier, Copyright 2022). (b) UV-Vis absorption spectrum of VOPc/CN photocatalysts and molecular flat model of the π–π interactions formed between them. ((b) Reproduced from ref. 124 with permission from Elsevier, Copyright 2019). (c) π–π stacking structure between O-CN and SA-TCPP. ((c) Reproduced from ref. 125 with permission from Elsevier, Copyright 2021).

structure due to the absence of π-orbitals in its short alkyl terminal chains. Similarly, hp-PDI-BA also failed to form a biplane structure despite having a benzene ring at the terminal position. In contrast, hp-PDI-NA achieved double π–π conjugation through its biplanar structure (the primary plane of the PDI molecule and the nicotinic plane of the aminonicotinic acid), which enhances the π–π interactions and shortens the interlayer spacing, thus facilitating the photogenerated carriers' transport and separation. The study reveals that hp-PDI-NA exhibits photocatalytic phenol removal activity that is 3.5 times more excellent than that of standard PDI nanoparticles underneath visible light, along with excellent pollutant mineralization capabilities. This research highlights a novel approach to designing efficient PDI-based supramolecular photocatalysts through strategic end-group substitution and morphological control. Additionally, different drying strategies can also impact π–π interactions. Freeze-drying, in particular, helps preserve the π–π stacking within the PDI structure, which subsequently influences its photocatalytic performance.[123] In a word, the π–π stacking interaction not only plays an important role to form self-assembled PDI supramolecules with different shapes (such as nanofiber and nanobelt) but can also be used as an efficient strategy to get composite photocatalysts with other π-conjugated materials, which finally improve the PDI-based photocatalyst performance.

3.2.2. Phthalocyanine. Phthalocyanine is a planar cyclic tetrapyrrole compound characterized by π-electron delocalization and an 18-π conjugated network, offering exceptional optical and electrochemical properties.[124,126] This includes strong absorption in the Q band between 600 and 800 nm, which imparts a deep blue color.[124] Phthalocyanine molecules engage in π–π stacking with π-electron conjugated materials, enhancing the photocatalytic processes.[124,127] Metal phthalocyanines, which are derivatives formed by substituting the central hydrogen with metal ions (such as Zn, Fe, Cu *etc.*), extend absorption into the near-infrared spectrum, boosting the photosensitization effect and photocatalytic performance.[28,99,124,128–130] Additionally, their π–π conjugation with π-electron-rich materials enhances molecular attraction, improving photocatalytic efficiency.[28,128] Liu *et al.* examined the photocatalytic H_2 production performance of vanadium phthalocyanine oxynitride-modified carbon nitride (VOPc/CN).[124] As illustrated in Fig. 7b, VOPc/CN demonstrates significantly higher light absorption in the visible spectrum compared to g-C_3N_4, with VOPc exhibiting a noticeable red shift within the VOPc/CN composite, indicating π–π stacking interactions between VOPc and g-C_3N_4. The 4 wt%-VOPc/CN system displayed a hydrogen production efficiency six times more wonderful than that of g-C_3N_4 alone. This enhancement is imputed primarily to the π–π interactions between VOPc and g-C_3N_4, which facilitate charge separation and enhance the efficiency of photocatalytic hydrogen evolution.

3.2.3. Porphyrin. Porphyrin is a tetrapyrrole macromolecule with an 18π electron conjugation system, consisting of four pyrrole units connected by sp^2 hybridized carbon bridges to form a planar square structure, which is widely used in the fields of catalysts, photosynthesis, phototherapy and sensors.[131–133] As organic semiconductors with large π-conjugated systems, porphyrins have unique photochemical and redox capabilities, and their optical properties and easily tunable characteristics make them important in the field of chemical materials.[134–137] They are excellent photocatalysts because of their selective absorption of visible light, and their self-assembly improves carrier mobility through π–π bonding, which further enhances photocatalytic performance.[136,137] In addition, planar layer materials with π-electron conjugation can

Open Access Article. Published on 24 January 2025. Downloaded on 11/7/2025 6:47:57 AM.
This article is licensed under a Creative Commons Attribution 3.0 Unported Licence.

be assembled with the porphyrin *via* π–π stacking interactions,[138–140] and the rigid planar surfaces of the porphyrin and abundant π-electrons can also enhance the adsorption of organic pollutants on the surface of the photocatalysts *via* π–π stacking interactions.[141] Further, the porphyrin's tetrapyrrole macrocyclic core is an idealistic binding site for metals and is easily functionalized by metallization.[132] During metallization, the porphyrin loses protons to form a double anionic ligand, and the residual nitrogen atoms are coordinated to the metal ions *via* a lone pair of electrons. The free-base porphyrin and metalloporphyrin units act as acceptors and influence the type of binding to the guest, where the free-base porphyrin binds the guest mainly through π–π interactions, while the metalloporphyrin forms a coordination bond with the guest through the metal center.[132] Compared to porphyrins, metallized porphyrins also have an 18π conjugated planar structure, which effectively absorbs long-wave visible light and exhibits excellent electron transport, and the metal active sites of metalloporphyrins help to reduce charge complexation and further enhance photocatalytic ability.[137] Xu *et al.* synthesized oxidized carbon nitride (O-CN) through thermal exfoliation and hydrothermal treatment, and combined it with porphyrin molecules *via* supramolecular self-assembly (TCPP) to create SA-TCPP/O-CN composites (Fig. 7c). SA-TCPP/O-CN-40% composites showed enhanced degradation capabilities for organic pollutants, with phenol degradation rates 2.5 times and 3.1 times more excellent than SA-TCPP and O-CN, respectively. Oxygen production rates for the SA-TCPP/O-CN-40% composite were 2.7 times and 4.7 times more excellent than that of SA-TCPP and O-CN, respectively, and the sterilization efficiency increased significantly to 62.5%, surpassing both SA-TCPP and O-CN. These improvements are attributed to the 0D/2D heterostructure formed *via* π–π interactions between SA-TCPP and O-CN, which generate built-in electric fields and electron departure domain effects. These enhancements promote interfacial charge transfer and the generation of a large amount of reactive oxygen radicals, thereby improving the photocatalytic performance.[125]

3.2.4. Complexes. Complex is a type of compound formed by a central atom or ion and a molecule or ion (ligand) containing a lone pair of electrons through a coordination bond. The π–π interaction within a complex is a crucial determinant of its internal chemical structure, material stability, morphology, and functionality.[142–145] It modifies the photophysical properties by adjusting the rotational conformations of aromatic ligands.[142] This interaction enables the transition from zero-dimensional to one-dimensional,[143] one-dimensional to two-dimensional,[143,146] two-dimensional to three-dimensional,[147] and directly from one-dimensional to three-dimensional,[148] forming a versatile supramolecular network. In addition to the inherent changes within complexes, π–π interactions also occur between π-conjugated complexes and other π-conjugated complexes, reaction substrates and semiconductor materials.[149–156] These interactions facilitate charge migration and transmission, thereby enhancing photocatalytic performance.[149–156] Zhang *et al.* constructed mononuclear Zn(II) molecular complex-coupled co-catalysts for CO_2 photoreduction, in which the introduction of $CoCl_2$ was the most effective, and the CO generation rate was as high as 494.4 μmol g^{-1} h^{-1} (100% selectivity), which was mainly attributed to the fact that the catalytic capacity could be extremely boosted by the ordered heterogeneousness of mononuclear Zn(II) molecular complexes *via* π–π stacking (Fig. 8a).[149] Qiu *et al.* constructed Re[4,4′-di(pyren-1-yl)-2,2′-bipyridine](CO)$_3$Cl (4,4′-dipyrenyl-Re) catalysts with bifunctional photosensitizer pyrenyl moiety (photosensitized and π-structured) units, which can achieve efficient CO_2 reduction under visible light, and TON_{CO} can be as high as 1367 ± 32, which is mainly imputed to the π–π interactions originating from the pyrene moiety in the catalyst structure and the extension of the π-conjugated system remarkably improves the electron transport efficiency and visible light trapping ability (Fig. 8b).[150]

3.3. Conjugated polymers

3.3.1. Carbon nitride. To date, various types of carbon nitride materials including graphitic carbon nitride (g-C_3N_4), poly heptazine imide (PHI), poly triazine imide (PTI), and other synthetic polymeric carbon nitrides have been synthesized and employed across diverse research areas in photocatalysis.[157–161] Among them, g-C_3N_4 is widely favored due to its extensive applications, frequent research focus, and distinct optoelectronic properties.[162] It is composed of sp^2 hybridized carbon and nitrogen atoms that form a π-conjugated planar structure akin to graphene, notable for its high stability and non-toxicity.[162]

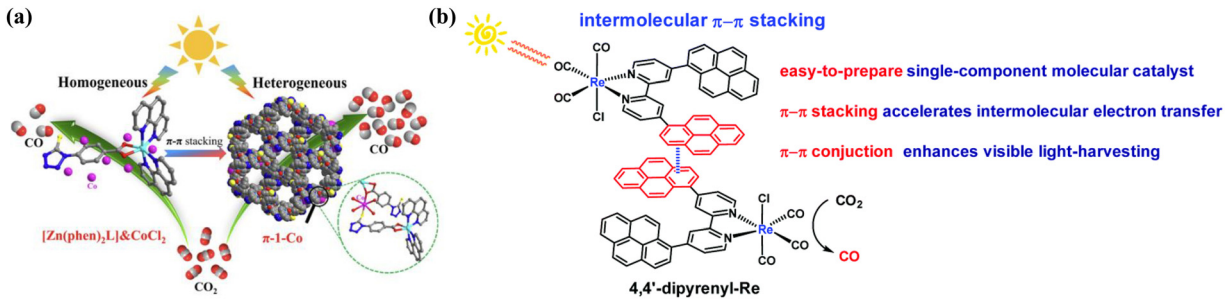

Fig. 8 (a) Schematic of CO_2 reduction based on heterogeneous (π-1) and homogeneous ([Zn(phen)2L]) photocatalysts. ((a) Reproduced from ref. 149 with permission from National Academies Press, Copyright 2022). (b) Design and mechanism of complex catalysts for the photoreduction of CO_2. ((b) Reproduced from ref. 150 with permission from Royal Society of Chemistry, Copyright 2020).

Open Access Article. Published on 24 January 2025. Downloaded on 11/7/2025 6:47:57 AM.
This article is licensed under a Creative Commons Attribution 3.0 Unported Licence.

The π–π conjugated bond structure within g-C_3N_4 provides active sites for catalytic reactions.[163] Furthermore, a π–π stacking structure is formed between the layers of g-C_3N_4 heptazine units (C_6N_7).[164,165] π–π stacking influences interlayer carrier transport and separation.[166] Additionally, g-C_3N_4 can be combined with various π-conjugated materials to create composites that enhance its photocatalytic performance.[167] The other two noteworthy materials, PHI and PTI, are nitrogen-containing polymers characterized by their cyclic nitrogen-containing heptazine and triazine units linked by imine bonds (–NH–).[161] This arrangement endows PHI and PTI with a rich π-electron system at the molecular level, facilitating π–π interactions due to their cyclic structures with extended π-electron systems.[161,168–170] Researchers can manipulate π–π interactions in carbon nitride materials by adjusting the materials' structure, layer stacking, or surface functionalization, thus leveraging their significant potential in photocatalysis. Tang *et al.* developed BCN/CN_x composite materials for the photoreduction of CO_2 by an ultrasonic self-assembly technology to combine two types of carbon nitride materials.[32] The process involves synthesizing boron-containing carbon nitride (BCN) and nitrogen-deficient ultrathin carbon nitride nanosheets (CN_x), and forming heterojunctions *via* π–π stacking interactions (Fig. 9a). The BCN/CN_x composite exhibits superior performance in converting CO_2 into CH_4, achieving higher yields than either BCN or CN_x alone, thanks to the strong π–π interactions and efficient electron transport within the composite structure. Xu *et al.* constructed a FePc/g-C_3N_4(CNFP)/H_2O_2 photo-Fenton system for the removal of oxytetracycline (OTC) by calcination.[171] The OTC removal rate of CNFP60 reached 88.48% at 1 h, which was significantly higher than that of g-C_3N_4 (41.30%), while the degradation rate of CNFP60 was 7.4 times more excellent than that of g-C_3N_4. The principal cause for the enhanced photocatalytic performance is the constitution of a fast electron transfer channel by the π–π interaction between FePc and g-C_3N_4, which realizes the rapid transfer of photogenerated electrons (Fig. 9b).

3.3.2. Other conjugated polymers. The π–π interactions in other conjugated polymers (traditional and novel) are influenced by their aromatic and conjugated nature. Traditional conjugated polymers such as polyaniline, polypyrrole, and polythiophene feature π–π conjugated structures within their polymer chains, facilitating the formation of π–π interactions.[172–178] These polymers are characterized by extensive π-conjugated skeletons, which impart high electrical conductivity, environmental stability, superior light absorption, and excellent carrier mobility, which contribute to better charge conversion during photocatalysis.[174–180] In addition to traditional conjugated polymers, new π-conjugated organic polymers have emerged as efficient visible light-driven photocatalysts. These materials exhibit a large specific surface area, adjustable structures, designable properties, low cost, and high stability.[135,181] Their π-delocalized systems respond effectively to sunlight, promoting charge migration and separation.[182] π-conjugation along the polymer chains and π-stacking between chains result in hybridized energy levels, which facilitate efficient charge transfer and separation.[183] Additionally, the π-conjugated skeleton and surface functional groups can adsorb pollutants, enhancing the photocatalytic performance.[182] Furthermore, hybridizing these polymers with other π-conjugated materials uses π–π stacking to improve charge transfer and dissociation, thereby boosting the photocatalytic activity.[184,185] In summary, researchers can control and design π–π interactions in conjugated polymers by selecting appropriate polymer structures, side groups, and processing conditions. This is essential for understanding and optimizing the behavior and properties of conjugated polymers in various applications, especially in the field of photocatalysis.

3.4. Carbon materials

Carbon-based materials such as graphenes, graphene oxides (GOs), reduced graphene oxides (RGOs), carbon nanotubes (CNTs), graphite, graphdiyne, biochar, carbon quantum dots (CQDs) and graphene quantum dots (GQDs) are known for their capacity to construct π–π interactions with other π-conjugated materials or aromatic compounds (Fig. 10a–c). Among them, graphenes and their derivatives are the most widely used. Graphene, a two-dimensional material, features a unique honeycomb structure comprising a single layer of carbon atoms arranged in a tightly bound sp^2 hybrid configuration.[41,186–189] This arrangement endows graphene with outstanding physical and chemical properties (high

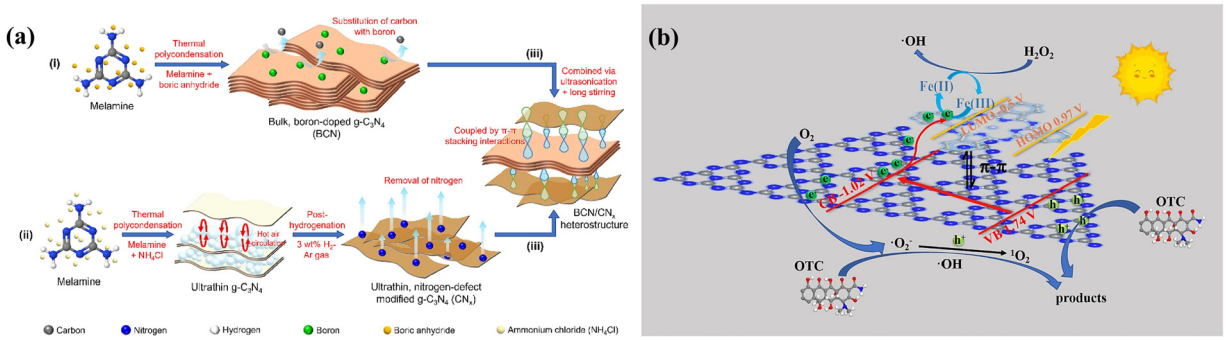

Fig. 9 (a) Preparation route of BCN/CNx hybrid materials ((a) Reproduced from ref. 32 with permission from Elsevier, Copyright 2023). (b) Illustration of the photo-Fenton reaction mechanism of FePc/g-C_3N_4 composites. ((b) Reproduced from ref. 171 with permission from Elsevier, Copyright 2023).

Open Access Article. Published on 24 January 2025. Downloaded on 11/7/2025 6:47:57 AM.
This article is licensed under a Creative Commons Attribution 3.0 Unported Licence.

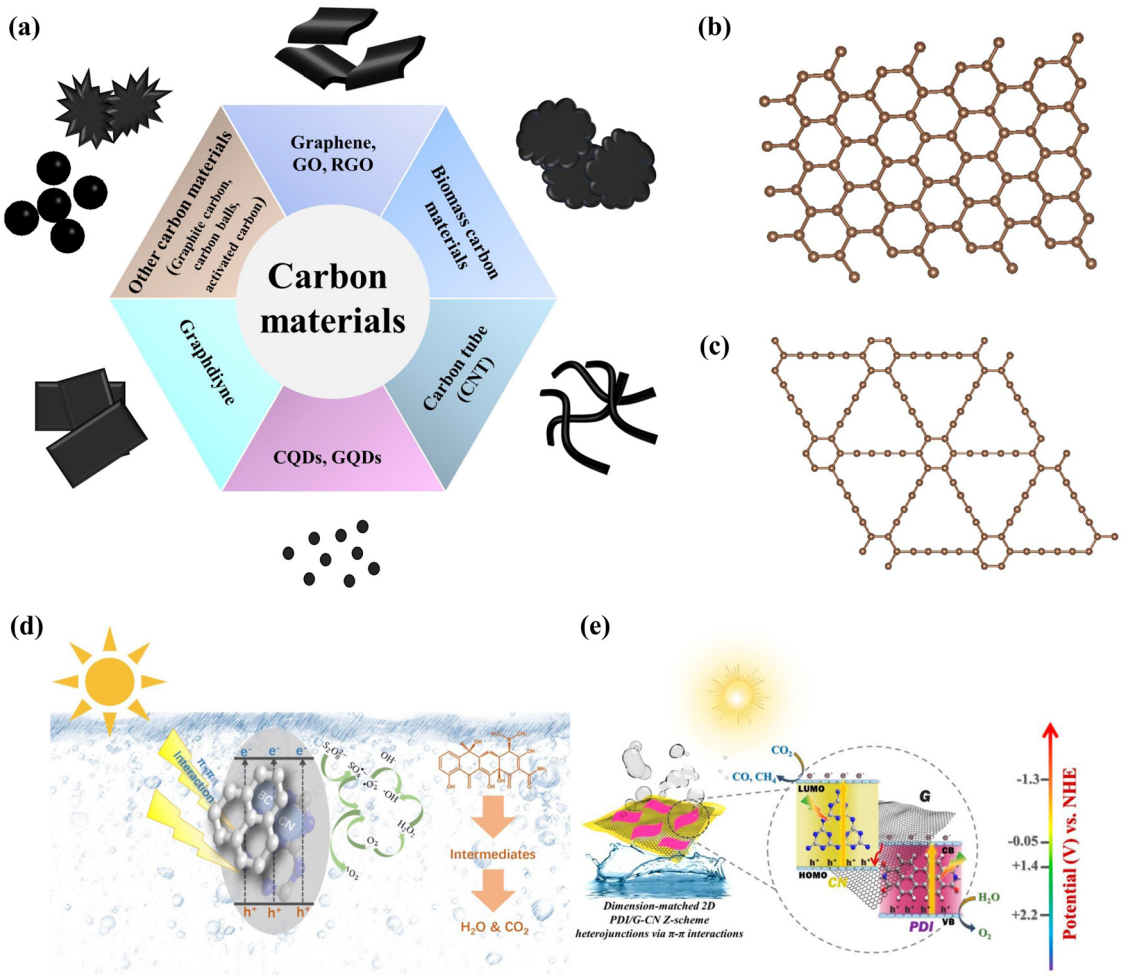

Fig. 10 (a) Summary of currently used carbon materials with π–π interactions, the main structural forms of the above materials. (b) Graphite (sp^2 hybridized carbon atoms) and (c) graphdiyne (sp^2 and sp hybridized carbon atoms). (d) Mechanistic diagram of the photodegradation of pollutants by biochar/g-C_3N_4 synergized PMS. ((d) Reproduced from ref. 211 with permission from Elsevier, Copyright 2022). (e) S-scheme electron migration pathway of PDI/G-CN composites and mechanistic diagram of photo-reduction of CO_2. ((e) Reproduced from ref. 101 with permission from American Chemistry Society, Copyright 2021).

conductivity and superior electron mobility).[41,186–188,190] The sp^2 hybridized carbon atoms in graphenes form covalent bonds that contribute to a delocalized π-electron cloud across their surface, creating an extensive π-conjugated structure.[186–188,191] This structure facilitates π–π interactions with other molecules or materials *via* π-electron cloud interactions.[41,186–188,192] Particularly, the π–π stacking interactions between graphenes and the aromatic rings of organic compounds in water make them highly effective in absorbing and removing pollutants.[186–188] Similarly, graphene derivatives (GOs, RGOs, and GQDs) and CNTs also have such extended π structures, which are extremely easy to form π–π interactions with other materials or pollutants with π conjugated structures.[102,127,193–201] Graphyne, an innovative material crafted from a fusion of sp and sp^2 hybridized carbon atoms, exhibits distinctive attributes such as an extensively conjugated π-system (easy to form π–π interaction), conformally arrayed pores, and tunable electronic properties, thereby unveiling its burgeoning promise in the realm of photocatalysis.[202–204] While the aforementioned carbon materials are widely utilized, their intricate synthesis processes and high costs hinder large-scale application. Consequently, biochar has attracted attention for its easy availability, low cost, porous structure, rich functional groups, excellent adsorption capabilities, and tunable chemical and physical properties.[205–209] Notably, biochar also possesses a π-conjugated electron system through π–π stacking and ether bond formation, demonstrating significant potential in the field of photocatalytic degradation.[210–212] Currently, carbon materials are primarily utilized in photocatalysis for the degradation of pollutants. This effectiveness is largely due to the π-conjugated systems within their structures, which engage in π–π interactions with pollutants to enhance the photocatalytic activity. Additionally, there is a small but growing body of research focused on combining carbon materials with other π-conjugated semiconductor materials through π–π interactions, broadening their application in various areas of photocatalysis. Tang *et al.* constructed graphene-like marl biochar-modified g-C_3N_4 (BC/CN) by calcination, and photocatalytic

Open Access Article. Published on 24 January 2025. Downloaded on 11/7/2025 6:47:57 AM.
This article is licensed under a Creative Commons Attribution 3.0 Unported Licence.

synergistic persulfate (PMS) removal of tetracycline could be achieved under visible light (1 h, 90% removal rate), which was principally due to the electron-absorbing property of the biochar that could modulate g-C_3N_4's electronic constitution, and meantime, the formation of the π–π interaction between them can accelerate the photogenerated electron transport channel (Fig. 10d).[211] Sun *et al.* developed a perylene diamide/graphene-g-C_3N_4 composite photocatalyst (PDI/G-CN) that is responsive across the entire light spectrum. This photocatalyst is capable of photo-reducing CO_2 to produce CO and CH_4 with an efficiency 16 times more excellent than that of g-C_3N_4 alone. This enhanced performance is primarily owing to the creation of an S-type heterojunction among the three components *via* π–π interactions, which markedly improves the efficiency of charge separation (Fig. 10e).[101]

3.5. Other materials

In addition to the previously mentioned examples, π–π interactions can occur in a wide variety of materials (BN, dyes, some organic molecules, *etc.*) in which aromatic rings or conjugated π-electron systems are present, and the principle of their π–π interactions is essentially based on the presence of aromatic or conjugated structures and the ability of these structures to participate in attractive interactions.[26,97,213–224] In summary, researchers can control and design π–π interactions in these materials by modifying the chemical structure, adjusting the distance between interacting structures, or introducing functional groups that enhance or inhibit interactions. Thus, π–π interactions can occur in a variety of materials in addition to the examples discussed earlier.

3.6. Summary

The choice of photocatalysts forming π–π interactions hinges on the particular application and requirements. The advantages and disadvantages of different types of photocatalysts that can form π–π interactions are as follows: (a) most of the conjugated polymers, organic small molecules, and organic framework materials have the advantages of excellent charge transport properties, high absorbance in the visible and near-infrared areas, flexible design and synthesis for various applications, and obvious π–π interactions between conjugated structures. Their disadvantages are mainly limited stability in certain environments (*e.g.*, UV and pH) and the need for some additional modification or protection. In addition, the raw materials for synthesizing these materials are very expensive and not suitable for large extent production, and some of them are toxic (potential environmental problem). Nevertheless, among them, there are also special materials that can be stabilized. For instance, g-C_3N_4 has excellent physical and chemical stability at room temperature, and its layered structure is very easy to modulate. However, because it generally forms a disordered structure, the π–π interactions are difficult to adjust, and its light absorption ability is weak. Therefore, directional modulation of the g-C_3N_4 structure is ineffective, which limits its charge separation and capability and, consequently, restricts its development. (b) Carbon materials possess unique characteristics making them attractive for π–π interactions, and their advantages are mainly high stability, wonderful electrical conductivity, large specific surface area, dimensional diversification, and excellent compatibility. Their disadvantages are mainly their lack of specificity in forming π–π interactions with various aromatic or conjugated compounds, the ease of aggregation between their layered structures, the difficult control of surface functionalization, the fact that some of the carbon materials are also polluted by the production process, and the high cost of synthesis of advanced carbon materials (single-walled carbon nanotubes, high-quality graphenes, graphyne, *etc.*). These drawbacks need to be addressed when designing and using these materials in various applications. In addition, Table S1 (ESI†) also shows the advantages and disadvantages of other related materials and the difficulty of regulating the π–π interaction, which is still a great challenge in general. In summary, the selection of the most favorable photocatalyst depends on the specific photocatalytic reaction, environmental conditions, and desired properties. The trade-offs between advantages and disadvantages must be carefully considered and the photocatalytic materials and systems optimized accordingly to meet the desired performance criteria.

4. π–π interaction between photocatalytic materials and reactant organic molecules

Besides the π–π interactions within aromatic photocatalysts themselves that indirectly affect their catalytic performance, the π–π interactions between aromatic photocatalysts (such as carbon nitride, COFs, MOFs, PDIs, and various types of composites modified with carbon materials) and organic conjugated reaction molecules exist in various photochemical and photophysical processes, which directly affect the efficiency and selectivity of photocatalytic reactions. Therefore, it makes sense to investigate the π–π interactions of aromatic photocatalysts and organic conjugated reaction molecules and to discuss the influence on photocatalyst performance.

4.1. Formation of π–π interaction between photocatalysts and organic pollutants

First, π–π interactions were found between aromatic photocatalysts and organic pollutants, which mainly include polycyclic aromatic hydrocarbons (PAHs), dyes, drugs, and aromatic pesticides.[206,208,225–235] It significantly affects degradation and removal of organic pollutants.[135,236–240] During the photocatalytic process, the π electron clouds between the photocatalyst and the organic pollutant may overlap and result in the π–π interaction. In addition, it further enhances the pollutant's adsorption on the photocatalyst's surface, which is beneficial for the subsequent photocatalytic degradation reaction. Therefore, researchers often use the strategy, enhancing the π–π interaction by exploring new photocatalysts with aromatic structure, towards improving the efficiency of aromatic pollutant molecules. For example, Gao *et al.* successfully designed

Open Access Article. Published on 24 January 2025. Downloaded on 11/7/2025 6:47:57 AM.
This article is licensed under a Creative Commons Attribution 3.0 Unported Licence.

the photocatalytic adsorbent MIL-53(Fe) and found that it exhibited a good adsorption capacity (0.57 mmol g^{-1}) of carbamazepine (CBZ) from water, which is mainly due to π–π interactions between MIL-53(Fe) and CBZ.[241] Similarly, Du *et al.* constructed a composite (NHCS/$Zn_2In_2S_5$) of self-assembled $Zn_2In_2S_5$ and N-doped hollow carbon spheres (NHCS) with the rich π-conjugated aromatic backbone structure. Therefore, the organic pollutants (phenol or bisphenol A (BPA)) with abundant π bonds can be gathered onto the surface of the composite (NHCS/$Zn_2In_2S_5$), which leads to reduce activation energies of the phenol*/BPA*.[242] Therefore, both phenol (97.6%) and BPA (79.7%) were efficiently removed. In addition, the separated electrons were quickly transferred to the dissolved oxygen, resulting in higher H_2O_2 yields of 1.31 mmol L^{-1} from phenol and 2.31 mmol L^{-1} from BPA, respectively. Zhang *et al.* further confirmed that the π–π interactions between g-C_3N_4 (CNN-500) and pollutant molecule (flumequine, FLU) facilitated efficient charge separation and transfer, finally accelerating the photocatalytic degradation rate of FLU. That is, CNN-500 can photocatalytically remove 62.9% of FLU in 30 min.[243]

4.2. Formation of π–π interactions between photocatalysts and organic reaction substrates

In addition, π–π interactions were confirmed to be able to promote the conversion of organic conjugated reaction substrates. These substrates containing aromatic or conjugated structures, such as aromatics, some biomass molecules or aromatic molecules with π-electron systems, can form π–π interactions with these photocatalysts *via* van der Waals forces, enhance the adsorption of substrates onto the catalyst surface, and affect the reaction efficiency and selectivity.[24,33,244] In the presence of light, the substrate molecules are more likely to participate in photochemical processes, such as electron transfer, and the π–π interaction leads to selective activation of the substrate and controls the reaction outcome. Researchers use these interactions to design and optimize photocatalytic systems such as photoredox, cross-coupling, and photodissociation reactions. Das *et al.* used a chemically stable two-dimensional microporous COF (PCR-1) with a dangling phenyl group as a photocatalyst for H_2O_2 generation (adding benzyl alcohol as a sacrificial agent). This induced the strong π–π interactions of PMCR-1 and benzyl alcohol that facilitates efficient hole transfer, obviously increasing the production of H_2O_2 and a higher selective oxidation of benzyl alcohol to the corresponding aldehyde. Based on these inspired findings, the catalyst (PMCR-1) was highly selective for other benzene ring species (benzylamine and methyl sulfide derivatives).[24] Different from the above-mentioned sections, Bai *et al.* explored the heterojunction $Zn_{0.5}Cd_{0.5}S$/graphene oxide (ZCS/GO) composites that induced charge separation and then formed reduction and oxidation centers.[33] Meanwhile, the π–π interactions of GO and benzene ring promoted charge carriers' spatial distribution, which improved interfacial charges transfer and photocatalytic hydrogenation/oxidation activities of ZCS/GO. Therefore, ZCS/GO realized the cascade conversion from *p*-xylene to *p*-methylbenzaldehyde and finally to selected *p*-methylbenzyl alcohol. Additionally, other mesoporous 2D organic photocatalysts show a similar property when the π-conjugated material is used as the reaction substrate. Liu *et al.* found that the mesoporous graphitic carbon nitride (mpg-C_3N_4) photocatalyst also formed the favorable π–π interactions with a lignin model molecule, finally realizing 90% conversion rate of lignin model molecule *via* photocatalytic oxidation (cleavage of the C–C structure: β-O-4 and β-1 bonds) under visible light.[244]

5. Influence of π–π interaction on photocatalysis

The π–π interactions, esteemed as one of the most fascinating and important intermolecular noncovalent interactions, affect greatly the crystal size and crystallinity of conjugated organic photocatalysts, subsequently impacting their multiple physicochemical traits. Moreover, they can directly influence charge transfer, thereby significantly enhancing the efficiency and stability of photocatalytic systems. The mechanisms underlying π–π interactions in photocatalytic reactions are intricate and contingent upon the specific materials and reactions involved. In general, π–π interactions can affect photocatalytic reactions in the following ways (Fig. 11 and Table S2, ESI†).

5.1. Enhancing light absorption

π–π interactions can lead to stacking or close proximity of aromatic or conjugated systems within the photocatalyst material, which enhance the light absorption properties of the material by better π–π interactions.[245] Stacked aromatic systems with extended π-electron systems can absorb photons over a wider wavelength range, including UV and visible light. π–π interactions can affect the energy level and electronic structure of photocatalysts. The stacking of π-conjugated systems can lead to changes in energy levels, which is important for matching the band gap of the photocatalyst to the energy of the incident photon.[121,122,246] This extended light absorption is essential for triggering photocatalytic reactions.

5.2. Promoting electron–hole pair separation

Photocatalytic reactions implicate the creation of e^-–h^+ pairs when the photocatalyst absorbs photons. Effective charge separation is essential for these reactions to occur. π–π interactions can play a role in separating these charge carriers.[154,166] In materials with π–π stacks, photogenerated electrons and holes may be located in different parts of the stack structure, leading to spatial separation. This spatial separation reduces the likelihood of electron–hole pair complexation, which would otherwise reduce the efficiency of the photocatalytic process.[121,155,247] In addition, π–π interactions can facilitate electron transfer between aromatic or conjugated units within the photocatalyst. These units are in close proximity, enabling efficient electron transfer pathways that promote electron mobility and transfer to active sites on the surface of the material, where the chemical reaction occurs.[42,248] Due to the presence of π–π stacks, excitons generated by light absorption

Open Access Article. Published on 24 January 2025. Downloaded on 11/7/2025 6:47:57 AM.
This article is licensed under a Creative Commons Attribution 3.0 Unported Licence.

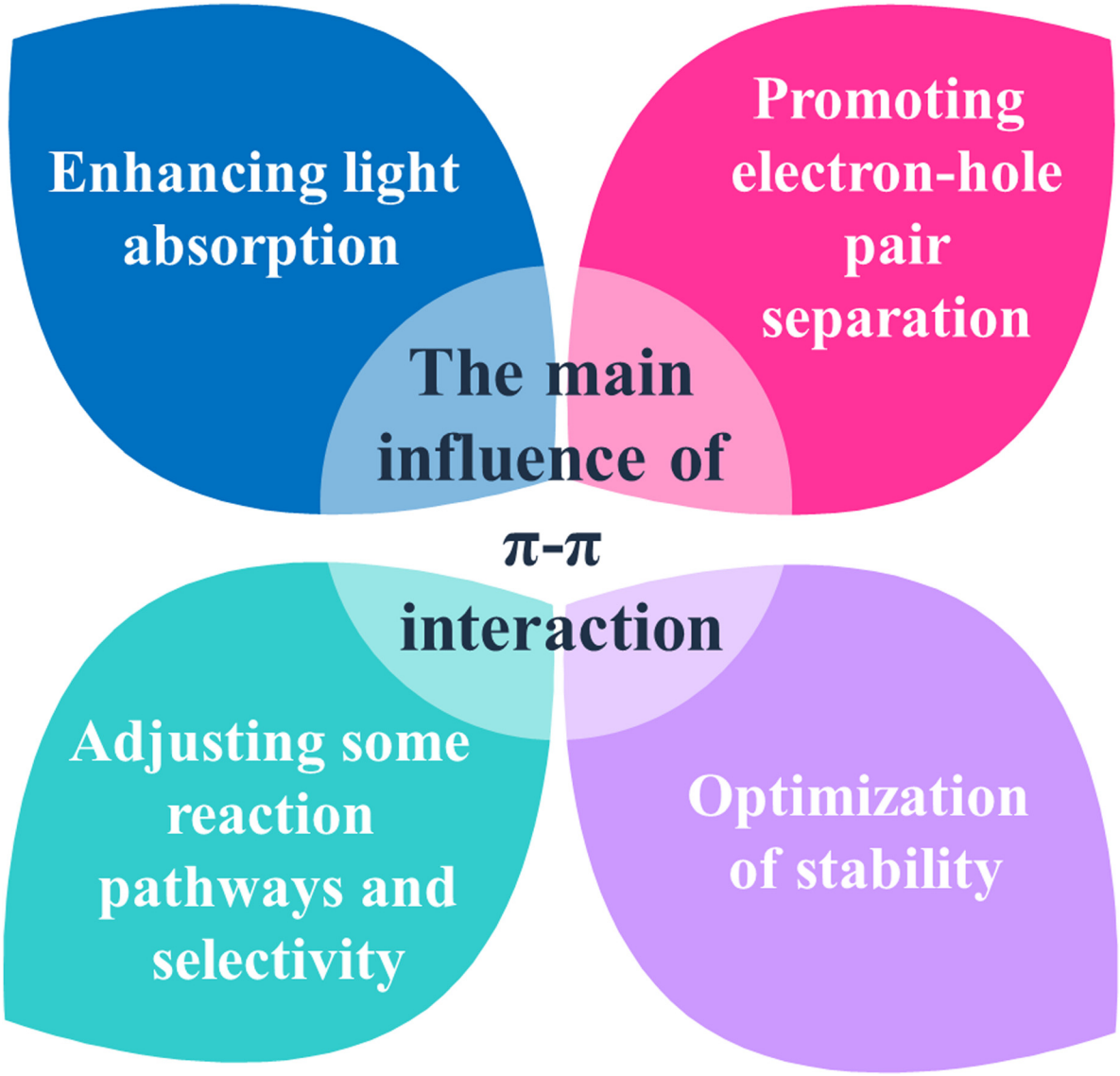

Fig. 11 Main influence of π–π interactions on photocatalysis.

can move along π-conjugated paths, thus improving the chances of charge separation and reaction at the active site.[249] Furthermore, it has been found that only moderate π–π interactions at appropriate distances can balance charge transfer and recombination, thereby optimizing carrier generation and transition processes in photocatalytic systems.[23] In some photocatalytic systems, π–π interactions may be convoluted in heterojunctions' constitution, in which different semiconductor materials (organic semiconductors or inorganic semiconductors) are combined together.[250–253] These connections can improve charge separation at their interface, so the construction of composites with π–π interactions can advance carrier separation and thus reduce recombination.

5.3. Optimization of stability

π–π interactions also contribute to the stability of the photocatalyst.[175] π–π interactions on the surfaces of photocatalysts improve crystalline stability, enhance mechanical stability, and improve charge separation.[78,175,254–256] These combined effects lead to improved stability and performance of photocatalysts, ensuring their long-term effectiveness across a broad spectrum of applications.

5.4. Adjusting reaction pathways and selectivity

π–π interactions can significantly affect the selectivity and pathways of photocatalytic reactions by influencing the adsorption, activation, and transformation of reactant molecules on the surface of the photocatalyst.[257,258] π–π interactions serve multiple roles in photocatalytic reactions including regulating the adsorption orientation of substrates on the photocatalyst surface, activating and stabilizing reaction intermediates.[170,258–260] These effects collectively favor specific reaction pathways while inhibiting others, thereby enhancing product selectivity. Overall, π–π interactions offer a valuable

Open Access Article. Published on 24 January 2025. Downloaded on 11/7/2025 6:47:57 AM.
This article is licensed under a Creative Commons Attribution 3.0 Unported Licence.

approach for designing and optimizing photocatalysts by precisely controlling various aspects of the photocatalytic process to achieve efficient and selective conversions tailored to particular applications.

It is worth noting that the specific role and impact of π–π interactions on photocatalytic reactions hinge on the nature of photocatalysts, the reactants involved, and the reaction environments. By careful design and engineering of photocatalytic materials, these interactions are used to enhance the performance of various applications such as pollutant removal, hydrogen peroxide production, water splitting, CO_2 reduction and synthesis of valuable chemicals.

6. Modulating π–π interaction for photocatalysis

Based on above-mentioned effects of π–π interactions on photocatalysts' properties, the design and selection of appropriate materials with optimized π–π interactions can improve the efficiency and selectivity of photocatalysis. Therefore, it makes sense to modulate carefully π–π interactions for high-performance photocatalysts. To date, researchers have proposed several effective strategies including side-chain engineering, substituent engineering, and doping of main aromatic structures in photocatalysts. The detailed discussion is shown as follows:

6.1. Side-chain and substituent engineering

Although π–π interactions depend on the main aromatic structure stacking in photocatalysts, different types of side-chains and halogen substituents on main aromatic structure also influence the π–π interactions between aromatic units of photocatalysts, because of the steric hindrance and the electron push–pull property, which can tune the light absorption and crystallinity of related photocatalysts, and enhance their charge separation.[254,261,262] For instance, Liu *et al.* designed three linearly conjugated polymers (ethylenediamine-PDI, oxamide-PDI, and oxamide-NDI) based on two aromatic cores (perylene diimide (PDI) and naphthalene diimide (NDI)) and two different covalently linked sections (ethylenediamine and oxamide) (Fig. 12a).[254] Fig. 12b demonstrates that highly crystallized oxamide-PDI shows the best photocatalytic oxygen production performance. It was mainly attributed to the fact that oxamide-PDI not only yielded a higher π–π stacking interaction energy and enlarged light absorption from expanded π-conjugation of oxamide, but also produced a strong built-in electric field from a strong internal dipole moment and ordered crystalline structure that facilitates the efficient migration and separation of charge carriers. In addition, the length of the side chain influences its π–π stacking mode in organic aromatic photocatalysts. Wang *et al.* developed H/J-type aggregated PDI (perylene tetracarboxylic acid diimide) supramolecular nanostructures using two PDI derivatives modified with linear carboxyl-substituted side chains of different lengths.[117] H-PDI demonstrated superior efficiency in photocatalytic pollutant removal and oxygen production, particularly for phenol removal. This enhanced performance is attributed to H-PDI's stronger π–π interactions and a narrower band gap, which facilitate more effective photogenerated carrier migration and produce a higher yield of superoxide radicals and potent oxidizing holes. Surprisingly, a few studies have noted that regioisomers also influence π–π interactions in organic aromatic photocatalysts. Wang *et al.* developed regioisomeric benzotriazole-based COFs, where the symmetrical isomer (BTz-COF-S), due to its more ordered π–π stacking, exhibits stronger light absorption and exciton dissociation capabilities. This results in superior photocatalytic hydrogen production activity to the asymmetric isomer (BTz-COF-AS).[263] Different from the above-mentioned side-chain tactics, using halogen substituents (such as F and Cl) represents another efficient way to facilitate π–π interactions of organic aromatic photocatalysts. Wang *et al.* introduced electronegative halogen atoms (F and Cl) into benzothiadiazole as a acceptor unit, which combine 1,3,5-tricarbonylresorcinol (TP) as a donor unit to successfully synthesize donor–acceptor (D–A) conjugated COFs (COF-Cl and COF-F) (Fig. 12c).[261] Through theoretical calculations, COF-F showed the lower charge (1.191) of the TP donor unit and the highest charge (0.286) of the acceptor component compared with those of COF-H and COF-Cl. It indicates that the electronegative F substituent enhances the internal segregation driving force and promotes charge separation. In addition, due to the formation of intramolecular hydrogen bonds between the F atom and the hydrogen atoms of adjacent benzene rings, the smaller torsion angle and center distance of the benzene rings in COF-F not only provide a better planarity of COF-F, but also improve the conjugation degree and π–π interactions between COF-F molecule interlayers. This helps to increase the crystallinity of COF-F, and obtain the faster axial carrier charge transfer and lower the carrier recombination rate based on the maintained beneficial face-to-face stacking (AA′ positive stacking mode). Therefore, COF-F finally exhibits a higher photocatalytic hydrogen production activity than COF-Cl and COF-H (Fig. 12d). In addition, based on the two above-mentioned strategies' synergistic effects, An *et al.* constructed a series of benzothiadiazole (BT)-based polymeric materials with adjusting different side chains and substituents for hydrogen production.[262] As seen from Fig. 12e, compared with the P1 polymer, the P2 polymer was introduced by a linear oligo (ethylene glycol) (OEG) side chain and the P3 polymer was incorporated by both the OEG side chain and the backbone fluorine substituent. It was found that the hydrophilic OEG side chains not only promoted water uptake but also enhanced intermolecular packing and efficient exciton separation. Additionally, the fluorine substituents on the polymer backbone improved the noncovalent coulombic interactions, resulting in a planar chain conformation in polymer's structure. This enhanced polymer's self-assembling capability. Therefore, the P3 polymer showed the π–π stacking enhancement and the higher long-lived polarons' yield, ultimately realizing the higher hydrogen production activity, as shown in Fig. 12f. Therefore, the side-chain and substituents are regarded as

Open Access Article. Published on 24 January 2025. Downloaded on 11/7/2025 6:47:57 AM.
This article is licensed under a Creative Commons Attribution 3.0 Unported Licence.

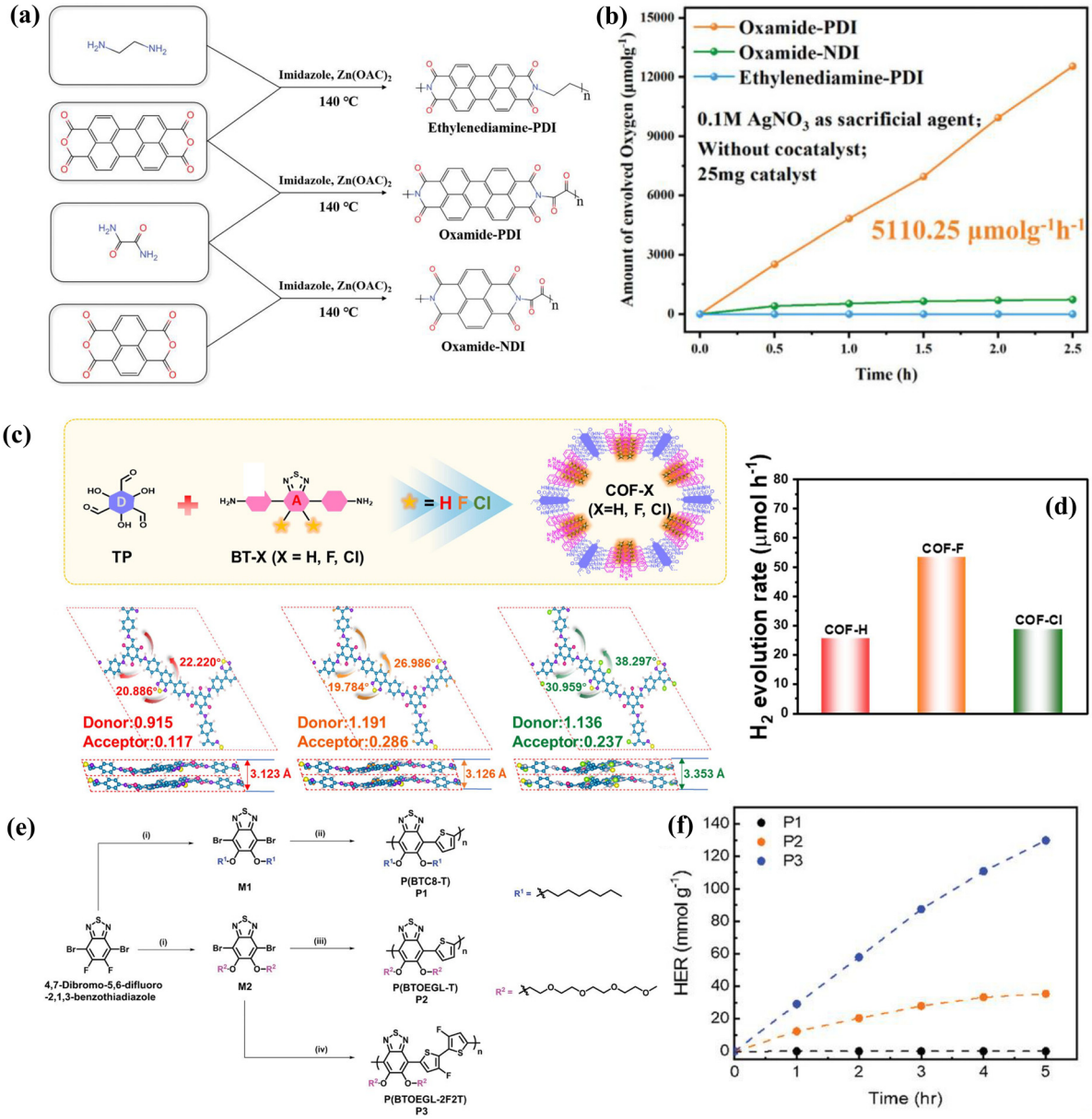

Fig. 12 (a) Preparation routes of several linear conjugated polymers and (b) their corresponding photocatalytic oxygen production performance comparison plots. ((a) and (b) Reproduced from ref. 254 with permission from Wiley-VCH, Copyright 2023). (c) Preparation roadmap of several COFs and (d) comparative photocatalytic hydrogen precipitation performances of the above three COF materials. ((c) and (d) Reproduced from ref. 261 with permission from American Chemistry Society, Copyright 2023). (e) Preparation roadmap of three conjugated polymers. (f) Comparative photocatalytic hydrogen production performance of three conjugated polymers. ((e) and (f) Reproduced from ref. 262 with permission from Wiley-VCH, Copyright 2023).

indirect strategies to change the density of the π-electron cloud and the π–π stacking distance of adjacent main aromatic structures, finally influencing related photocatalysts' catalytic performance.

6.2. Doping and extending of main aromatic structures in photocatalysts

Doping the main aromatic structure of organic semiconductors or expanding the π-electron cloud can influence the π–π interactions between the aromatic units of photocatalysts. This modification adjusts the charge distribution in the photocatalysts, impacting their light absorption and charge separation capabilities.[122,255,264,265] Miao *et al.* successfully synthesized two different two-dimensional β-ketoenamine-linked COFs with hexagonal skeleton structures: TpTAPT-COF and TpTAPB-COF by combining different organic units (1,3,5-tris(4-aminophenyl)triazine (TAPT) and 1,3,5-tris(4-aminophenyl)benzene (TAPB)) with 1,3,5-triformylphloroglucinol (Tp) (Fig. 13a), respectively.[255] The high rigidity and planarity of the triazine ring in TpTAPT-COF result in better crystallinity and more pronounced π–π interactions, as evidenced by the sharper diffraction peak at around 26° (Fig. 13b). Consequently,

Open Access Article. Published on 24 January 2025. Downloaded on 11/7/2025 6:47:57 AM.
This article is licensed under a Creative Commons Attribution 3.0 Unported Licence.

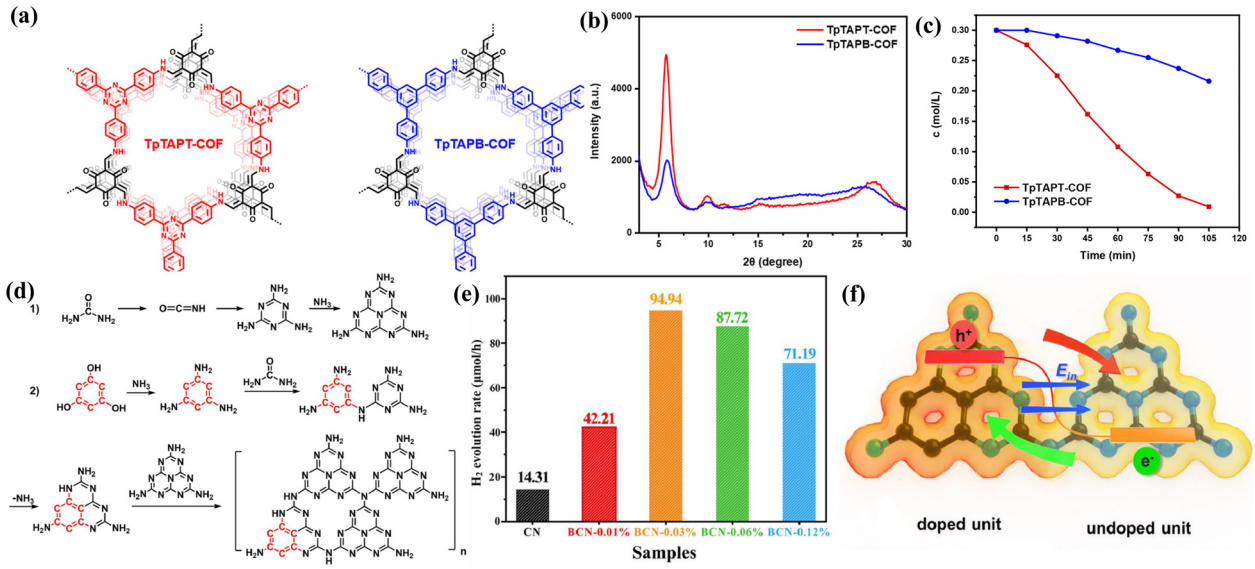

Fig. 13 (a) Structural diagrams of the two COFs and (b) their corresponding PXRD patterns. (c) Reaction time curves for the conversion of phenylmethyl sulfide by the two COFs. ((a) and (c) Reproduced from ref. 255 with permission from Royal Society of Chemistry, Copyright 2023). (d) Preparation process of introducing a benzene ring structure in g-C_3N_4. (e) Graph of photocatalytic hydrogen production results of all the materials under visible-light irradiation. (f) Roadmap of photogenerated carriers' charge transport on the novel carbon nitride. ((d)–(f) Reproduced from ref. 266 with permission from Elsevier, Copyright 2022).

TpTAPT-COF exhibits superior catalytic activity and selectivity in the photocatalytic oxidation of benzyl sulfide (Fig. 13c). The minimal steric hindrance of the triazine unit allows TpTAPT-COF to maintain stable planarity and tight π–π stacking, enhancing light absorption and facilitating charge separation and migration. Building on previous research, Han *et al.* substituted the benzene ring with a pyridine ring on the side chain of the triazine ring, forming a new covalent triazine framework (T3N-CTF).[265] This modification expanded the π electron clouds on the triazine ring, enhancing electron delocalization and conjugation length. The resulting increase in π–π stacking contributed to superior carrier separation and transmission efficiency, leading to a higher photocatalytic hydrogen production rate. As a representative organic semiconductor material with π–π interactions, Chen *et al.* improved the π–π conjugated structure of carbon nitride by doping with 1,3,5-benzenetriol (Fig. 13d).[266] This doping replaced the triazine ring with a benzene ring in the π-electron delocalized heptazine ring structure, affecting π–π interactions, broadening light absorption, and improving charge separation. The optimized BCN-0.03% sample exhibited a H_2 output rate underneath visible light irradiation 6.6 times more excellent than that of g-C_3N_4 (Fig. 13e). This increase in efficiency is primarily attributed to the dopant choice, which facilitates the formation of unique coplanar heterojunctions (Fig. 13f). These heterojunctions not only retain the g-C_3N_4's original network formation but also significantly enhance the separation and transfer of photogenerated carriers by an improved π-conjugated endogenic electric field.

6.3. Regulation of metal ions

At present, the effect of metal ions on the conjugation and π–π interaction in material structure has not been widely concerned. Metal ions are found to many influence the π–π interactions in MOF materials, and can significantly influence these interactions *via* coordination with organic ligands, regulating electronic properties, and interfering with π–π packing.[86] The coordination between metal ions and organic ligands not only determines the pore structure, conductivity and crystallinity of MOFs, but also affects the π–π stacking pattern between molecules.[86] The size, coordination mode and geometry of metal ions affect the distance and arrangement between ligands, thus changing the strength of the π–π interaction.[86] However, in the photocatalytic reaction system, no researchers have carried out in-depth research on this yet. In addition, we expect that later work can carry out more studies on the influence of metal ions on π–π interaction in photocatalytic systems; reasonable design and selection of metal ions may significantly improve the photocatalytic performance of materials.

7. Construction of π–π interactions in heterojunction systems

In some photocatalytic systems, π–π interactions may be involved in the formation of heterojunctions, in which different semiconductor materials are combined together. These connections can improve charge separation and promote more efficient photocatalytic reactions.

7.1. Hybridization of different organic photocatalysts

Organic semiconductor molecules are usually composed of macromolecules with π-electrons, which form conjugated molecular orbitals, so that this structure can form a low bandgap and generate photoelectron excitation. The complex electronic structure of organic semiconductors can easily cause scattering

Open Access Article. Published on 24 January 2025. Downloaded on 11/7/2025 6:47:57 AM.
This article is licensed under a Creative Commons Attribution 3.0 Unported Licence.

and compounding of carriers, and hence, the construction of composites with π–π interactions can promote the separation of carriers and thus reduce compounding, as well as enhance the stability of catalysts.[32,185,214,250,251,267] Xu *et al.* constructed a large π-isolated domain direct Z-type polymer composite structure (g-C_3N_4/P1Cl-T) by combining a two-dimensional (2D) donor–acceptor conjugated polymer (P1Cl-T) with g-C_3N_4 *via* the π–π stacking interaction between them, and the various characterization results also showed that the π–π interaction between them successfully formed an extended π network on the whole polymer heterojunction, which facilitated the full-spectrum absorption, formation of the built-in electric field, exciton dissociation and charge transport, and ultimately realized the substantial improvement of the hydrogen production performance.[184] The orbital overlap between the triazine unit with a π-electronic structure in the g-C_3N_4 structure and the polymer with a D–A structure and its π-electronic cloud can be easily realized, which is very conducive to the photogenerated charge migration. Compared with g-C_3N_4 (2.31 mmol h^{-1} g^{-1}) or P1Cl-T (0.33 mmol h^{-1} g^{-1}), the hydrogen production performance of g-C_3N_4/P1Cl-T photocatalysts was significantly enhanced (g-C_3N_4/P1Cl-T_7 had the best performance, 49.22 mmol h^{-1} g^{-1}), and the photocatalytic hydrogen production performance of g-C_3N_4/P1Cl-T_7 was further enhanced by the further introduction of Pt, reaching 111.8 mmol h^{-1} g^{-1}. Therefore, we can conclude that the reconstructed extended π-network on the Z-type heterojunction is responsible for the substantial increase in the hydrogen production activity.

7.2. Hybridization of inorganic photocatalysts and organic photocatalysts

In addition to the above-mentioned considerations, hybrid systems of inorganic and organic semiconductors can combine the many advantages offered by inorganic and organic semiconductors, taking full advantage of the unique properties of each material class. For example, the flexible structure of organic semiconductors can be easily incorporated into the surface of inorganic semiconductors, organic semiconductors can be designed to achieve energy band matching with inorganic semiconductors, organic semiconductors can also increase the light absorption of the hybrid system, and the stability of inorganic semiconductors can enable organic–inorganic hybrid materials to exhibit better long-term stability compared to pure organic semiconductors. Overall, combining inorganic and organic semiconductors in hybrid materials has a wide range of advantages that make them promising candidates for photocatalytic applications. These advantages from the synergistic combination of the strengths of both material classes mitigate their respective weaknesses.[104,105,111,113,252] Yang *et al.* constructed a full-spectrum Ag_2S/PDI composite system for photocatalytic removal of phenol and photocatalytic oxygen production performance.[253] The construction process of Ag_2S/PDI composites is mainly due to the formation of hydrogen bonding and π–π stacking from PDI tightly bound by electrostatic self-assembly. The apparent rate constants for visible light degradation of phenol by Ag_2S/PDI composites (1 : 0.6) exhibited the fastest degradation rate (0.0259 min^{-1}), which was 6.93 times higher than that of pure PDI (0.00374 min^{-1}). Further, Ag_2S/PDI (1 : 0.6) could remove 94.48% of phenol within 2 h. The degradation rate of Ag_2S/PDI (0.0259 min^{-1}) was 6.93 times higher than that of pure PDI (0.00374 min^{-1}). In addition, the oxygen production performance of Ag_2S/PDI (1 : 0.6) (34.6256 μmol h^{-1} g^{-1}) was improved by 1.79-fold compared to that of PDI (19.3312 μmol h^{-1} g^{-1}). The above-mentioned results indicated that Ag_2S and PDI form a built-in electric field, which helps the photogenerated electrons to migrate along the direction of π–π stacking, thus generating more reactive radicals and more powerful oxidizing ability.

8. Application of materials involving π–π interaction during photocatalysis

Fig. 14a and b show the applications and distribution of photocatalysts with π–π interactions in various fields of

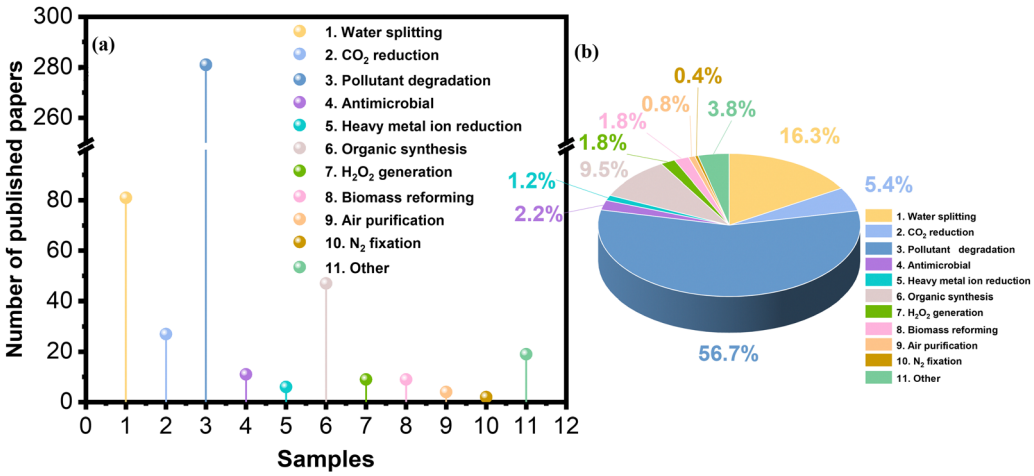

Fig. 14 Publication status (a) and proportion of papers (b) of photocatalysts with π–π interaction based on keyword search of "π–π" and "photocata*" in the Web of Science (as of September 1, 2024).

Open Access Article. Published on 24 January 2025. Downloaded on 11/7/2025 6:47:57 AM.
This article is licensed under a Creative Commons Attribution 3.0 Unported Licence.

photocatalysis since 2002, in which we can find that more than half of the papers are related to the photodegradation of pollutants, most of which are related to the degradation of aromatic pollutants. We find that the proportions of reported reactions are, in descending order, pollutant degradation (56.7%), water splitting (19.8%), organic synthesis (9.5%), and CO_2 reduction (5.4%) that are the main categories of applications, the details of which will be introduced next. In addition, we will introduce in detail the two popular areas of H_2O_2 generation and biomass conversion. Other photocatalytic applications are relatively rare, mainly through the built-in electric field generated by π–π interaction to improve their photocatalytic performance.

8.1. π–π interactions: synergistic effects of photocatalysts and aromatic organics

While discussing the application of π–π interaction in the field of photocatalysis, the degradation of organic pollutants, aromatic organic conversion and biomass conversion are three major reactions largely relying on the π–π interaction between the photocatalyst and the aromatic organic matter, which has been widely and mostly discussed and studied by researchers.

8.1.1 Pollutant degradation. In the photocatalytic degradation of pollutants, π–π interactions between different semiconductors and between semiconductors and pollutants, and synergistic effects of these interactions provide various advantages that contribute to the efficiency and effectiveness of pollutant degradation.[240–243,268–272] The main advantages of π–π interactions between semiconductors are enhanced charge transfer, increased surface area, and expanded light absorption. The main advantages of π–π interactions between semiconductors and pollutants are enhanced pollutant adsorption, optimized selective adsorption and improved reactivity. The synergistic effect of the two above-mentioned π–π interactions can lead to the efficient removal of difficult-to-degrade organic pollutants (*e.g.* polycyclic aromatic hydrocarbons, dyes, drugs, and aromatic pesticides).[206,208,225–235] For instance, Sun *et al.* developed a new supramolecular photocatalyst, hp-PDI-NA, by combining PDI (perylene diimide) with nicotinic acid (NA). This structure boosts the transport and separation of photogenerated carriers through reduced steric hindrance and enhanced π–π interaction, thereby resulting in a 3.5 times higher phenol degradation efficiency under the visible illumination than that of nano-PDI (Fig. 15a).[122] Li *et al.* synthesized a new 0D/2D S-type heterojunction photocatalyst *via* the π–π conjugated self-assembly of nitrogen-doped carbon dots (N-CDs) and sulfur-doped carbon nitride (S-C_3N_4). This heterojunction, stabilized by π–π interactions, effectively promotes the separation and migration of photogenerated charges, substantially boosting the photocatalytic degradation and hydrogen production from water (Fig. 15b).[273] Ning *et al.* substantially ameliorated the degradation efficiency of 2,4-dichlorophenol by synthesizing a 3D/0D structure Co–N–C/SA-TCPP photocatalyst, achieving a degradation rate 10.9 times higher than that of SA-TCPP alone and enhancing the oxygen production rate by 1.9 times. The enhancement is imputed to the π–π interaction between SA-TCPP and Co–N–C, which facilitates photogenerated charges' movement. Additionally, the cobalt nanoparticles and nitrogen-

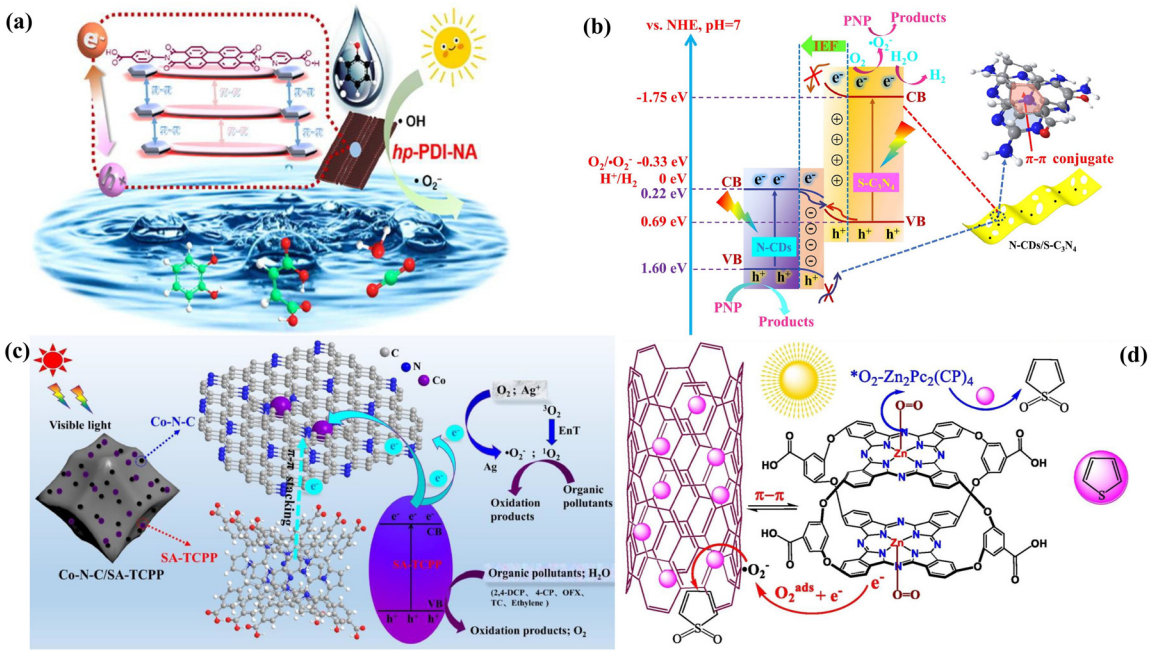

Fig. 15 (a) Mechanism chart of phenol's hp-PDI-NA photocatalytic elimination. ((a) Reproduced from ref. 122 with permission from Elsevier, Copyright 2022). (b) Photo-reactivity mechanism diagram of N-CDs/S-C_3N_4 constructing S-type heterojunction through π–π interaction. ((b) Reproduced from ref. 273 with permission from Elsevier, Copyright 2022). (c) Schematic of the mechanism of photocatalytic degradation of various pollutants by Co–N–C/SA-TCPP composite materials. ((c) Reproduced from ref. 274 with permission from Elsevier, Copyright 2022). (d) Photo-reactivity mechanism chart of MWCNTs/$Zn_2Pc_2(CP)_4$. ((d) Reproduced from ref. 275 with permission from Springer, Copyright 2021).

Open Access Article. Published on 24 January 2025. Downloaded on 11/7/2025 6:47:57 AM.
This article is licensed under a Creative Commons Attribution 3.0 Unported Licence.

doped carbon matrix in Co–N–C serve as electron traps and expedite electron transport (Fig. 15c).[274] Tian *et al.* synthesized a series of dinuclear metal phthalocyanines ($M_2Pc_2(CP)_4$, M = Fe^{2+}, Co^{2+}, and Zn^{2+}) and encapsulated them on the surface of multi-walled carbon nanotubes (MWCNTs) to enhance the desulfurization performance *via* a facile "*in situ* hydrothermal" approach. The π–π interaction plays a fundamental role in the constitution of MWCNTs/$M_2Pc_2(CP)_4$ composites, which not only enhances the dispersion of $M_2Pc_2(CP)_4$ on the surface of MWCNTs, but also significantly improves the photocatalytic performance of the composites by increasing the photogenerated charge separation efficiency (Fig. 15d).[275]

The above paragraph mainly describes the constitution of powerful built-in electric fields dictated by π–π interactions between semiconductors in the photocatalytic degradation of pollutants, and the next part of the work is more inclined to describe the significance of π–π interactions between semiconductors and pollutants in the degradation of pollutants.[135,236–240] Wang *et al.* developed an organic–inorganic hybrid heterostructure, NC@PDI/MZO, consisting of a benzimidazole-modified nitrogen-doped carbon skeleton and manganese-doped zinc oxide.[276] DFT calculations indicated that the adsorption energy of tetracycline (TC) on this material predominantly originates from hydrogen bonding (-140.0 kJ mol^{-1}) and π–π interactions (-61.5 kJ mol^{-1}), totaling an adsorption energy of -211.2 kJ mol^{-1} (Fig. 16a). NC@PDI/MZO demonstrated exceptional photocatalytic degradation of TC, achieving a degradation rate of 99.9% for 50 mg L^{-1} TC within 40 minutes of illumination (Fig. 16b). This high efficiency is largely due to the pivotal role of π–π interactions and hydrogen bonds in forming the composite material, which enhances TC adsorption and thus photocatalytic degradation efficiency *via* synergistic effects. The formation of the S-scheme heterostructure also aids in the

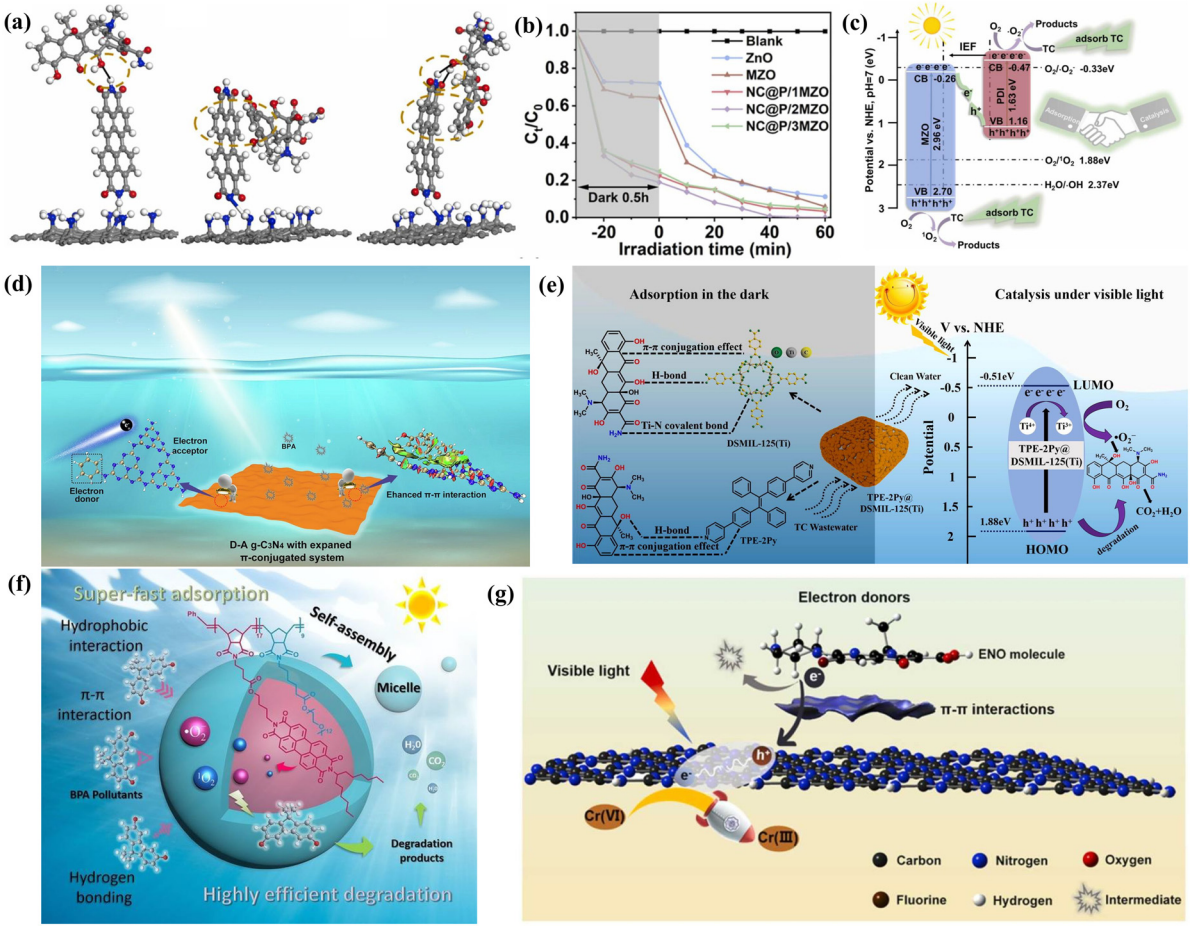

Fig. 16 (a) Model diagram of hydrogen bond adsorption, π–π adsorption, hydrogen bond adsorption and π–π interaction co-adsorption of NC@PDI/MZO sample for TC. (b) Performance of synergistic photocatalytic removal of TC by adsorption of different samples. (c) Mechanism diagram of NC@PDI/MZO adsorption synergistic photocatalytic removal of TC. ((a)–(c) Reproduced from ref. 276 with permission from Elsevier, Copyright 2024). (d) Mechanism diagram of D–A g-C_3N_4 enhancing the π–π adsorption with BPA and efficiently photodegrading BPA. ((d) Reproduced from ref. 233 with permission from Elsevier, Copyright 2022). (e) Mechanism diagram of TPE-2Py@DSMIL-125(Ti) coupling various synergistic effects to achieve efficient photodegradation of TC. ((e) Reproduced from ref. 277 with permission from Elsevier, Copyright 2023). (f) Mechanism diagram of micelles coupling various synergistic effects to achieve efficient photodegradation of BPA. ((f) Reproduced from ref. 232 with permission from Wiley-VCH, Copyright 2022). (g) Mechanism diagram of ultra-thin g-C_3N_4-coupled Cr(VI) reduction to achieve efficient photodegradation of ENO. ((g) Reproduced from ref. 278 with permission from Elsevier, Copyright 2022).

Open Access Article. Published on 24 January 2025. Downloaded on 11/7/2025 6:47:57 AM.
This article is licensed under a Creative Commons Attribution 3.0 Unported Licence.

separation and transfer of photogenerated carriers, further boosting photocatalytic performance (Fig. 16c). Zhang *et al.* prepared a novel donor–acceptor-type graphitic phase carbon nitride (D–A g-C_3N_4) to boost the photocatalytic degradation of bisphenol A (BPA) by an extended π-conjugation system. DFT calculations revealed that the extended π-conjugation system of D–A g-C_3N_4 enhances the π–π interactions between the catalyst and BPA molecules, which contributes to the adsorption of BPA and the electron transfer, thereby improving the photocatalytic degradation efficiency (Fig. 16d).[233] Song *et al.* enhanced the adsorption and photocatalytic degradation properties of tetracycline hydrochloride (TC) by modifying TPE-2Py on the surface of the metal–organic framework (MOF) MIL-125(Ti). π–π conjugation is a key factor in the adsorption of TC by TPE-2Py@DSMIL-125(Ti), which helps to enhance the material-TC molecular interactions, thereby improving the photocatalytic performance (Fig. 16e).[277] Wang *et al.* developed a perylene-based amphiphilic micelle for the efficient adsorption and photodecomposition of BPA in aqueous solutions. This micelle system exhibited an eightfold increase in BPA degradation efficiency compared to perylene nanorods. This enhancement is credited to the partially ordered stacking structure of perylene units formed through self-assembly within the micelle. This π–π stacking augments visible light absorption, catalytic ability, and cycling stability. Additionally, the micelle structure facilitates the production and separation of e^-–h^+ pairs in the photocatalytic reaction. The micelle's adsorption capacity for BPA is bolstered by hydrophobic interactions, hydrogen bonding, and π–π interactions (perylene units and BPA), enriching BPA molecules on the micelle surface and significantly boosting the degradation efficiency (Fig. 16f).[232] Zhang *et al.* investigated the mechanism of simultaneous removal of enoxacin (ENO) and hexavalent chromium (Cr(VI)) using ultrathin g-C_3N_4 during photocatalysis, highlighting the significant role of the antibiotic's molecular structure. DFT calculations indicated that ENO molecules preferentially adsorbed onto the surface of g-C_3N_4 by π–π interactions, facilitating crucial electron transfer and enhancing synergistic removal effects. These findings emphasize π–π interactions' decisive function in the photocatalytic elimination of pollutants and provide a theoretical foundation for designing and optimizing photocatalysts (Fig. 16g).[278]

8.1.2. Organic synthesis. π–π interactions play a vital role in photocatalytic organic synthesis by enhancing the concentration of substrates near the active sites of photocatalysts. This is achieved by promoting the adsorption and activation between substrates and photocatalysts, which, in turn, improve the reaction efficiency and selectivity. These interactions help stabilize the transition state of reactions, reduce activation energy, facilitate electron transfer, accelerate reaction rates, and increase product yields.[24,33,257,279–284] Specifically, π–π interactions exhibit high selectivity in the activation of aromatic or conjugated substrates, facilitating the synthesis of complex molecules. Additionally, these interactions enable the efficient conversion of substrates with various functional groups and support a range of photocatalytic reactions, including carbon–carbon bond constitution, carbon–heteroatom bond constitution, and redox reactions.[24,33,257,279–284] Shi *et al.* developed a two-dimensional sp^2 carbon-conjugated covalent organic framework (Por-sp^2c-COF) and synergistically combined it with a pyridine-anchored TEMPO cocatalyst (Fig. 17a), enhancing photocatalytic performance *via* π–π stacking. This configuration enables the pyridine moiety of the cocatalyst to intercalate within the Por-sp^2c-COF layers, boosting the efficiency of photoinduced hole transport and enhancing stability for selective sulfide to sulfoxide oxidation under 623 nm red LED irradiation (Fig. 17b). The photogenerated holes are effectively transferred to the TEMPO cocatalyst *via* π–π interactions, enhancing the photocatalytic activity. The HOMO state of the TEMPO portion is situated in the TEMPO moiety, while the LUMO state is focused on the COF, which suggests enhanced spatial charge separation. Electrons move from Por-sp^2c-COF to O_2 to generate $^{\bullet}O_2^-$, while holes are injected into pyridine-2-TEMPO to form a reversible transition state, facilitating the oxidation of sulfide to sulfoxide (Fig. 17c).[285] Liu *et al.* developed crystalline triazineimine polymers (PTI) featuring nitrile groups to boost the photocatalytic regeneration of nicotinamide cofactor (NADH) efficiency *via* π–π interactions.[170] The study highlighted that strong π–π interactions between the optimized PTI (D-PTI-350) and NADH facilitated charge transfer, achieving a NADH-to-NAD^+ conversion efficiency of 98.2% within 60 minutes. This performance substantially exceeded that of both the original PTI (88.1%) and amorphous poly carbon nitride (PCN, 56.8%) (Fig. 17d). This enhancement is attributed to the π-electron cloud of the aromatic ring in NADH, which promotes directional transport of photogenerated charges and ameliorates the energy conversion efficiency in the photo-enzymatic coupling system (Fig. 17e). The research presents a novel approach to designing photo-enzymatic catalytic systems for biological cofactor regeneration, leveraging extended π-conjugated systems and noncovalent π–π stacking interactions, thus offering fresh perspectives for covalent-dependent photo-enzymatic catalysis development.

8.1.3. Biomass reforming. In photocatalytic biomass reforming, π–π interactions have several advantages that contribute to the efficiency and selectivity of the process, some of which overlap with the photocatalytic organic synthesis part.[258,286] π–π interactions significantly enhance photocatalytic biomass conversion by improving substrate adsorption on the photocatalyst surface and concentrating molecules near active sites, leading to more efficient and selective reactions.[29,258] These interactions facilitate electron transfer, enhance hydrogenation or deoxygenation reaction efficiencies, lower activation energy, speed up reaction rates, and boost product yields.[244,286] Specifically, for biomass with aromatic or conjugated structures such as lignin, π–π interactions effectively activate these substrates, facilitating selective functionalization or depolymerization.[244,286] This capability enables photocatalysis to produce not only biofuels and platform chemicals but also high-value products, positioning π–π interactions as a key mechanism for enhancing biomass conversion under visible light. Xu *et al.* effectively synthesized S-type

Open Access Article. Published on 24 January 2025. Downloaded on 11/7/2025 6:47:57 AM.
This article is licensed under a Creative Commons Attribution 3.0 Unported Licence.

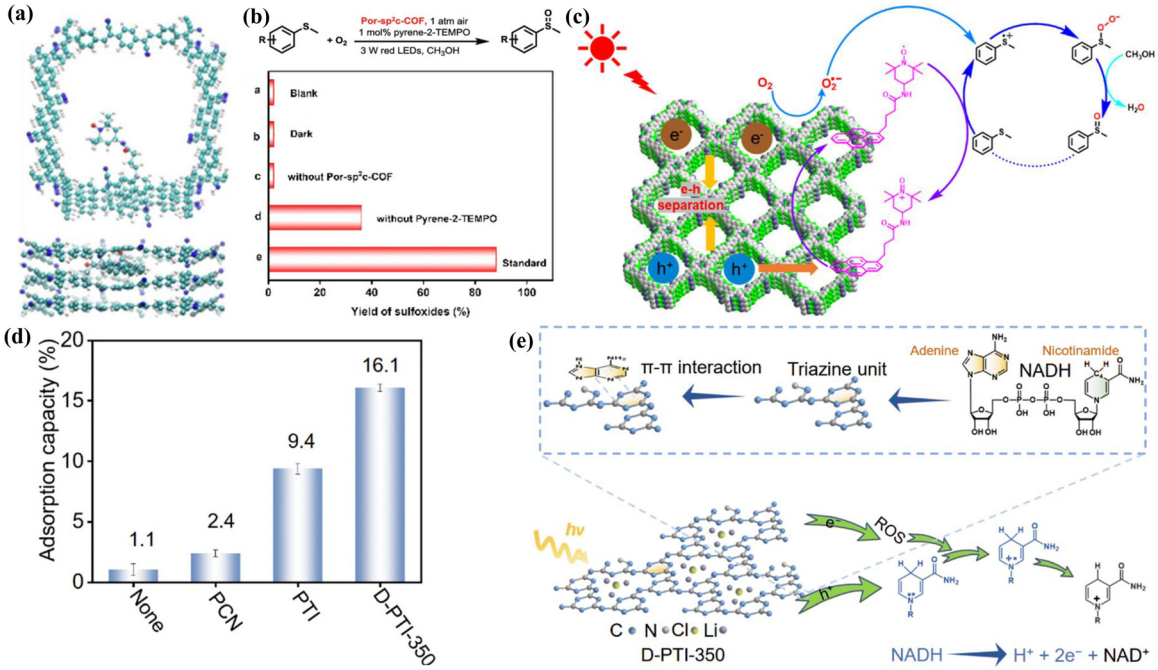

Fig. 17 (a) Theoretical calculation results of π–π interaction between Por-sp^{2}c-COF and pyrene-2-TEMPO. (b) Synergistic photocatalytic red light-induced selection of Por-sp^{2}c-COF and pyrene-2-TEMPO performance of selective aerobic oxidation of phenyl sulfide in different environments. (c) Reaction mechanism diagram of synergistic photocatalytic selective aerobic oxidation of phenyl sulfide by Por-sp^{2}c-COF and pyrene-2-TEMPO. ((a)–(c) Reproduced from ref. 285 with permission from Wiley-VCH, Copyright 2021). (d) Comparison of the NADH adsorption capacity of different samples under dark conditions. (e) Reaction mechanism diagram of D-PTI-350 photocatalytic oxidation of NADH. ((d) and (e) Reproduced from ref. 170 with permission from the Royal Society of Chemistry, Copyright 2024).

heterojunction photocatalysts of p-CN/P-PDI for efficient photocatalytic cleavage of a lignin model, using polyhedral oligomeric sesquisiloxanes (POSS) at both ends of PDI. The incorporation of POSS strengthens the π–π interactions with p-CN, promoting the formation of stable heterojunctions. At the same time, due to the π–π interaction between certain aromatic molecules present in the β-O-4 model and the electron-rich p-CN, this would contribute to molecular activation. As demonstrated in Fig. 18a and b, p-CN/p-PDI-3 accomplished more than 99% conversion of lignin β-O-4 model molecules with 96% C–C bond selectivity. This high efficiency is primarily due to the crucial roles of photogenerated h^+ and reactive oxygen species (ROS) in the photocatalytic oxidization process (Fig. 18c). By enhancing the π–π interaction between different materials and the π–π interaction between materials and lignin model molecules, this study provides a new idea for designing efficient photocatalytic polymerization models of activated and depolymerized lignin.[107] Li *et al.* enhanced the photocatalytic efficiency of carbon nitride (g-C_3N_4-Cl-A5) by means of Cl doping and high-temperature oxidation, significantly boosting the cleavage of lignin's β-O-4 bond and increasing the yield of benzaldehyde (1.74 mg h^{-1}) (Fig. 18d). This enhancement was credited to the superoxide radicals' heightened generation and the improved efficiency of photogenerated electron transport. The π–π conjugated planar constitution of g-C_3N_4 facilitated the adsorption of benzene rings from lignin by π–π stacking. This noncovalent interaction enhanced the targeted transport of photogenerated charges and increased the energy conversion efficiency, contributing to the superior photocatalytic performance.[29] Liu *et al.* discovered that the mesoporous graphitic carbon nitride (mpg-C_3N_4) photocatalyst also formed the favorable π–π interactions with the lignin model molecule, finally realizing 90% conversion rate of the lignin model molecule through photocatalytic oxidation under visible light (cleavage of the C–C structure: β-O-4 and β-1 bonds) (Fig. 18e).[244]

8.2. π–π interaction: the photocatalyst itself and the synergy between different photocatalysts

Although reactants such as water and CO_2 do not have aromatic structures, the aromatic or conjugated structures contained in the photocatalyst can stabilize the active center of the catalyst through π–π interaction and improve the catalytic efficiency. Therefore, even if the reactants themselves do not participate in the π–π interaction, this interaction still plays a key role in the photocatalysis process, mainly by regulating the properties of the catalyst to affect the reaction efficiency and selectivity.

8.2.1 Water splitting. In the photocatalytic water splitting reaction, which employs sunshine to convert water into hydrogen and oxygen, π–π interactions contribute to the efficiency and effectiveness of the process.[42,287] π–π interactions boost photocatalytic water splitting primarily by establishing a built-in electric field, modifying the interfacial electron density of composite materials to enhance charge separation, lowering

Open Access Article. Published on 24 January 2025. Downloaded on 11/7/2025 6:47:57 AM.
This article is licensed under a Creative Commons Attribution 3.0 Unported Licence.

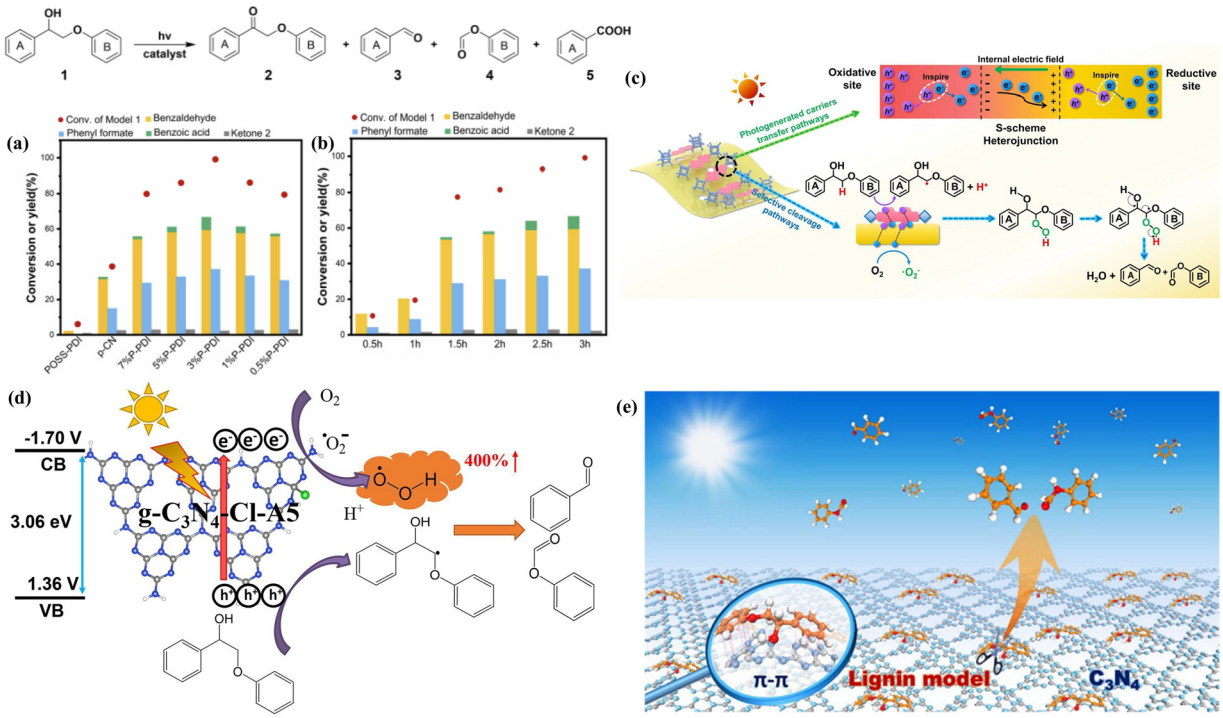

Fig. 18 (a) Conversion of 1 using p-CN/P-PDI with different POSS-PDI contents in 3 h. (b) Conversion of 1 using p-CN/P-PDI-3 in different irradiation times. Reaction conditions: 10 mg of catalyst, 1 mL of CH_3CN, 0.006 mmol of substrate 1, Xe lamp (300 W), O_2 (1 atm). (c) Reaction mechanism for the photocatalytic selective cleavage of β-O-4 model compound on p-CN/P-PDI S-type heterojunction. ((a)–(c) Reproduced from ref. 107 with permission from Wiley-VCH, Copyright 2023). (d) Mechanism diagram of g-C_3N_4-Cl-A5 photocatalytic decomposition of lignin model compounds. ((d) Reproduced from ref. 29 with permission from Elsevier, Copyright 2023). (e) Schematic of the mechanism of selective conversion of lignin model compounds by mesoporous carbon nitride. ((e) Reproduced from ref. 244 with permission from the American Chemistry Society, Copyright 2018).

the reaction energy barriers associated with hydrogen evolution, and facilitating proton transfer.[155,162,194,249,273,288] Through π–π interactions, PTCDA and PTA formed a close-contact heterostructure by face-to-face arrangement at the molecular level, which strengthened the electron communication between PTA and PTCDA. Fig. 19a demonstrates that the PTCDA/PTA heterostructure exhibits much higher photocatalytic hydrogen production rate (45.06 mmol g^{-1} h^{-1}) than PTA and PTCDA alone. The calculation results in Fig. 19b show that the LUMO of PTCDA/PTA at the interface is distributed on the PTA, while the HOMO is principally located on the PTCDA, indicating that PTA and PTCDA serve as an electron donor and electron acceptor, respectively. Fig. 19c reveals that the particular asymmetric planar structure formed *via* π–π stacking increases the dipole moment to generate a giant internal electric field, which significantly facilitates the separation and migration of photogenerated charges.[249] π–π interactions also promote the transport of photogenerated electrons from ZnCd-ZIF-8 to GO, enhancing the charge separation efficiency and thereby significantly improving the photocatalytic hydrogen production efficiency (Fig. 19d and e).[193] Additionally, π–π interactions help the self-organization of the thiophene-based trimers (TBTs) to form ordered structures and tight stacking, which increases the π–π orbital overlap and thus affects the size and crystallinity of the aggregates. TBTs with tuned aggregation *via* methyl side-chain engineering with small size and higher crystallinity have more surface-active sites, shortened charge transfer distance, and fewer charge recombination centers, exhibiting remarkably improved photocatalytic activity for hydrogen generation (Fig. 19f–h).[289]

In addition to hydrogen production reactions, π–π interactions have also demonstrated promising applications in photocatalytic oxygen evolution and total water splitting. Strong interfacial π–π interactions can push the spontaneous adsorption of perylene diimide polymer (PDIP) onto carbon paper (CP), resulting in the redistribution of interfacial electrons, constitution of built-in electric field, narrowing of the band gap, downward shift of valence band edges, and prolongation of photogenerated charge carrier lifetime. The constructed PDIP/CP photocatalyst displays considerable boosted photocatalytic water oxidization activity (Fig. 20a and b).[290] A conceivable mechanism of the PDIP/CP photocatalyst sheet was recommended (Fig. 20c): the PDIP generates photogenerated e^- and h^+ through visible light excitation; the photogenerated e^- move to the CP that is forced through the built-in electric field and are eaten through Ag^+ ions' reduction; meantime, photogenerated h^+ immediately oxidizes adsorbed water molecules to generate oxygen molecules. Moreover, π–π interactions can collaborate with metal ligands to construct *via* self-assembly nanorods (NRs) of peroxydimethylene diimide (PDI), which demonstrates an excellent photocatalytic oxygen production performance of CuPDI-Hm (25 900 μmol g^{-1} h^{-1}), owing to

Open Access Article. Published on 24 January 2025. Downloaded on 11/7/2025 6:47:57 AM.
This article is licensed under a Creative Commons Attribution 3.0 Unported Licence.

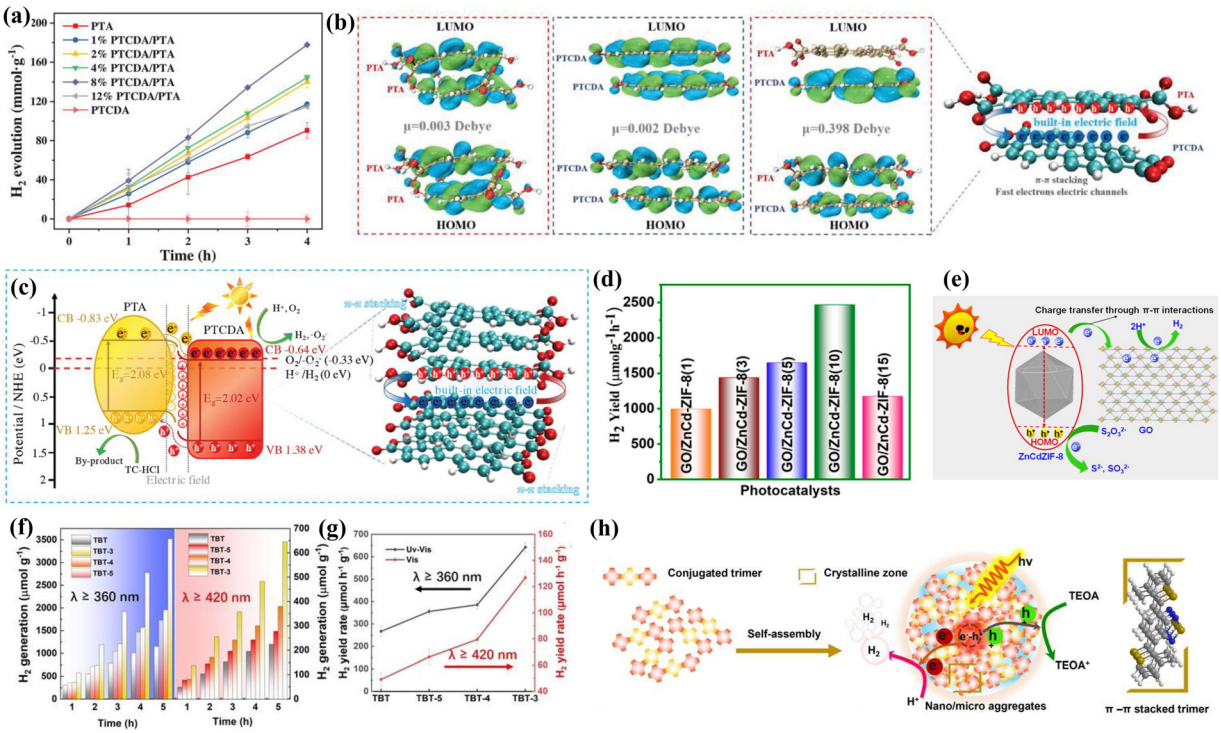

Fig. 19 (a) Photocatalytic H_2 evolution performance of distinct samples underneath simulated sunlight irradiation. (b) Frontier molecular orbital distribution and dipole moment within different materials and within stacked units between each other. (c) Schematic of the charge transfer mechanism on PTCDA/PTA photocatalyst. ((a)–(c) Reproduced from ref. 249 with permission from Wiley-VCH, Copyright 2023). (d) Performance of photocatalytic hydrogen production of different GO/ZnCd-ZIF-8 samples. (e) Mechanism diagram of GO/ZnCd-ZIF-8 improving photocatalytic hydrogen production through π–π interaction. ((d) and (e) Reproduced from ref. 193 with permission from the American Chemistry Society, Copyright 2024). (f) Performance of photocatalytic hydrogen production from aggregates under UV-visible light and visible light irradiation. (g) Comparison of photocatalytic hydrogen production rates of different aggregates under UV-visible light and visible light. (h) Microaggregate synthesis process and possible photocatalytic hydrogen production mechanism. ((f)–(h) Reproduced from ref. 289 with permission from Wiley-VCH, Copyright 2024).

the optimized molecular alignment, built-in electric fields, and improved charge separation efficiency (Fig. 20d and e).[291] However, excessively strong π–π interactions may be detrimental to photocatalytic water splitting because it may lead to close packing of molecules or layers, resulting in strong intermolecular forces that hinder the separation and transport of photogenerated charge carriers. By optimizing the π–π stacking interactions by changing the conjugation system of g-C_3N_4 and providing more channels for charge and mass transfer by forming a large number of in-plane holes, alkali treatment can enhance the activity of photocatalytic water decomposition over Pt/CQDs/CN (B) by 24.6 times (Fig. 20f–h). This means that a suitable π–π interaction strength is critical for photocatalysis in these π–π conjugated systems.[292]

8.2.2. H_2O_2 generation. In photocatalytic hydrogen peroxide (H_2O_2) generation, π–π interactions offer several advantages that contribute to the efficiency and effectiveness of the process.[90,293] In addition to the general benefits of π–π interactions in photocatalytic systems (such as enhancing charge separation, promoting electron transfer, increasing the utilization of visible light, and improving catalyst stability), these interactions offer unique advantages including the selective adsorption and activation of oxygen molecules.[294,295] Essentially, this interaction helps to align the reactant molecules more effectively at the photocatalyst surface, optimizing the reaction conditions for H_2O_2 production. Shan *et al.* substantially ameliorated the photocatalytic H_2O_2 generation performance through introducing a small amount of dopamine (PDA) between carboxylated cellulose nanofibers (CNFs) and graphitic carbon nitride (CN) to form a composite material with an extended hydrogen-bond/π-bond network (CN/CNF_P, Fig. 21a).[294] Fig. 21b and d demonstrate that CN/CNF_P exhibits excellent photocatalytic H_2O_2 generation performance, optimally up to 130.7 μmol L^{-1} h^{-1}, which is a great deal more excellent than that of CN/CNF (75.2 μmol L^{-1} h^{-1}) and original CN (20.2 μmol L^{-1} h^{-1}). Such improvement was mainly attributed to the enhanced O_2 adsorption capacity of CNF_P (a composite of dopamine and CNF) *via* multiple π–π stacking effect/hydrogen bonding with CN, and the enhanced photogenerated charge transport and separation efficiency, which facilitated the superior photocatalytic H_2O_2 production (Fig. 21e). Guo *et al.* developed PDA@BCN S-type heterostructures by incorporating 3,4,9,10-perylene tetracarboxylic dianhydride (PTCDA) into BCN, significantly enhancing light absorption through π–π stacking interactions and achieving a H_2O_2 yield of up to 285.47 μmol h^{-1} g^{-1}. The π–π stacking interactions between PTCDA and BCN are the primary driving force for the formation of the PDA@BCN heterostructures,

Open Access Article. Published on 24 January 2025. Downloaded on 11/7/2025 6:47:57 AM.
This article is licensed under a Creative Commons Attribution 3.0 Unported Licence.

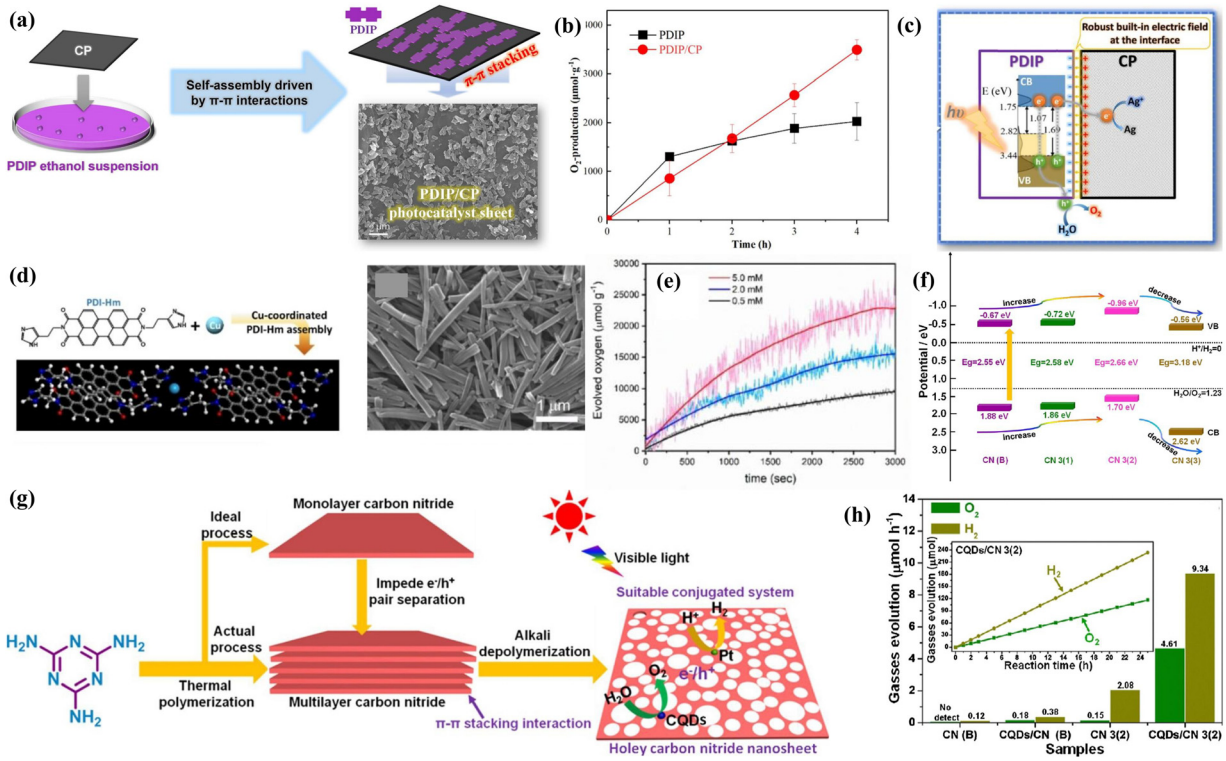

Fig. 20 (a) Schematic of the preparation process of PDIP/CP photocatalyst. (b) Comparative effect of photocatalytic oxygen production performance of PDIP and PDIP/CP. (c) Photocatalytic oxygen production mechanism diagram of PDIP/CP composite material. ((a)–(c) Reproduced from ref. 290 with permission from Elsevier, Copyright 2024). (d) Schematic of PDI-Hm assembly connected through Cu-imidazole coordination and SEM image of crystallized CuPDI-Hm nanorods, (e) photocatalytic production of CuPDI-Hm nanorods at different $AgNO_3$ concentrations. ((d) and (e) Reproduced from ref. 291 with permission from Wiley-VCH, Copyright 2023). (f) Energy band structure diagrams of different samples. (g) Synthetic routes of different CN samples and mechanism diagrams of their photoreaction processes. (h) Performance of photocatalytic total water splitting of different CN and CQDs/CN composite materials. ((f)–(h) Reproduced from ref. 292 with permission from Elsevier, Copyright 2018).

facilitating the generation and efficient separation of photogenerated carriers under the visible light. Additionally, the S-type heterostructure between PTCDA and BCN optimizes charge transport and separation, further boosting the photocatalytic production of H_2O_2 (Fig. 21f).[295] Yang *et al.* constructed composites of polyaniline (PANI) and g-C_3N_4 to achieve efficient photocatalytic H_2O_2 production.[296] This was primarily owing to the forceful π–π interactions between the tri-*s*-triazine units in the g-C_3N_4 structure and PANI that helped to reduce charge recombination and enhance electron transport, which were crucial for H_2O_2 generation (Fig. 21g). In conclusion, π–π interactions played a key role in this study, which not only facilitated electron transport and separation, but also contributed to the enhancement of light absorption and conductivity of the photocatalytic materials, which significantly improved the photocatalytic H_2O_2 generation efficiency.

8.2.3. Carbon dioxide reduction. Photocatalytic carbon dioxide (CO_2) reduction is an effective way to convert solar energy into sustainable energy, wherein the selection of photocatalytic materials plays a crucial role. In recent years, π–π interactions are discovered to play a tremendous role in photocatalytic CO_2 reduction.[297–304] π–π interactions optimize the electron transfer efficiency and reaction selectivity in the photocatalytic CO_2 reduction process primarily by constructing directional built-in electric fields, influencing intramolecular and intermolecular conjugation, forming carrier transmission channels, and accelerating the transfer of photoexcited electrons.[150,218,299,305] Hierarchical π–π interactions enable the self-assembly of metal–organic layers to form a quadruple π-bonded metal–organic layer (πMOL) with a tessellated lattice of about 1.0 nm thickness (Fig. 22a), on which the catalytic selectivity at individual metal sites could be controlled for efficient CO_2 reduction reactions (CO_2RRs) and hydrogenolysis reactions (HERs).[306] In saturated CO_2 acetonitrile aqueous solutions, Fe-πMOL achieved an efficient CO_2RR with a yield of about 3.98 mmol g^{-1} h^{-1} and a selectivity of 91.7% towards CO. In contrast, isomeric Co-πMOL as well as mixed-metal FeCo-πMOL exhibited excellent activity toward the HER under similar conditions (Fig. 22b). This was mainly attributed to the π–π interactions contributing to the uniform distribution of monometallic active sites in the 2D MOLs and the facilitated electron transfer *via* spatial electron transport pathways, which were essential for the improvement of the photocatalytic efficiency (Fig. 22c). The π–π interaction-driven formation of the heterojunction between 2D carbon nitride (2D CN) and a covalent organic framework based on triazine (COF-TD) accelerates charge carriers' migration and consequently improves the production of CO (Fig. 22d and e).[307] π–π interactions,

Open Access Article. Published on 24 January 2025. Downloaded on 11/7/2025 6:47:57 AM.
This article is licensed under a Creative Commons Attribution 3.0 Unported Licence.

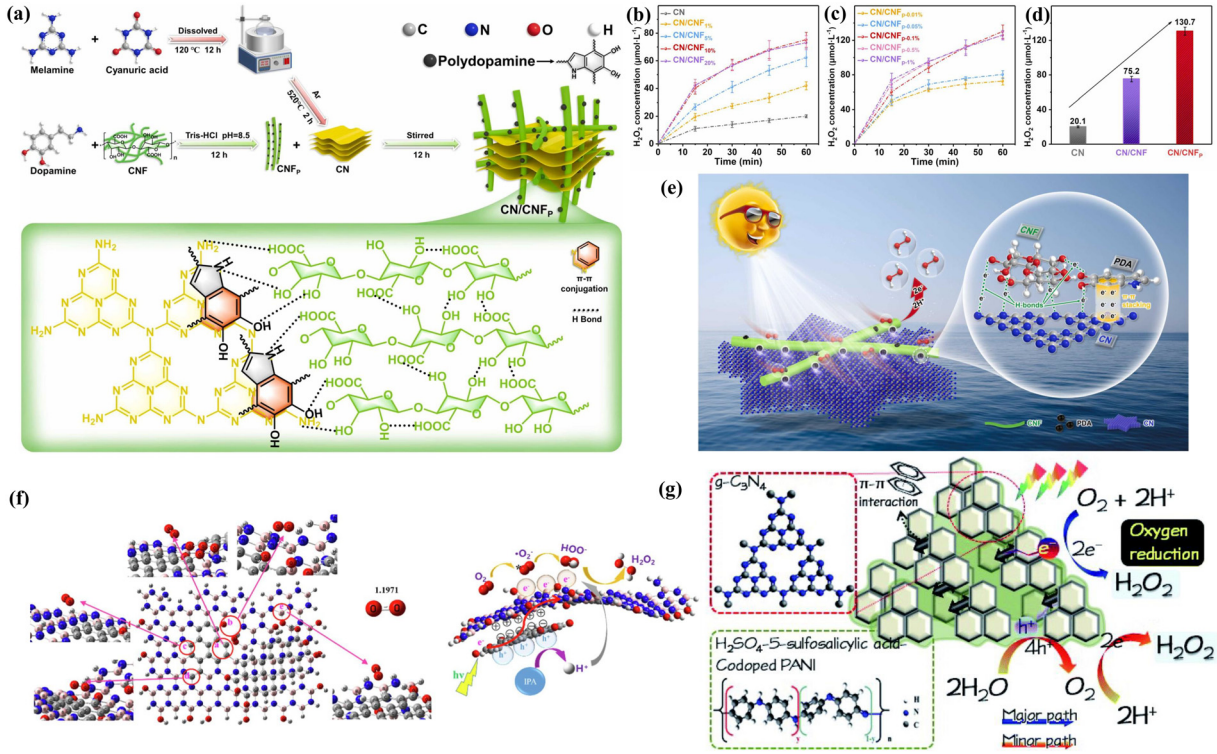

Fig. 21 (a) Synthesis process of CN/CNF$_P$ composite materials and the types of effects involved. (b) Photocatalytic production of H_2O_2 from distinct CN/CNF composites. (c) Photocatalytic production of H_2O_2 from distinct CN/CNF$_P$ composites. (d) Comparison of photocatalytic production of H_2O_2 by CN, CN/CNF and CN/CNF$_P$. (e) Reaction mechanism diagram of photocatalytic production of H_2O_2 by CN/CNF$_P$. ((a)–(e) Reproduced from ref. 294 with permission from Elsevier, Copyright 2024). (f) Mechanism chart of photocatalytic synthesis of H_2O_2 by the PDA@BCN composite constructed through π–π interaction. ((f) Reproduced from ref. 295 with permission from Elsevier, Copyright 2023). (g) Mechanism diagram of PANI/CN photocatalytic synthesis of H_2O_2. ((g) Reproduced from ref. 296 with permission from the Royal Society of Chemistry, Copyright 2020).

together with H-bonding, led to a close-contact Z-type heterojunction between ZnPc and PDI, which greatly enhanced the photogenerated charge transport and separation for the conversion of carbon dioxide (CO_2) into solar fuel (Fig. 22f).[99] π–π interactions between 4,4′-diaminostyrene-2,2′-disulfonic acid (DAS) and 4,4′-dinitrostyrene-2,2′-disulfonic acid disodium salt (DNS) in a parallel molecule arrangement promote the transfer of photoexcited electrons to the host anions when co-intercalated in Ni_2Mn-LDHs, to participate in CO_2 reduction, while the photogenerated holes are transferred to the HOMO of the guest anion to oxidize H_2 to release H_2O (Fig. 22g).[308] Wang *et al.* constructed a molecular model to study the π–π interaction between the photosensitizer and the catalyst by introducing pyridine groups between them. This design strategy enhanced the interaction between the photosensitizer and the catalyst. The coplanar π–π interaction between IrPPPY and Co-PYN5 enabled the photocatalytic CO_2-to-CO conversion with an excellent apparent quantum efficiency of 14.3 ± 0.8% and a high selectivity of 98%. This is mainly due to the speedy transport of the excited-state electrons from photoexcited IrPPPY to Co-PYN5 *via* coplanar π–π interactions, generating oxidized IrPPPY and one-electron-reduced Co-PYN5. This process significantly improves the performance of photocatalytic CO_2 reduction (Fig. 22h).[218] In general, the electron transfer channel constructed by π–π interaction is conducive to the efficient and selective photoreduction of CO_2.

9. Summary and prospects

This review primarily delineates the utilization of π–π interactions within photocatalytic systems, elucidating the various categories and detection techniques for π–π interactions. It also presents an overview of the prevalent photocatalysts capable of engaging in π–π interactions, detailing their types and operational mechanisms. This review further examines the influence of π–π interactions on the characteristics of photocatalysts and the overall photocatalytic system. Moreover, it highlights numerous strategies that have been engineered to augment photocatalytic efficiency *via* π–π interactions. Additionally, this review acknowledges the promising outcomes of π–π interactions in diverse photocatalytic application frameworks. While π–π interactions offer significant benefits in the realm of photocatalysis, this review also addresses the challenges encountered in their practical application and looks forward to their prospects. The following are the challenges and prospects of π–π interactions for photocatalysis:

(1) Consistently reproducing the desired π–π interactions at an appropriate level in different batches of photocatalysts may

Open Access Article. Published on 24 January 2025. Downloaded on 11/7/2025 6:47:57 AM.
This article is licensed under a Creative Commons Attribution 3.0 Unported Licence.

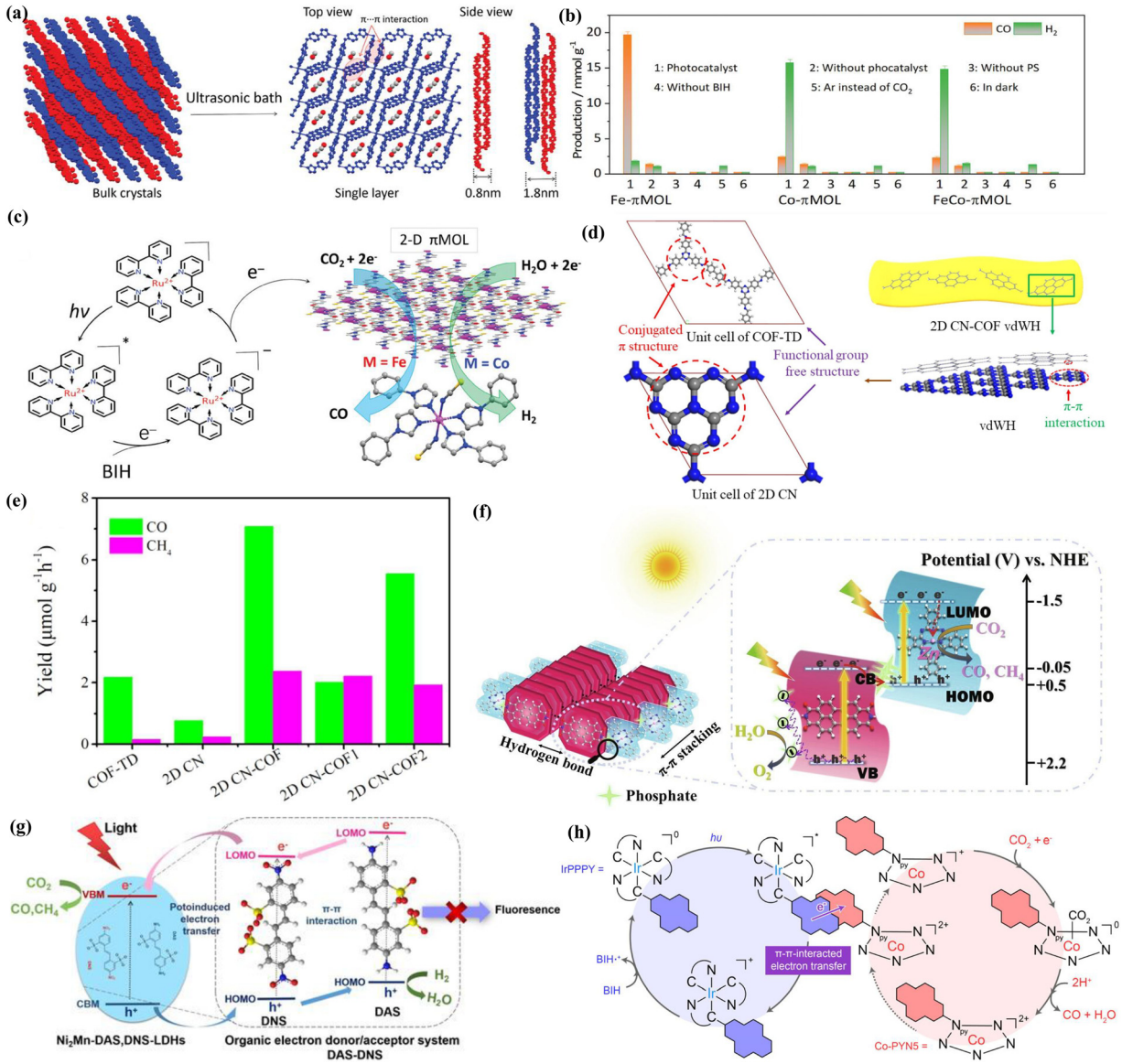

Fig. 22 (a) Schematic of the formation of a single layer of πMOL through solvent-assisted exfoliation. (b) Comparison of the experimental results of the photocatalytic CO_2/H_2O reduction activity of Co-πMOL, Fe-πMOL, and FeCo-πMOL. (c) Photocatalytic reduction of the studied FeCo-πMOL electron transfer pathways for CO_2 and H_2O. ((a)–(c) Reproduced from ref. 306 with permission from Wiley-VCH, Copyright 2023). (d) Composite material formed by COF-TD and 2D CN through π–π interaction. (e) Comparison of the yield effects of photoreduction of CO_2 to CO/CH_4 for distinct 2D CN-COF samples. ((d) and (e) Reproduced from ref. 307 with permission from Elsevier, Copyright 2021). (f) Mechanism chart of ZnPc/P-PDI's CO_2 photoreduction. ((f) Reproduced from ref. 99 with permission from Elsevier, Copyright 2021). (g) Mechanism diagram of Ni_2Mn-LDHs-DAS, DNS constructed through π–π interaction for the photoreduction of CO_2. ((g) Reproduced from ref. 308 with permission from Wiley-VCH, Copyright 2021). (h) Mechanism diagram of IrPPPY/Co-PYN5 photoreduction of CO_2 to generate CO. ((h) Reproduced from ref. 218 with permission from the American Chemistry Society, Copyright 2022).

be a challenge. Achieving precise control over the assembly of π-conjugated systems to ensure optimal π–π interactions remains a challenge. Therefore, the standardization of synthetic methods and improved characterization techniques is essential to enhance the reproducibility of π–π interactions in photocatalytic materials aiming to achieve a better control of the arrangement of aromatic units. The design of photocatalysts with specific π–π interactions can be tailored by adjusting the energy level to match with the energy of the incident photon, thus enabling the customized design of photocatalytic materials. Among them, organic/conjugated photocatalysts provide highly controllable π–π interactions due to their strong designability, which can significantly improve the selectivity, efficiency and stability of photocatalytic systems. By adjusting the intensity and arrangement of the π–π interaction, the photocatalytic reaction path can be accurately controlled, the reaction efficiency can be optimized and the stability of the catalyst can be enhanced. Although the regulation of π–π

Open Access Article. Published on 24 January 2025. Downloaded on 11/7/2025 6:47:57 AM.
This article is licensed under a Creative Commons Attribution 3.0 Unported Licence.

interaction still faces certain challenges, through molecular design and novel synthesis methods, these problems can be overcome and the performance of photocatalytic materials can be further improved, and the development of photocatalytic technology can be promoted.

(2) Tuning the strength of π–π interactions to achieve the desired balance between stability and reactivity is a challenge. We need to understand the factors that affect the strength of the interactions and employ computational methods that can help fine-tune the π–π interactions for specific applications. Prolonged exposure to light and harsh reaction conditions may lead to degradation of the π-conjugated system and affect the stability of the photocatalyst. The introduction of stabilizing groups or protective layers can improve the photostability of π–π interactions in photocatalytic materials. The rational construction of cocatalysts is an effective strategy to swiftly transfer photogenerated charge carriers from the bulk to the surface and then to the reactants, thus reducing the photocorrosion. Moreover, appropriate choice of the reaction medium including the solvent, pH and gas atmosphere as well as suitable sacrificial reagents will benefit the stability of these photocatalysts.

(3) Optimizing π–π interactions enables the development of photocatalysts that exhibit tailored selectivity and enhanced efficiency, facilitating precise manipulation of intricate organic transformations, including selective oxidation, reduction, and isomerization. In multi-stage photocatalytic processes, fine-tuning these interactions can steer reaction trajectories towards achieving high selectivity and product yields, exemplified by the targeted synthesis of specific compounds in photocatalytic systems. The rational design of photocatalytic systems can improve the selectivity by precisely controlling the molecular structure and electronic properties, which allows us to optimize the redox ability of the catalyst, free radical generation, and adsorption configuration of the reactants. It is very promising to design photocatalysts for different applications to realize the versatility of π–π interactions in photocatalysis. Combining π–π interactions with other types of interactions (*e.g.*, hydrogen bonding or metal–ligand interactions) may also be an effective strategy.

(4) *In situ* and *operando* characterization techniques such as infrared spectroscopy, Raman spectroscopy, nuclear magnetic resonance, transient absorption spectroscopy, X-ray diffraction, and electron microscopy (TEM and SEM) are poised to significantly advance our understanding of π–π interactions in materials science. These techniques allow for real-time monitoring and detailed analysis at the molecular level, which is crucial for revealing the characteristics, vibrational modes, electron transfers, interaction strengths, and changes in crystal structure associated with π–π stacking in organic semiconductors, carbon-based materials, MOFs, and COFs. As these methods evolve, they will provide a robust scientific basis for the comprehensive study of π–π interactions, furthering material design and optimization.

(5) In future research, the combined use of density functional theory (DFT) and machine learning (ML) is expected to significantly accelerate new photocatalyst discovery and also enhance the exploration of the mechanisms underlying π–π interactions. DFT will provide essential insights into the energy, geometric configuration, and electronic distribution of π–π interactions by accurately simulating the electronic structures of molecules. It will also optimize the geometric structures of stacked assemblies to elucidate electronic mechanisms. Concurrently, ML will expedite DFT calculations through data-driven predictive models, identify the characteristics of π–π interactions, and facilitate the screening of potential molecules from extensive molecular libraries. This integrated application of DFT and ML will profoundly advance the understanding of π–π interactions, accelerate the development of novel materials and catalysts, and bolster research in materials science and chemistry.

In conclusion, while there are challenges in exploiting and optimizing π–π interactions in photocatalysis, ongoing research and advances in materials science, synthesis techniques, and characterization methods offer promising prospects for addressing these challenges and unlocking the full potential of π–π interactions in photocatalysis.

Data availability

No primary research results, software or code have been included and no new data were generated or analysed as part of this review.

Conflicts of interest

There are no conflicts to declare.

Acknowledgements

This research was financially sustained through the Natural Sciences and Engineering Research Council of Canada-Discovery Grant (Canada).

Notes and references

1 W. Zhang, W. Huang, B. Wu, J. Yang, J. Jin and S. Zhang, *Coord. Chem. Rev.*, 2023, **491**, 215235.
2 A. Chawla, A. Sudhaik Sonu, P. Raizada, T. Ahamad, Q. V. Le, V.-H. Nguyen, S. Thakur, A. K. Mishra, R. Selvasembian and P. Singh, *Coord. Chem. Rev.*, 2023, **491**, 215246.
3 V. Thakur, S. Singh, P. Kumar, S. Rawat, V. Chandra Srivastava, S.-L. Lo and U. Lavrenčič Štangar, *Chem. Eng. J.*, 2023, **475**, 146100.
4 M. Wang, H. Yu and K. Yu, *Chem. Eng. J.*, 2023, **470**, 144100.
5 L. Jing, Y. Xu, M. Xie, Z. Li, C. Wu, H. Zhao, N. Zhong, J. Wang, H. Wang, Y. Yan, H. Li and J. Hu, *Small*, 2024, **20**, 2304404.

Open Access Article. Published on 24 January 2025. Downloaded on 11/7/2025 6:47:57 AM.
This article is licensed under a Creative Commons Attribution 3.0 Unported Licence.

6 I. Ahmad, Y. Zou, J. Yan, Y. Liu, S. Shukrullah, M. Y. Naz, H. Hussain, W. Q. Khan and N. R. Khalid, *Adv. Colloid Interface Sci.*, 2023, **311**, 102830.
7 H. Huang, L. Jiang, J. Yang, S. Zhou, X. Yuan, J. Liang, H. Wang, H. Wang, Y. Bu and H. Li, *Renewable Sustainable Energy Rev.*, 2023, **173**, 113110.
8 Y. Sun, Y. Ahmadi, K.-H. Kim and J. Lee, *Renewable Sustainable Energy Rev.*, 2022, **170**, 112967.
9 S. Naghdi, M. M. Shahrestani, M. Zendehbad, H. Djahaniani, H. Kazemian and D. Eder, *J. Hazard. Mater.*, 2023, **442**, 130127.
10 F. Deng, J. Peng, X. Li, X. Luo, P. Ganguly, S. C. Pillai, B. Ren, L. Ding and D. D. Dionysiou, *J. Clean. Prod.*, 2023, **416**, 137957.
11 P. Bhavani, D. Praveen Kumar, J. Suk Yoo, M. Hussain, S. Weon, W. Kim and Y.-K. Park, *Chem. Eng. J.*, 2023, **467**, 143429.
12 I. Ahmad, A. Idrees, N. S. Alatawi, S. B. Ahmed, M. Shaban and Y. Y. Ghadi, *Adv. Colloid Interface Sci.*, 2023, **321**, 103032.
13 L. Jing, Y. Xu, M. Xie, Z. Li, C. Wu, H. Zhao, J. Wang, H. Wang, Y. Yan, N. Zhong, H. Li and J. Hu, *Nano Energy*, 2023, **112**, 108508.
14 Z. Li, L. Zhang, Y. Liu, C. Shao, Y. Gao, F. Fan, J. Wang, J. Li, J. Yan, R. Li and C. Li, *Angew. Chem., Int. Ed.*, 2020, **59**, 935–942.
15 Z. Li, R. Li, H. Jing, J. Xiao, H. Xie, F. Hong, N. Ta, X. Zhang, J. Zhu and C. Li, *Nat. Catal.*, 2023, **6**, 80–88.
16 J. Yang, D. Wang, H. Han and C. Li, *Acc. Chem. Res.*, 2013, **46**, 1900–1909.
17 R. Yang, Y. Fan, Y. Zhang, L. Mei, R. Zhu, J. Qin, J. Hu, Z. Chen, Y. Hau Ng, D. Voiry, S. Li, Q. Lu, Q. Wang, J. C. Yu and Z. Zeng, *Angew. Chem., Int. Ed.*, 2023, **62**, e202218016.
18 J. Li, L. Zhu, C.-H. Tung and L.-Z. Wu, *Angew. Chem., Int. Ed.*, 2023, **62**, e202301384.
19 M. Z. Rahman, F. Raziq, H. Zhang and J. Gascon, *Angew. Chem., Int. Ed.*, 2023, **62**, e202305385.
20 Y. Shi, Z. Zhao, D. Yang, J. Tan, X. Xin, Y. Liu and Z. Jiang, *Chem. Soc. Rev.*, 2023, **52**, 6938–6956.
21 X. Tao, Y. Zhao, S. Wang, C. Li and R. Li, *Chem. Soc. Rev.*, 2022, **51**, 3561–3608.
22 W. Liu, C. He, S. Huang, K. Zhang, W. Zhu, L. Liu, Z. Zhang, E. Zhu, Y. Chen, C. Chen and Y. Zhu, *Angew. Chem., Int. Ed.*, 2023, **62**, e202304773.
23 S. Liu, Q. Chen, Y. Chen, P. Lin, H. Zhuzhang, M. Han, Z.-A. Lan, X. Chen, X. Wang, Q. Li and Z. Li, *J. Mater. Chem. A*, 2023, **11**, 14682–14689.
24 P. Das, J. Roeser and A. Thomas, *Angew. Chem., Int. Ed.*, 2023, **62**, e202304349.
25 P.-D. Liu, Y. Chen, A.-G. Liu, Z.-T. Chen and B. Li, *J. Mater. Chem. A*, 2023, **11**, 25322–25331.
26 X. Gong, F. Ma, Y. Zhang, Y. Li, Z. Wang, Y. Liu, P. Wang, H. Cheng, Y. Dai, Y. Fan, B. Huang and Z. Zheng, *ACS Catal.*, 2023, **13**, 12338–12349.
27 K. Zhang, L. Wang, Y. Hong, X. Duan, C. Ai, L. Zhang, T. Zhang, Y. Chen, X. Lin, W. Shi and F. Guo, *J. Alloys Compd.*, 2023, **966**, 171580.
28 M. K. T. Chee, B.-J. Ng, W.-K. Chong, L.-L. Tan, W. S. Chang and S.-P. Chai, *ACS Appl. Energy Mater.*, 2023, **6**, 7935–7943.
29 X. Li, G. Fang, T. Wu, Q. Tian, Q. Yang and Z. Chen, *Appl. Surf. Sci.*, 2023, **635**, 157717.
30 S. S. Zhao, J. Liang, D.-H. Si, M.-J. Mao, Y. B. Huang and R. Cao, *Appl. Catal., B*, 2023, **333**, 122782.
31 Z. Liu, S. Yao, A. Zhang, Y. Li, Y. Fu and Q. Zhou, *Appl. Catal., B*, 2023, **338**, 123023.
32 J.-Y. Tang, C.-C. Er, X. Y. Kong, B.-J. Ng, Y.-H. Chew, L.-L. Tan, A. R. Mohamed and S.-P. Chai, *Chem. Eng. J.*, 2023, **466**, 143287.
33 X. Bai, M. She, Y. Ji, Z. Zhang, W. Xue, E. Liu, K. Wan, P. Liu, S. Zhang and J. Li, *Adv. Sci.*, 2023, **10**, 2207250.
34 M. A. Hamza, S. A. Rizk, E.-E. M. Ezz-Elregal, S. A. A. El-Rahman, S. K. Ramadan and Z. M. Abou-Gamra, *Sci. Rep.*, 2023, **13**, 12929.
35 Z. Mou, Y. Dong, S. Li, Y. Du, X. Wang, P. Yang and S. Wang, *Int. J. Hydrogen Energy*, 2011, **36**, 8885–8893.
36 Y.-Q. Xing and S.-Y. Liu, *Chin. J. Struct. Chem.*, 2022, **41**, 2209056–2209068.
37 F. Jin, B. Yang, X. Wang, T. Li, N. Tsubaki and Z. Jin, *Chin. J. Struct. Chem.*, 2023, **42**, 100198.
38 J. Wang, Z. Wang, J. Zhang and K. Dai, *Chin. J. Struct. Chem.*, 2023, **42**, 100202.
39 W.-R. Zhuang, Y. Wang, P.-F. Cui, L. Xing, J. Lee, D. Kim, H.-L. Jiang and Y.-K. Oh, *J. Controlled Release*, 2019, **294**, 311–326.
40 T. Chen, M. Li and J. Liu, *Cryst. Growth Des.*, 2018, **18**, 2765–2783.
41 E. M. Pérez and N. Martín, *Chem. Soc. Rev.*, 2015, **44**, 6425–6433.
42 Y. Liu, H. Wu and Q. Wang, *J. Mater. Chem. A*, 2023, **11**, 21470–21497.
43 J. Ji, X. Wei, W. Wu and C. Yang, *Acc. Chem. Res.*, 2023, **56**, 1896–1907.
44 S. J. Olusegun, T. G. F. Souza, G. D. O. Souza, M. Osial, N. D. S. Mohallem, V. S. T. Ciminelli and P. Krysinski, *J. Water Process Eng.*, 2023, **51**, 103457.
45 Y. Hao, Y.-L. Lu, Z. Jiao and C.-Y. Su, *Angew. Chem., Int. Ed.*, 2024, **63**, e202317808.
46 S. Hu, M.-L. Gao, J. Huang, H. Wang, Q. Wang, W. Yang, Z. Sun, X. Zheng and H.-L. Jiang, *J. Am. Chem. Soc.*, 2024, **146**, 20391–20400.
47 C. Janiak, *J. Chem. Soc., Dalton Trans.*, 2000, **21**, 3885–3896.
48 R. Thakuria, N. K. Nath and B. K. Saha, *Cryst. Growth Des.*, 2019, **19**, 523–528.
49 T. F. Headen, C. A. Howard, N. T. Skipper, M. A. Wilkinson, D. T. Bowron and A. K. Soper, *J. Am. Chem. Soc.*, 2010, **132**, 5735–5742.
50 R. Zhao and R.-Q. Zhang, *Phys. Chem. Chem. Phys.*, 2016, **18**, 25452–25457.
51 X. Xu, K. Jia, Q. Qi, G. Tian and D. Xiang, *Phys. Chem. Chem. Phys.*, 2024, **26**, 14607–14612.
52 S. Samanta, S. Sanyal, M. Maity, M. Chaudhury and S. Ghosh, *J. Lumin.*, 2017, **190**, 403–412.

 This journal is © The Royal Society of Chemistry 2025

Open Access Article. Published on 24 January 2025. Downloaded on 11/7/2025 6:47:57 AM.
This article is licensed under a Creative Commons Attribution 3.0 Unported Licence.

53 B. J. J. Timmer and T. J. Mooibroek, *J. Chem. Educ.*, 2021, **98**, 540–545.
54 T. Yang, Y. Chen, Y. Wang, X. Peng and A. Kong, *ACS Appl. Mater. Interfaces*, 2023, **15**, 8066–8075.
55 J. Zhang, Y. Xu, L. Cui, A. Fu, W. Yang, C. Barrow and J. Liu, *Composites, Part A*, 2015, **71**, 1–8.
56 F. C.-M. Leung, S. Y.-L. Leung, C. Y.-S. Chung and V. W.-W. Yam, *J. Am. Chem. Soc.*, 2016, **138**, 2989–2992.
57 M.-M. Shi, Y. Chen, Y.-X. Nan, J. Ling, L.-J. Zuo, W.-M. Qiu, M. Wang and H.-Z. Chen, *J. Phys. Chem. B*, 2011, **115**, 618–623.
58 Y. Shao, G.-Z. Yin, X. Ren, X. Zhang, J. Wang, K. Guo, X. Li, C. Wesdemiotis, W.-B. Zhang and S. Yang, *RSC Adv.*, 2017, **7**, 6530–6537.
59 L. Chen, H. Wang, J. Liu, R. Xing, X. Yu and Y. Han, *J. Polym. Sci., Part B:Polym. Phys.*, 2016, **54**, 838–847.
60 S. Yao, X. Zhang, H. Wang, H. Wang, X. Gan, Z. Wu, Y. Tian, Z. Pan and H. Zhou, *Dyes Pigm.*, 2017, **145**, 152–159.
61 L. Liu, J. Hao, Y. Shi, J. Qiu and C. Hao, *RSC Adv.*, 2015, **5**, 3045–3053.
62 Q. Yang, M. Luo, K. Liu, H. Cao and H. Yan, *Appl. Catal., B*, 2020, **276**, 119174.
63 E. Asayesh-Ardakani, M. Rahmani, A. Hosseinian, S.-B. Ghaffari and M.-H. Sarrafzadeh, *Coord. Chem. Rev.*, 2024, **518**, 216087.
64 J. Tan, S. Namuangruk, W. Kong, N. Kungwan, J. Guo and C. Wang, *Angew. Chem., Int. Ed.*, 2016, **55**, 13979–13984.
65 T. Wang, Y. Zhang, Z. Wang, Y. Chen, P. Cheng and Z. Zhang, *Dalton Trans.*, 2023, **52**, 15178–15192.
66 Y. Zhu, P. Shao, L. Hu, C. Sun, J. Li, X. Feng and B. Wang, *J. Am. Chem. Soc.*, 2021, **143**, 7897–7902.
67 X. Guan, Q. Fang, Y. Yan and S. Qiu, *Acc. Chem. Res.*, 2022, **55**, 1912–1927.
68 Z. Ting, G. Yi-fan and G. Jia, *J. Funct. Polym.*, 2018, **31**, 189–215.
69 C. Liu, Z. Wang, L. Zhang and Z. Dong, *J. Am. Chem. Soc.*, 2022, **144**, 18784–18789.
70 A. Zhang and Y. Ai, *Prog. Chem.*, 2020, **32**, 1564–1581.
71 W. H. X. Yu and Y. Li, *Acta Chim. Sin.*, 2022, **80**, 1494–1506.
72 F. Guo, W. Zhang, S. Yang, L. Wang and G. Yu, *Small*, 2023, **19**, 2207876.
73 W. Liu, X. Li, P. He, B. Li, N. Liu, Y. Li and L. Ma, *Small*, 2024, **20**, 2403684.
74 Y. Li, J. Sui, L.-S. Cui and H.-L. Jiang, *J. Am. Chem. Soc.*, 2023, **145**, 1359–1366.
75 M. Guo, S. Jayakumar, M. Luo, X. Kong, C. Li, H. Li, J. Chen and Q. Yang, *Nat. Commun.*, 2022, **13**, 1770.
76 S. Kandambeth, K. Dey and R. Banerjee, *J. Am. Chem. Soc.*, 2019, **141**, 1807–1822.
77 H. Yuan, Z. Lu, Y. Li, C. Zhang and G. Li, *Chin. J. Chromatogr.*, 2022, **40**, 109–122.
78 J. Li, S.-Y. Gao, J. Liu, S. Ye, Y. Feng, D.-H. Si and R. Cao, *Adv. Funct. Mater.*, 2023, **33**, 2305735.
79 T. Shi, L. Li, Z. Li, G. Chen, H. Wang, X. Zhang and Y. Xie, *J. Phys. Chem. Lett.*, 2022, **13**, 10364–10369.
80 S. Yu, H. Pang, S. Huang, H. Tang, S. Wang, M. Qiu, Z. Chen, H. Yang, G. Song, D. Fu, B. Hu and X. Wang, *Sci. Total Environ*, 2021, **800**, 149662.
81 J. Li, Q. Lv, L. Bi, F. Fang, J. Hou, G. Di, J. Wei, X. Wu and X. Li, *Coord. Chem. Rev.*, 2023, **493**, 215303.
82 S. Sağlam, F. N. Türk and H. Arslanoğlu, *J. Environ. Chem. Eng.*, 2023, **11**, 110568.
83 Y. Chai, Y. Zhang, L. Wang, Y. Du, B. Wang, N. Li, M. Chen and L. Ou, *Sep. Purif. Technol.*, 2022, **295**, 121225.
84 G. Xu, C. Zhu and G. Gao, *Small*, 2022, **18**, 2203140.
85 S. A. A. Razavi, W. Chen, H.-C. Zhou and A. Morsali, *Coord. Chem. Rev.*, 2024, **517**, 216004.
86 P. Thanasekaran, C.-H. Su, Y.-H. Liu and K.-L. Lu, *Coord. Chem. Rev.*, 2021, **442**, 213987.
87 H. Dai, X. Yuan, L. Jiang, H. Wang, J. Zhang, J. Zhang and T. Xiong, *Coord. Chem. Rev.*, 2021, **441**, 213985.
88 V. Anh Tran, K. B. Vu, T.-T. Thi Vo, V. Thuan Le, H. H. Do, L. G. Bach and S.-W. Lee, *Appl. Surf. Sci.*, 2021, **538**, 148065.
89 Y. Wang, A. Liu, Y. Zheng, J. Song, H. Xian and T. Jiang, *Surf. Interfaces*, 2024, **46**, 104069.
90 N. A. Nordin, M. A. Mohamed, N. S. N. Hasnan, S. F. M. Yusoff, M. S. Mastuli, T. Sugiura and K. Manseki, *J. Sol-Gel Sci. Technol.*, 2024, DOI: 10.1007/s10971-024-06331-x.
91 Y. Sun, J. Wei, Z. Fu, M. Zhang, S. Zhao, G. Xu, C. Li, J. Zhang and T. Zhou, *Adv. Mater.*, 2023, **35**, 2208625.
92 Y. Sun, Y. Li, X. Song, S. Zhao, T. Zhou and J. Zhang, *Adv. Funct. Mater.*, 2024, 2413107.
93 W.-H. Deng, X. Wang, K. Xiao, Y. Li, C. Liu, Z. Yao, L. Wang, Z. Cheng, Y. Lv, S. Xiang and Z. Zhang, *Chem. Eng. J.*, 2024, **497**, 154457.
94 C. Ma, L. Qin, T. Zhou and J. Zhang, *Energy Environ. Sci.*, 2024, **17**, 8992–9026.
95 W.-K. Qin, C.-H. Tung and L.-Z. Wu, *J. Mater. Chem. A*, 2023, **11**, 12521–12538.
96 A. A. Zhang, Z. X. Wang, Z. B. Fang, J. L. Li and T. F. Liu, *Angew. Chem., Int. Ed.*, 2024, **63**, e202412777.
97 B. Yu, L. Li, S. Liu, H. Wang, H. Liu, C. Lin, C. Liu, H. Wu, W. Zhou, X. Li, T. Wang, B. Chen and J. Jiang, *Angew. Chem., Int. Ed.*, 2021, **60**, 8983–8989.
98 C. Huang, S. Barlow and S. R. Marder, *J. Org. Chem.*, 2011, **76**, 2386–2407.
99 R. Sun, Y. Wang, Z. Zhang, Y. Qu, Z. Li, B. Li, H. Wu, X. Hua, S. Zhang, F. Zhang and L. Jing, *Chem. Eng. J.*, 2021, **426**, 131266.
100 J. Lu, Z. Li, H. Gao and W. Cui, *Appl. Surf. Sci.*, 2021, **537**, 148003.
101 R. Sun, H. Yin, Z. Zhang, Y. Wang, T. Liang, S. Zhang and L. Jing, *J. Phys. Chem. C*, 2021, **125**, 23830–23839.
102 X. Bai, L. Guo, T. Jia, D. Hao, C. Wang, H. Li and R. Zong, *J. Hazard. Mater.*, 2022, **435**, 128992.
103 P. Liu, T. Liang, J. Bian, Z. Li, Z. Zhang and L. Jing, *Mater. Res. Bull.*, 2023, **167**, 112370.
104 X. Zhang, L. Shi and Y. Zhang, *J. Taiwan Inst. Chem. Eng.*, 2022, **132**, 104111.
105 L. Yan, W. Wang, Q. Zhao, Z. Zhu, B. Liu and C. Hu, *J. Colloid Interface Sci.*, 2022, **606**, 898–911.

Open Access Article. Published on 24 January 2025. Downloaded on 11/7/2025 6:47:57 AM.
This article is licensed under a Creative Commons Attribution 3.0 Unported Licence.

106 S. Dong, Y. Zhao, J. Yang, X. Liu, W. Li, L. Zhang, Y. Wu, J. Sun, J. Feng and Y. Zhu, *Appl. Catal., B*, 2021, **291**, 120127.
107 X. Xu, S. Dai, S. Xu, Q. Zhu and Y. Li, *Angew. Chem., Int. Ed.*, 2023, **62**, e202309066.
108 R. Wang, J. Liu, B. Wang, R. Yang, S. Zhu, Y. Song, Y. Hua, J. Yan, M. Cheng, H. Xu and H. Li, *J. Alloys Compd.*, 2022, **925**, 166370.
109 R. Tang, D. Gong, Y. Deng, S. Xiong, J. Deng, L. Li, Z. Zhou, J. Zheng, L. Su and L. Yang, *Chem. Eng. J.*, 2022, **427**, 131809.
110 J. Yang, H. Miao, J. Jing, Y. Zhu and W. Choi, *Appl. Catal., B*, 2021, **281**, 119547.
111 Y. Wang, Z. Zhao, R. Sun, J. Bian, Z. Zhang and L. Jing, *Nanoscale*, 2022, **14**, 8041–8049.
112 S. Dai, Y. Xu, W. Zhang, S. Li, Q.-Y. Guo, J. Cui, Y. Song, J. Yuan, W. Peng and M. Huang, *J. Mater. Chem. A*, 2022, **10**, 20248–20253.
113 R. Yang, G. Song, L. Wang, Z. Yang, J. Zhang, X. Zhang, S. Wang, L. Ding, N. Ren, A. Wang and X. Yu, *Small*, 2021, **17**, 2102744.
114 A. Kumari and S. Sengupta, *ChemCatChem*, 2024, **16**, e202301033.
115 F. Würthner, *Chem. Commun.*, 2004, 1564–1579.
116 H. Wu, L. Xue, Y. Shi, Y. Chen and X. Li, *Langmuir*, 2011, **27**, 3074–3082.
117 J. Wang, D. Liu, Y. Zhu, S. Zhou and S. Guan, *Appl. Catal., B*, 2018, **231**, 251–261.
118 K. Balakrishnan, A. Datar, R. Oitker, H. Chen, J. Zuo and L. Zang, *J. Am. Chem. Soc.*, 2005, **127**, 10496–10497.
119 H. Li, C. Wang, X. Bai, X. Wang, B. Sun, D. Li, L. Zhao, R. Zong and D. Hao, *Mater. Chem. Front.*, 2020, **4**, 2673–2687.
120 K. Kong, S. Zhang, Y. Chu, Y. Hu, F. Yu, H. Ye, H. Ding and J. Hua, *Chem. Commun.*, 2019, **55**, 8090–8093.
121 Z. Zhang, J. Wang, D. Liu, W. Luo, M. Zhang, W. Jiang and Y. Zhu, *ACS Appl. Mater. Interfaces*, 2016, **8**, 30225–30231.
122 Y. Sun, D. Wang and Y. Zhu, *Chem. Eng. J.*, 2022, **438**, 135667.
123 G. Aimaiti, Y. Zou, Y. Ma, Y. Shi, K. Qi, W. Zhan, Z. Qian, Z. Liu and Y. Dong, *Chem. Eng. J.*, 2024, **496**, 153852.
124 Y. Liu, L. Ma, C. Shen, X. Wang, X. Zhou, Z. Zhao and A. Xu, *Chin. J. Catal.*, 2019, **40**, 168–176.
125 J. Xu, Q. Gao, Z. Wang and Y. Zhu, *Appl. Catal., B*, 2021, **291**, 120059.
126 S. Bettini, L. Valli and G. Giancane, *Molecules*, 2020, **25**, 3742.
127 D. M. Mafukidze and T. Nyokong, *J. Mol. Struct.*, 2019, **1180**, 307–317.
128 K. Shi, M. Zhou, F. Wang, X. Li, W. Huang, K. Lu, K. Yang and C. Yu, *Chemosphere*, 2023, **329**, 138617.
129 M. Pei, K. Li, X. Li, C. Song and X. Guo, *Ind. Eng. Chem. Res.*, 2023, **62**, 2698–2709.
130 S. Xu, W. Sun, X. Meng, Y. Dong and Y. Ding, *J. Phys. Chem. C*, 2021, **125**, 24413–24421.
131 T. Ikeda, J. M. Lintuluoto, N. Aratani, Z. S. Yoon, D. Kim and A. Osuka, *Eur. J. Org. Chem.*, 2006, 3193–3204.
132 V. Valderrey, G. Aragay and P. Ballester, *Coord. Chem. Rev.*, 2014, **258–259**, 137–156.
133 K. Yamasumi and H. Maeda, *Bull. Chem. Soc. Jpn.*, 2021, **94**, 2252–2262.
134 S. Chen, X. Ren, S. Tian, J. Sun and F. Bai, *MRS Adv.*, 2020, **5**, 2147–2155.
135 J. Han, Z. Zhu, N. Li, D. Chen, Q. Xu, H. Li, J. He and J. Lu, *Appl. Catal., B*, 2021, **291**, 120108.
136 B. Zhao, D. Lu, K. K. Kondamareddy, W. Gu, J. Li, T. Tian, L. Li, H. Fan and W. Ho, *J. Alloys Compd.*, 2024, **984**, 174004.
137 B. Das, L. P. R. Pala, M. K. Mohanta, M. Devi, D. Chakraborty, N. R. Peela, M. Qureshi and S. S. Dhar, *J. Mater. Chem. A*, 2022, **10**, 23691–23703.
138 D. Chen, K. Wang, W. Hong, R. Zong, W. Yao and Y. Zhu, *Appl. Catal., B*, 2015, **166–167**, 366–373.
139 R. Bera, B. Jana, B. Mondal and A. Patra, *ACS Sustainable Chem. Eng.*, 2017, **5**, 3002–3010.
140 W. Li, X. He, R. Ge, M. Zhu, L. Feng and Y. Li, *Sustainable Mater. Technol.*, 2019, **22**, e00114.
141 S. Liu, S. Zhou, C. Hu, M. Duan, M. Song, F. Huang and J. Cai, *J. Mater. Sci.: Mater. Electron.*, 2020, **31**, 10677–10688.
142 T. Morimoto, C. Nishiura, M. Tanaka, J. Rohacova, Y. Nakagawa, Y. Funada, K. Koike, Y. Yamamoto, S. Shishido, T. Kojima, T. Saeki, T. Ozeki and O. Ishitani, *J. Am. Chem. Soc.*, 2013, **135**, 13266–13269.
143 Y.-J. Huang and J. Zhang, *Inorg. Chim. Acta*, 2020, **501**, 119244.
144 T.-T. Zhu, Y.-T. Tao, Y. Sun, X. Wang, X.-W. Zhang, J.-L. Chai, J. Han, X.-L. Zhao and X.-D. Chen, *J. Mol. Struct.*, 2021, **1236**, 130289.
145 S. Adhikari, A. H. Sheikh, S. Kansız, N. Dege, N. Baildya, G. Mahmoudi, N. A. Choudhury, R. J. Butcher, W. Kaminsky, S. Talledo, E. M. Lopato, S. Bernhard and J. Kłak, *J. Mol. Struct.*, 2023, **1285**, 135481.
146 X.-Y. Zhang, R.-X. Wu, C.-F. Bi, X. Zhang and Y.-H. Fan, *Inorg. Chim. Acta*, 2018, **483**, 129–135.
147 X.-L. Hao, Y.-Y. Ma, Y.-H. Wang, W.-Z. Zhou and Y.-G. Li, *Inorg. Chem. Commun.*, 2014, **41**, 19–24.
148 Z. Xu, X. Mao, P. Zhang, H. Li, Y. Wang, M. Liu and L. Jia, *J. Mol. Struct.*, 2017, **1128**, 665–673.
149 J.-H. Zhang, Y.-N. Gong, H.-J. Wang, Y.-C. Wang, W. Yang, J.-H. Mei, D.-C. Zhong and T.-B. Lu, *Proc. Natl. Acad. Sci. U. S. A.*, 2022, **119**, e2118278119.
150 L.-Q. Qiu, K.-H. Chen, Z.-W. Yang and L.-N. He, *Green Chem.*, 2020, **22**, 8614–8622.
151 J. Li, Y. Wei, X.-Y. Chen, Z.-L. Zhu and Y. Gao, *Inorg. Chem. Commun.*, 2017, **86**, 10–13.
152 S. Scoditti, E. Dabbish, G. E. Pieslinger, E. Rezabal, X. Lopez, E. Sicilia and L. Salassa, *Phys. Chem. Chem. Phys.*, 2022, **24**, 5323–5329.
153 S. Tang, Z. Fu, Y. Li and Y. Li, *Appl. Catal., A*, 2020, **590**, 117342.
154 M. Kombo, H.-B. Chong, L.-B. Ma, S. Sahar, X.-X. Fang, T. Zhao, C. Ling, X.-J. Lu and A.-W. Xu, *ACS Appl. Nano Mater.*, 2020, **3**, 10659–10667.

 This journal is © The Royal Society of Chemistry 2025

Open Access Article. Published on 24 January 2025. Downloaded on 11/7/2025 6:47:57 AM.
This article is licensed under a Creative Commons Attribution 3.0 Unported Licence.

155 Y. Zhang, Q. Cao, X. Wu, Y. Xiao, A. Meng, Q. Zhang, Y. Yu and W.-D. Zhang, *Chem. Eng. J.*, 2022, **427**, 132042.
156 J. Wei, D. Luo, M. Shi, Q. Yuan, M. Wang, Y. Huang and Y. Ni, *Inorg. Chem.*, 2023, **62**, 10973–10983.
157 S. Cao, J. Low, J. Yu and M. Jaroniec, *Adv. Mater.*, 2015, **27**, 2150–2176.
158 X.-L. Song, L. Chen, J.-T. Ren, L.-J. Gao and Z.-Y. Yuan, *Coord. Chem. Rev.*, 2024, **507**, 215752.
159 M. Chen, M. Sun, X. Cao, H. Wang, L. Xia, W. Jiang, M. Huang, L. He, X. Zhao and Y. Zhou, *Coord. Chem. Rev.*, 2024, **510**, 215849.
160 H. Li, B. Cheng, J. Xu, J. Yu and S. Cao, *EES Catal.*, 2024, **2**, 411–447.
161 H. Song, L. Luo, S. Wang, G. Zhang and B. Jiang, *Chin. Chem. Lett.*, 2024, **35**, 109347.
162 H. Che, C. Liu, H. Dong, C. Li, X. Liu and G. Che, *Int. J. Hydrogen Energy*, 2019, **44**, 20029–20041.
163 W. Wang, Y. Huang and Z. Wang, *Acta Phys. Chim. Sin.*, 2020, 2011073.
164 J. Huang, M. Klahn, X. Tian, X. Dai, J. Rabeah, V. Aladin, B. Corzilius, S. Bartling, H. Lund, N. Steinfeldt, T. Peppel, A. J. Logsdail, H. Jiao and J. Strunk, *ACS Appl. Nano Mater.*, 2024, **7**, 7442–7452.
165 F. Fina, S. K. Callear, G. M. Carins and J. T. S. Irvine, *Chem. Mater.*, 2015, **27**, 2612–2618.
166 X. Cai, Y. Li, Y. Zhang and W. Lin, *ACS Catal.*, 2023, **13**, 15877–15885.
167 M. Majdoub, Z. Anfar and A. Amedlous, *ACS Nano*, 2020, **14**, 12390–12469.
168 T. Banerjee, F. Podjaski, J. Kröger, B. P. Biswal and B. V. Lotsch, *Nat. Rev. Mater.*, 2021, **6**, 168–190.
169 S. Wang, H. Zhang, R. Nie, Y. Ning, C. Zhao, Z. Xia, P. Niu, L. Li and S. Wang, *Dalton Trans.*, 2022, **51**, 13015–13021.
170 J. Liu, J. Li, F. Xing and J. Liu, *Catal. Sci. Technol.*, 2024, **14**, 903–911.
171 F. Xu, C. Lai, M. Zhang, D. Ma, L. Li, S. Liu, X. Zhou, H. Yan, N. Wang, M. Xu, L. Qin and H. Yi, *Sep. Purif. Technol.*, 2023, **308**, 122829.
172 L. Liu, L. Ding, Y. Liu, W. An, S. Lin, Y. Liang and W. Cui, *Appl. Catal., B*, 2017, **201**, 92–104.
173 X. Wang, J. Zhu, X. Yu, X. Fu, Y. Zhu and Y. Zhang, *J. Mater. Sci. Technol.*, 2021, **77**, 19–27.
174 Y. Qing, Y. Li, L. Cao, Y. Yang, L. Han, P. Dansawad, H. Gao and W. Li, *Sep. Purif. Technol.*, 2023, **314**, 123545.
175 S. Yan, H. Song, Y. Li, J. Yang, X. Jia, S. Wang and X. Yang, *Appl. Catal., B*, 2022, **301**, 120820.
176 N. A. Chopan and A. H. Bhat, *New J. Chem.*, 2023, **47**, 15922–15941.
177 Y. Yu, Q. Yang, X. Yu, Q. Lu and X. Hong, *ChemistrySelect*, 2017, **2**, 5578–5586.
178 S. Wang, C. T. Nai, X.-F. Jiang, Y. Pan, C.-H. Tan, M. Nesladek, Q.-H. Xu and K. P. Loh, *J. Phys. Chem. Lett.*, 2012, **3**, 2332–2336.
179 Y. Liang, X. Wang, W. An, Y. Li, J. Hu and W. Cui, *Appl. Surf. Sci.*, 2019, **466**, 666–672.
180 L. Ding, H. Zhou, S. Li, X. Lan, X. Chen and S. Zeng, *Colloids Surf., A*, 2022, **648**, 129296.
181 X. Yuan, N. Sunyer-Pons, A. Terrado, J. L. León, G. Hadziioannou, E. Cloutet and K. Villa, *ChemSusChem*, 2023, **16**, e202202228.
182 C. Lu, J. Han, N. Li, D. Chen, Q. Xu, H. Li and J. Lu, *J. Colloid Interface Sci.*, 2024, **668**, 59–67.
183 H. Yang, H. Hou, Y. Jiang, Z. Zhang, L. Wang, R. Wang, X. Zhan, Y. Luo and W. Yang, *Opt. Mater.*, 2024, **149**, 115015.
184 L. Xu, B. Tian, T. Wang, Y. Yu, Y. Wu, J. Cui, Z. Cao, J. Wu, W. Zhang, Q. Zhang, J. Liu, Z. Li and Y. Tian, *Energy Environ. Sci.*, 2022, **15**, 5059–5068.
185 X. Zhu, M. Guan, R. Gong, X. Gong, C. Dai and J. Tang, *Sustainable Energy Fuels*, 2023, **7**, 1537–1543.
186 Q. Zhu, J. Wang, L. Zhang, D. Yan, H. Yang, L. Zhang and X. Miao, *Bull. Mater. Sci.*, 2023, **46**, 17.
187 K. Thakur and B. Kandasubramanian, *J. Chem. Eng. Data*, 2019, **64**, 833–867.
188 V. Georgakilas, J. N. Tiwari, K. C. Kemp, J. A. Perman, A. B. Bourlinos, K. S. Kim and R. Zboril, *Chem. Rev.*, 2016, **116**, 5464–5519.
189 G. Sheng, Y. Shao, W. Ye, C. Sun, C. Chen, J. C. Crittenden and C. Liu, *ACS Sustainable Chem. Eng.*, 2018, **6**, 6711–6717.
190 Q. Wang, H. Li, J.-H. Yang, Q. Sun, Q. Li and J. Yang, *Appl. Catal., B*, 2016, **192**, 182–192.
191 F. Li, M. Tang, T. Li, L. Zhang and C. Hu, *Appl. Catal., B*, 2020, **268**, 118397.
192 Q. Hao, S. Hao, X. Niu, X. Li, D. Chen and H. Ding, *Chin. J. Catal.*, 2017, **38**, 278–286.
193 S. Gonuguntla, C. S. Vennapoosa, B. M. Abraham, A. V. S. Sainath and U. Pal, *ACS Appl. Nano Mater.*, 2024, **7**, 18146–18156.
194 P. Karthik, R. Vinoth, P. Zhang, W. Choi, E. Balaraman and B. Neppolian, *ACS Appl. Energy Mater.*, 2018, **1**, 1913–1923.
195 M. P. Croxall, R. T. Lawrence, R. Ghosh Biswas, R. Soong, A. J. Simpson and M. C. Goh, *J. Phys. Chem. Lett.*, 2024, **15**, 3653–3657.
196 Z. Luo, D. Zhang, C. Ma, M. Zhu, B. Li, L. Song and S. Yang, *ACS Omega*, 2023, **8**, 4072–4080.
197 T. Li, M. Wang, Q. Hou, Y. Hou, K. Xuan and Y. Hao, *Appl. Surf. Sci.*, 2022, **605**, 154672.
198 A. Jilani, S. Z. Hussain, M. O. Ansari, R. Kumar, M. R. Dustgeer, M. H. D. Othman, M. A. Barakat and A. A. Melaibari, *J. Mater. Sci.*, 2021, **56**, 7434–7450.
199 S. J. Park, S. Kim, T. F. Anjong, S. E. Lee and J. Kim, *Carbon*, 2015, **94**, 448–454.
200 G. Jenita Rani, M. A. Jothi Rajan and G. Gnana Kumar, *Res. Chem. Intermed.*, 2017, **43**, 2669–2690.
201 Z. Zhu, L. Pan, Z. Liu, J. Zhao, Z. Tao and Y. He, *RSC Adv.*, 2021, **11**, 33408–33415.
202 W. Zhou, H. Shen, Y. Zeng, Y. Yi, Z. Zuo, Y. Li and Y. Li, *Angew. Chem., Int. Ed.*, 2020, **59**, 4908–4913.
203 H.-Y. Si, C.-J. Mao, J.-Y. Zhou, X.-F. Rong, Q.-X. Deng, S.-L. Chen, J.-J. Zhao, X.-G. Sun, Y. M. Shen, W.-J. Feng, P. Gao and J. Zhang, *Carbon*, 2018, **132**, 598–605.

Open Access Article. Published on 24 January 2025. Downloaded on 11/7/2025 6:47:57 AM.
This article is licensed under a Creative Commons Attribution 3.0 Unported Licence.

204 H. Si, Q. Deng, C. Yin, J. Zhou, S. Zhang, Y. Zhang, Z. Liu, J. Zhang, J. Zhang and J. Kong, *J. Alloys Compd.*, 2020, **833**, 155054.
205 C. M. Navarathna, N. B. Dewage, A. G. Karunanayake, E. L. Farmer, F. Perez, E. B. Hassan, T. E. Mlsna and C. U. Pittman, *J. Inorg. Organomet. Polym. Mater.*, 2020, **30**, 214–229.
206 C. X. Yang, Q. Zhu, W. P. Dong, Y. Q. Fan and W. L. Wang, *Langmuir*, 2021, **37**, 9253–9263.
207 F. Guo, C. Shi, W. Sun, Y. Liu, X. Lin and W. Shi, *Chin. J. Chem. Eng.*, 2022, **48**, 1–11.
208 N. Cheng, B. Wang, M. Chen, Q. Feng, X. Zhang, S. Wang, R. Zhao and T. Jiang, *Environ. Pollut.*, 2023, **336**, 122409.
209 Y. Lan, Y. Luo, S. Yu, H. Ye, Y. Zhang, M. Xue, Q. Sun, Z. Yin, X. Li, C. Xie, Z. Hong and B. Gao, *Sep. Purif. Technol.*, 2024, **330**, 125543.
210 L. Meng, W. Yin, S. Wang, X. Wu, J. Hou, W. Yin, K. Feng, Y. S. Ok and X. Wang, *Chemosphere*, 2020, **239**, 124713.
211 R. Tang, D. Gong, Y. Deng, S. Xiong, J. Zheng, L. Li, Z. Zhou, L. Su and J. Zhao, *J. Hazard. Mater.*, 2022, **423**, 126944.
212 J. Yang, L. Wang, J. Yang, C. Li and S. Zhong, *J. Environ. Chem. Eng.*, 2024, **12**, 111768.
213 X. Ji, X. Liu, Y. Guo and J. Zhang, *Chem. Eng. J.*, 2021, **425**, 131260.
214 C.-C. Li, I. Ullah, G. Wang and A.-W. Xu, *Catal. Sci. Technol.*, 2023, **13**, 5456–5461.
215 J. Wang, H. Li, Y. Zhu, M. Yang, J. Huang, X. Zhu, Z. P. Yu, Z. Lu and H. Zhou, *Chem. Sci.*, 2023, **14**, 323–330.
216 X. Peng, J. Ma, Z. Zhou, H. Yang, J. Chen, R. Chen, K. Wu, G. Xi, S. Liu, Y. Shen and Y. Zhang, *Chem. Sci.*, 2023, **14**, 4319–4327.
217 X. J. Zhao, Y. Li, M. Li, Y. L. Tian, W. P. Wang, B. S. Zhang and X. C. Wang, *Org. Biomol. Chem.*, 2022, **20**, 5139–5144.
218 J.-W. Wang, H.-H. Huang, P. Wang, G. Yang, S. Kupfer, Y. Huang, Z. Li, Z. Ke and G. Ouyang, *JACS Au*, 2022, **2**, 1359–1374.
219 X.-D. Su, B.-B. Zhang, Q. Liu, J.-T. Cheng, Z.-X. Wang and X.-Y. Chen, *Org. Lett.*, 2021, **23**, 8262–8266.
220 L.-B. Ma, K. Liang, G. Wang, X.-X. Fang, C. Ling, T. Zhao, M. Kombo, T.-Y. Cheang and A.-W. Xu, *Catal. Sci. Technol.*, 2019, **9**, 5441–5446.
221 B. Chandra Garain and S. K. Pati, *ChemPhysChem*, 2023, **24**, e202200753.
222 V. J. K. Lourdusamy, M. R. N. Thomas and S. Subramani, *Environ. Sci. Pollut. Res.*, 2023, **30**, 18113–18122.
223 S. Saita, M. Anzai, N. Mori and H. Kawasaki, *Colloids Surf., A*, 2021, **617**, 126360.
224 G. Son, J. Kim and C. B. Park, *ACS Appl. Energy Mater.*, 2020, **3**, 1215–1221.
225 W. Shahzad, A. K. Badawi, Z. A. Rehan, A. M. Khan, R. A. Khan, F. Shah, S. Ali and B. Ismail, *Ceram. Int.*, 2022, **48**, 24979–24988.
226 W. Yao, M. Li, C. Sun, Y. Liu, M. Ma, F. Chen, L. Zhou and Y. Zheng, *J. Clean. Prod.*, 2022, **372**, 133745.
227 M. Tang, L. Qin, M. Luo, H. Shen, S.-Z. Kang, T. Zhang and X. Li, *J. Environ. Chem. Eng.*, 2022, **10**, 108040.
228 K. Karuppasamy, I. Rabani, D. Vikraman, C. Bathula, J. Theerthagiri, R. Bose, C.-J. Yim, A. Kathalingam, Y.-S. Seo and H.-S. Kim, *Environ. Pollut.*, 2021, **272**, 116018.
229 L. Yan, H. Gao and Y. Chen, *ACS Appl. Nano Mater.*, 2021, **4**, 7746–7757.
230 D. Mohanta and M. Ahmaruzzaman, *J. Alloys Compd.*, 2020, **828**, 154093.
231 V. A. Tran, A. N. Kadam and S.-W. Lee, *J. Alloys Compd.*, 2020, **835**, 155414.
232 G. Wang, H. Li, N. Li, D. Chen, J. He, Q. Xu and J. Lu, *Angew. Chem., Int. Ed.*, 2022, **61**, e202210619.
233 Q. Zhang, J. Chen, X. Gao, H. Che, P. Wang, B. Liu and Y. Ao, *Sep. Purif. Technol.*, 2022, **300**, 121947.
234 F. Li, T. Li, L. Zhang, Y. Jin and C. Hu, *Appl. Catal., B*, 2021, **296**, 120316.
235 Y. Shen, C. Zhu, B. Chen, J. Chen, Q. Fang, J. Wang, Z. He and S. Song, *Environ. Sci.: Nano*, 2020, **7**, 1525–1538.
236 A. Saadati and S. Sheibani, *Ceram. Int.*, 2022, **48**, 30294–30306.
237 S. Qin, Y. Xiong, J. Li, H. Wan, S. Fang, M. Duan, R. Li and D. Liao, *J. Phys. Chem. C*, 2021, **125**, 4027–4040.
238 H. Wang, X. Yuan, Y. Wu, G. Zeng, H. Dong, X. Chen, L. Leng, Z. Wu and L. Peng, *Appl. Catal., B*, 2016, **186**, 19–29.
239 L. Yue, S. Wang, G. Shan, W. Wu, L. Qiang and L. Zhu, *Appl. Catal., B*, 2015, **176–177**, 11–19.
240 K. L. V. Joseph, J. Lim, A. Anthonysamy, H.-I. Kim, W. Choi and J. K. Kim, *J. Mater. Chem. A*, 2015, **3**, 232–239.
241 Y. Gao, G. Yu, K. Liu, S. Deng, B. Wang, J. Huang and Y. Wang, *Chem. Eng. J.*, 2017, **330**, 157–165.
242 C. Du, W. Feng, S. Nie, X. Su, H. Liu, J. Feng, J. Sun, C. Hu and S. Dong, *Appl. Catal., B*, 2022, **310**, 121298.
243 Q. Zhang, J. Chen, X. Gao, H. Che, Y. Ao and P. Wang, *J. Hazard. Mater.*, 2022, **430**, 128386.
244 H. Liu, H. Li, J. Lu, S. Zeng, M. Wang, N. Luo, S. Xu and F. Wang, *ACS Catal.*, 2018, **8**, 4761–4771.
245 L. Wang, X. Liu, L. Ji, Q. Luo, Y. Duan, J. An, X. Chen, Y. Zhang, J. Ren and D. Wang, *Chem. Eng. J.*, 2022, **433**, 134502.
246 Y. Wei, M. Ma, W. Li, J. Yang, H. Miao, Z. Zhang and Y. Zhu, *Appl. Catal., B*, 2018, **238**, 302–308.
247 H. Yang, C. Li, T. Liu, T. Fellowes, S. Y. Chong, L. Catalano, M. Bahri, W. Zhang, Y. Xu, L. Liu, W. Zhao, A. M. Gardner, R. Clowes, N. D. Browning, X. Li, A. J. Cowan and A. I. Cooper, *Nat. Nanotechnol.*, 2023, **18**, 307–315.
248 Y. Shiraishi, K. Miura, M. Jio, S. Tanaka, S. Ichikawa and T. Hirai, *ACS Mater. Au*, 2022, **2**, 709–718.
249 W. Yu, N. Fang, R. Wang, Z. Liu, Y. Chu and C. Huang, *Adv. Funct. Mater.*, 2024, **34**, 2314894.
250 W. Liu, R. Xu, Y. Wang, N. Huang, T. Shimada and L. Ye, *Int. J. Hydrogen Energy*, 2022, **47**, 16005–16013.
251 T. Sun, S. Li, L. Zhang and Y. Xu, *Angew. Chem., Int. Ed.*, 2023, **62**, e202301865.
252 W. Wei and Y. Zhu, *Small*, 2019, **15**, 1903933.

 This journal is © The Royal Society of Chemistry 2025

Open Access Article. Published on 24 January 2025. Downloaded on 11/7/2025 6:47:57 AM.
This article is licensed under a Creative Commons Attribution 3.0 Unported Licence.

253 J. Yang, H. Miao, W. Li, H. Li and Y. Zhu, *J. Mater. Chem. A*, 2019, **7**, 6482–6490.
254 D. Liu, X. Yang, P. Chen, X. Zhang, G. Chen, Q. Guo, H. Hou and Y. Li, *Adv. Mater.*, 2023, **35**, 2300655.
255 X. Miao, F. Zhang, Y. Wang, X. Dong and X. Lang, *Sustainable Energy Fuels*, 2023, **7**, 1963–1973.
256 C. Yan, J. Dong, Y. Chen, W. Zhou, Y. Peng, Y. Zhang and L.-N. Wang, *Nano Res.*, 2022, **15**, 3835–3858.
257 T. Xue, C. Ma, L. Liu, C. Xiao, S.-F. Ni and R. Zeng, *Nat. Commun.*, 2024, **15**, 1455.
258 Y. Zhang, W. Zhang, F. Zhang, Y. Xiao, G. Jia, W. Wang, F.-S. Ke and Z. Guo, *Angew. Chem., Int. Ed.*, 2024, **63**, e202402694.
259 Z. Zhang, W. Liu, Y. Zhang, J. Bai and J. Liu, *ACS Catal.*, 2021, **11**, 313–322.
260 Y. Zhang, X. Huang, J. Li, G. Lin, W. Liu, Z. Chen and J. Liu, *Chem. Res. Chin. Univ.*, 2020, **36**, 1076–1082.
261 M. Wang, Z. Wang, M. Shan, J. Wang, Z. Qiu, J. Song and Z. Li, *Chem. Mater.*, 2023, **35**, 5368–5377.
262 S. An, Z. Wu, H. Jeong, J. Lee, S. Y. Jeong, W. Lee, S. Kim, J. W. Han, J. Lim, H. Cha, H. Y. Woo and D. S. Chung, *Small*, 2023, **19**, 2204905.
263 T. Wang, M. Li, Y. Chen, X. Che, F. Bi, Y. Yang, R. Yang and C. Li, *ACS Catal.*, 2023, **13**, 15439–15447.
264 B. Wang, X. Guo, Y. Zhang, Y. Wang, G. Huang, H. Chao, W. Wang, Z. Hu and X. Yan, *ACS Appl. Energy Mater.*, 2022, **5**, 7479–7489.
265 X. Han, F. Zhao, Q. Shang, J. Zhao, X. Zhong and J. Zhang, *ChemSusChem*, 2022, **15**, e202200828.
266 Z. Chen, B. Chong, N. Wells, G. Yang and L. Wang, *Chin. Chem. Lett.*, 2022, **33**, 2579–2584.
267 X. Liu, Z. Wang, S. Feng, X. Zhang, H. Xu, G. Wei, X. Gong, X. Wu and J. Hua, *Macromolecules*, 2023, **56**, 8275–8289.
268 B. Rabeie and N. M. Mahmoodi, *J. Colloid Interface Sci.*, 2024, **654**, 495–522.
269 C. Sun, Z. Wang, H. Zheng, S. Zhao, X. Luo, C. Li, L. Chen and F. Li, *Sep. Purif. Technol.*, 2024, **331**, 125586.
270 X. Wang, X. Li, G. Che, E. Zhu, H. Guo, P. A. Charpentier, W. Z. Xu and C. Liu, *ACS Appl. Mater. Interfaces*, 2024, **16**, 6367–6381.
271 J. Jin, Z. Liu, W. Wang, X. Cai, Y. Zhang, M. Muddassir, H. Sakiyama, J. Wang and C. Xie, *J. Mol. Struct.*, 2022, **1250**, 131867.
272 J. Han, Y. Deng, N. Li, D. Chen, Q. Xu, H. Li, J. He and J. Lu, *J. Colloid Interface Sci.*, 2021, **582**, 1021–1032.
273 X. Li, Q. Luo, L. Han, F. Deng, Y. Yang and F. Dong, *J. Mater. Sci. Technol.*, 2022, **114**, 222–232.
274 L. Ning, J. Xu, Y. Lou, C. Pan, Z. Wang and Y. Zhu, *J. Mater. Sci. Technol.*, 2022, **124**, 53–64.
275 M. Tian, Y. He and G. Zhang, *J. Nanopart. Res.*, 2021, **23**, 223.
276 Y. Wang, X. Li, W. Xu, D. Chen, N. Li, Q. Xu, H. Li and J. Lu, *Appl. Catal., B*, 2024, **348**, 123839.
277 X. Song, J. He, Y. Wang, J. Wang and S. Zhang, *J. Colloid Interface Sci.*, 2023, **645**, 918–932.
278 Q. Zhang, J. Chen, X. Gao, H. Che, P. Wang and Y. Ao, *Appl. Catal., B*, 2022, **313**, 121443.
279 Z. Khazaee, Y. Ouyang, Y. Zhang, O. Bogojevic, T. Jess Plesner and Z. Guo, *Chem. – Eur. J.*, 2024, **30**, e202303615.
280 L. Yang, J. Wang, K. Zhao, Z. Fang, H. Qiao, L. Zhai and L. Mi, *ChemPlusChem*, 2022, **87**, e202200281.
281 J. Jiao, T. Zhang, J. Xu, K. Guo, J. Li and Q. Han, *Chem. Commun.*, 2023, **59**, 3114–3117.
282 T. Zhang, J. Vanderghinste, A. Guidetti, S. V. Doorslaer, G. Barcaro, S. Monti and S. Das, *Angew. Chem., Int. Ed.*, 2022, **61**, e202212083.
283 N. Sun, D. Qi, Y. Jin, H. Wang, C. Wang, C. Qu, J. Liu, Y. Jin, W. Zhang and J. Jiang, *CCS Chem.*, 2022, **4**, 2588–2596.
284 L. Zhao, W. Cai, G. Ji, J. Wei, Z. Du, C. He and C. Duan, *Inorg. Chem.*, 2022, **61**, 9493–9503.
285 J.-L. Shi, K. Feng, H. Hao, C. Ku, P. H. L. Sit, W. Y. Teoh and X. Lang, *Sol. RRL*, 2022, **6**, 2100608.
286 Y.-Y. Lin and S.-Y. Lu, *J. Taiwan Inst. Chem. Eng.*, 2019, **97**, 264–271.
287 J. Cheng, Y. Wu, W. Zhang, J. Zhang, L. Wang, M. Zhou, F. Fan, X. Wu and H. Xu, *Adv. Mater.*, 2024, **36**, 2305313.
288 Y. Liu and Z. Xiang, *ACS Appl. Mater. Interfaces*, 2019, **11**, 41313–41320.
289 X. Yuan, K. Yang, C. Grazon, C. Wang, L. Vallan, J. D. Isasa, P. M. Resende, F. Li, C. Brochon, H. Remita, G. Hadziioannou, E. Cloutet and J. Li, *Angew. Chem., Int. Ed.*, 2024, **63**, e202315333.
290 B. Xia, N. Qiu, L. Cheng, A. Shan, H. Ma, J. Yang and J. Liu, *Chem. Eng. Sci.*, 2024, **283**, 119427.
291 S. Lee, J. Ju, C. Keum, J. Bang, H. Lee, S. Vikneshvaran, H. Yoo, J. Park and S.-Y. Lee, *ChemSusChem*, 2024, **17**, e202301044.
292 T. Song, P. Zhang, T. Wang, A. Ali and H. Zeng, *Appl. Catal., B*, 2018, **224**, 877–885.
293 C. Shu, X. Yang, L. Liu, X. Hu, R. Sun, X. Yang, A. I. Cooper, B. Tan and X. Wang, *Angew. Chem., Int. Ed.*, 2024, **136**, e202403926.
294 T. Shan, Y. Wang, D. Luo, Z. Huang, F. Zhang, H. Wu, L. Huang, J. Li, L. Chen and H. Xiao, *Appl. Catal., B*, 2024, **349**, 123872.
295 Y. Guo, X. Miao, X. Zhang, H. Che and Y. Li, *Sep. Purif. Technol.*, 2023, **326**, 124807.
296 H.-D. Yang, J.-H. Huang, K. Shibata, D. Lu, K. Maeda and C. Hu, *Sustainable Energy Fuels*, 2020, **4**, 4186–4195.
297 Y. Liu, Y. Wang, J. Shang, J. Peng and T. Zhu, *Appl. Catal., B*, 2024, **350**, 123937.
298 S. Zhang, Y. Hou, L. Zhang, H. Zhu, J. Xiong, S. Wang and T. Liu, *Small*, 2024, **20**, 2311816.
299 Y. Li, L. Wang, X. Gao, Y. Xue, B. Li and X. Zhu, *J. Mater. Chem. A*, 2024, **12**, 7807–7816.
300 J. Song, S. Wang, L. Wang, Q. Luo, J. An, Y. Duan and D. Wang, *Appl. Catal., B*, 2024, **343**, 123582.
301 D. Sun, J. Han, M. Xiao, T. Cao, Y. Li and H. Dong, *Sep. Purif. Technol.*, 2024, **338**, 126610.

302 P. Zhang, J. Jia, Y. Wang, L. Tong, J. Wang, C. Li and H. Dong, *Sep. Purif. Technol.*, 2024, **330**, 125224.
303 J.-W. Wang, Z. Li, Z.-M. Luo, Y. Huang, F. Ma, S. Kupfer and G. Ouyang, *Proc. Natl. Acad. Sci. U. S. A.*, 2023, **120**, e2221219120.
304 Z. Wu, W. Li, L. Hou, Q. Wei, H. Yang, Y. Jiang and D. Tang, *Sep. Purif. Technol.*, 2023, **311**, 123322.
305 S. Wang, X. Hai, X. Ding, S. Jin, Y. Xiang, P. Wang, B. Jiang, F. Ichihara, M. Oshikiri, X. Meng, Y. Li, W. Matsuda, J. Ma, S. Seki, X. Wang, H. Huang, Y. Wada, H. Chen and J. Ye, *Nat. Commun.*, 2020, **11**, 1149.
306 Z. Liu, Y. Xie, L. Liu, X. Cai, H.-Q. Yin, M. Zuo, Y. Liu, S. Feng, W. Huang and D. Wu, *Small*, 2024, **20**, 2309194.
307 X. Song, Y. Wu, X. Zhang, X. Li, Z. Zhu, C. Ma, Y. Yan, P. Huo and G. Yang, *Chem. Eng. J.*, 2021, **408**, 127292.
308 Y. Li, J. Shi, L. Wu, J. Zhang and J. Lu, *Eur. J. Inorg. Chem.*, 2021, 620–627.

Open Access Article. Published on 24 January 2025. Downloaded on 11/7/2025 6:47:57 AM.
This article is licensed under a Creative Commons Attribution 3.0 Unported Licence.

 This journal is © The Royal Society of Chemistry 2025